Towards Rational Design of Peptides for Selective Interaction with Inorganic Materials

by

Eric Mark Krauland

Submitted to the Department of Biological Engineering
in partial fulfillment of the requirements for the degree of

Doctor of Philosophy

at the

MASSACHUSETTS INSTITUTE OF TECHNOLOGY

September 2007

Signature of Author

Department of Biological Engineering
August 18, 2007

Certified by... .....

Angela M. Belcher
Professor of Biological Engineering and Materials Science and Engineering
Thesis Supervisor

Accepted by..... .....

Alan J. Grodzinsky
Professor of Biological Engineering
Chairman, Committee for Graduate Studies

Towards Rational Design of Peptides for Selective Interaction with Inorganic Materials

by

Eric Mark Krauland

Submitted to the Department of Biological Engineering
on August 18, 2007, in partial fulfillment of the
requirements for the degree of
Doctor of Philosophy

Abstract

Utilizing molecular recognition and self-assembly, material-specific biomolecules have shown great promise for engineering and ordering materials at the nanoscale. These molecules, inspired from natural biomineralization systems, are now commonly selected against non-natural inorganic materials through biopanning random combinatorial peptide libraries. Unfortunately, the challenge of studying the biological-inorganic interface has slowed the understanding of interactions principles, and hence limited the number of downstream applications. This work focuses on the facile study of the peptide-inorganic interface using Yeast Surface Display. The general approach is to use combinatorial selection to suggest interaction principles followed by rational design to refine understanding. In this pursuit, two material groups—II-VI semiconductors and synthetic sapphire (metal oxides)—are chosen as inorganic targets due to their technological relevance and ease of study.

First, yeast surface display (YSD) was established as a broadly applicable method for studying peptide-material interactions by screening a human scFv YSD library against cadmium sulfide (CdS), a II-VI semiconductor. The presence of multiple histidine residues was found to be necessary for mediating cell binding to CdS. As a follow-up, a systematic screen with yeast displayed rationally designed peptides was performed on a panel of II-VI semiconductors and gold. Cell binding results indicated that peptide interaction was mediated by a limited number of amino acids that were influenced by locally situated residues. Interpretation of the results facilitated design of new peptides with desired material specificities. Next, the nature of peptide/metal oxide binding interface was interrogated using sapphire crystalline faces as model surfaces. Biopanning a random peptide YSD library and subsequent characterization of the identified binding partners revealed the importance of multiple basic amino acids in the binding event. Study of rationally designed basic peptides revealed a preference for those amino acids to be spaced in such a manner that maximized simultaneous interaction with the surface. Fusing peptides to maltose binding protein (MBP) allowed for quantitative affinity measurement with the best peptides having low nanomolar equilibrium dissociation constants. Finally, peptides were demonstrated as facile affinity tags for protein immobilization in micro-patterning and biosensor assays.

Thesis Supervisor: Angela M. Belcher
Title: Professor of Biological Engineering and Materials Science and Engineering

Acknowledgments

First and foremost, I would like to thank my advisor Angela Belcher for providing inspiration, constant intellectual and emotional support, and the flexibility to explore multiple paths on this scientific journey. Her enthusiasm to see "the latest" result was a tremendous motivator and made for a great working environment. I am also indebted to Dane Wittrup who used his expertise of Yeast Display get this project off the ground quickly. I would also like to thank Doug Lauffenburger for his insights into solving problems, as well as his early vision of Biological Engineering that played a large role in me choosing to attend MIT. I am proud to have be able to watch that vision take hold, largely through Dougs efforts, and transition BE from small division into a full department with cutting edge research and curricula, all while maintaining a strong collegial atmosphere. I would also like to thank my former advisor at Johns Hopkins, Justin Hanes, whose enthusiasm and guidance played a large part in fostering my initial love for research as an undergraduate and masters student.

I am also indebted to numerous co-workers and collaborators that had a direct hand in this work. Beau Peelle and I started this project together in my first year and he was directly involved in many aspects of this work, especially Chapters 2 and 3. His prior experience was instrumental in getting this project off the ground and I am truly grateful for his willingness to mentor me on a wide array of topics from molecular biology to wakeboarding. I would also like to acknowledge numerous collaborators, including Steve Kottmann for his computer simulations, Andrew Magyar for his help with all things electrical, Scott Knudsen and Jon Behr for their efforts with the SMR biosensor, Eugene Antipov and Steve Sazinsky for work with yeast expression, David Appleyard and his efforts with optical trapping, and Robbie Barbero for carrying forward some aspects of this work. In addition, thanks to Ki Tae Nam, Mo Khalil, Sreekar Bhaviripudi, Dan Solis, Rana Ghosh, and Andy Rakestraw for their availability in technical discussions. Also, I would like acknowledge the whole Belcher lab group, who provided a great social environment during my whole graduate career. A few others have also done well to keep my life at MIT balanced, including strongmen Ty Thomson and Nick Marcantonio, my roommates of four years Nate Tedford and Maxine Jonas, as well as a whole slew friends in BE and Boston. Thank you guys!

Finally, I would like to thank my family. My parents, Mark and Suzan, have provided unwavering support and encouragement to obtain the best education possible, regardless of the sacrifices necessary to make that happen. It has truly been a blessing and a main reason for my success at great institutions like Johns Hopkins and MIT. Thanks also to my brothers, Kevin and Greg, whom have taught me many life lessons and should also be credited for keeping my life balanced.

Contents

List of Figures

List of Tables

Chapter 1

Introduction

1.1 Background and motivation

The study of biomolecules for biotechnology applications has grown enormously in recent years with hopes of exploiting self-assembly and molecular recognition for integrating advanced materials into medicine and industry [46, 128, 133, 164]. The ability of biomolecules to direct the growth and organization of inorganic solids was first noticed in natural biomineralization systems [7, 94]. To acquire attributes such as increased structural integrity, physical protection, and orienteering, biology has evolved diverse structures ranging from bones and teeth, to mollusk shells and magnetosomes [93]. By utilizing the basic principle in which a pre-assembled organic scaffold templates formation of solids from inorganic precursors, natural systems have shown exquisite control on the molecular scale. Therefore, biomineralized materials often surpass their chemically-synthesized counterpart in important physical properties, such as hardness, fracture resistance [12], and abrasion resistance [90]. Additional advantages include spatial and temporal control over growth, remodeling mechanisms, and synthesis of mineral phases not possible otherwise possible at low temperature and pressure [155]. Due of these advantages, scientists and engineers have long been interested in biomineralization for novel routes to synthesize, and interface with, the next generation of advanced materials [11].

As the organic matrix is recognized as a critical component in biomineralization, several studies have focused on the identifying these genes and proteins [2, 3, 12, 13, 42, 134, 135, 136]. However, these natural systems suffer many drawbacks that make interrogation difficult. First, many biomineralizing organisms are not readily amenable to advanced genetic techniques such as gene transfection and culture of stable cell lines. Next, natural systems have evolved complex regulation and composition networks, and therefore can lose the ability to function outside the natural environment, or when network components are studied in isolation. Post-translational modification, which performs crucial functions in many biomineralization processes [59, 60, 154], necessitates the purification of proteins from a native state. Harsh de-mineralization conditions during purification may damage the organic proteins

present and prevent further studying the active biological components. Due to these difficulties, researchers have resorted to studying peptide analogues of native biomineralization proteins [77, 161, 163]. Even so, advances from studying biomineralization systems are limited to certain well studied organisms while the elucidation of broadly applicable molecular recognition principles elusive. Compounding the limited utility of natural systems is their inability to recognize and grow many technically important materials, since these natural systems evolved within a specialized biological niche.

An alternative strategy unencumbered by the drawbacks of natural systems is the use of genetically-controlled combinatorial libraries. Most generally, this method consists of creating a population (or library) of chemically diverse biomolecules through genetic mutation. Then using various schemes that maintain a physical link between genotype and phenotype, a subset of libraries members with the desired function are isolated and characterized. This method has been widely used to study and engineer novel and protein-protein and protein-small molecule interactions [50, 137, 158]. A common selection scheme, called biopanning, involves coupling a target molecule to a solid support that can then be used to physically separate bound and unbound library members. Biopanning is readily adaptable for selection against inorganic surfaces since the inorganic material can act directly as the solid support. This was first demonstrated in 1992 by Stanley Brown, when he panned bacterial-displayed polypeptides against iron oxide particulates and isolated binding peptides with specificity towards various oxide forms [22]. Shortly thereafter, Barbas et al. used synthetic phage displayed antibody libraries also pan against iron oxide (magnetite) [9]. Sequence analysis of consensus clones revealed regions of the heavy-chain CR3 enriched in basic amino acids with similarity to Stanley Brown's iron oxide-binding peptides. While these studies and others [49, 129] demonstrate the power of using large combinatory libraries to find novel interactions without prior knowledge, they limited themselves to minerals oxides typically found in natural systems. Utilizing the material-independent properties of this technique, in 1997 Stanley brown extended his bacterial-display method to find repeating polypeptides against metallic-gold and chromium [156]. Since these landmark studies, numerous researches have discovered inorganic-binding

peptides through combinatorial selection [21, 41, 72, 78, 102, 127, 146, 152].

Beyond binding, the ability of combinatorial selected-peptides to then nucleate material growth is necessary for this method to be a viable alternative to natural biomineralization systems. In 2000, Brown et al. extended their technique to identify gold-binding peptides to generate peptide that enhanced the nucleation of gold particles in solution [24]. Similarly, our laboratory has pioneered the ability to utilize affinity-selected peptides to nucleate and assemble important semi-conducting [47, 87, 95, 96] and magnetic [124] materials. Naik et al. have also reported several studies focused on identifying peptides from combinatorial libraries that selectively nucleate inorganic materials [108, 106, 107].

While combinatorial selection of peptides for adhesion and growth of inorganic materials has shown great promise for new applications in nanotechnology and medicine, the lack of mechanistic studies aimed at deducing general interfacial principles has limited understanding and slowed innovation. One concern is the difficulty in characterizing the nature of the interfacial interactions [55]. Many biochemical techniques are not amenable to studying direct binding interactions between a soluble molecule and solid material surface. Two techniques, surface plasmon resonance (SPR) [159] and quartz crystal microbalance (QCM) [27], require the material of interest to be deposited in a thin film, which is not always possible, or require custom modifications to the instruments. In light of this, coupling the display system to the direct study of binding interactions may be an attractive alternative. Unfortunately, phage display is not ideally suited for this process. The phage particles are of insufficient mass or size to evaluate binding strength using force detachment assays and require additional labeling, immunological assays, or time intensive AFM or TEM techniques for visualization, preventing rapid and direct quantification. Bacteria, being slightly larger than phage, have been used to a limited extent for measuring adhesion to inorganic surfaces but still recquired the use of a fluorescence stain to increase bacterial contrast with the surface [146].

Methodological issues have also slowed the development of basic principles governing peptide-material interactions. Genetic selection of peptides from random combi-

natorial libraries allows for answers to a problem without prior knowledge or intuition. While this aspect is crucial for exploring new areas, due to the technical difficulties is studying interfaces, researches have relied heavily on screening random libraries and not rational design to find novel interactions. Unfortunately, the consistent use of this technique may, counter-intuitively, slow the discovery of interaction principles. Issues with combinatorial selections for peptides to inorganics include inefficient coverage of sequence space, high sensitivity to display conditions and surface preparation, slow turnaround times, and limited ability for hypothesis testing. In addition, these selections rarely lead to a high degree of sequence convergence, which further compounds the problem of extracting meaningful information. Many selections are designed in hope of finding sequences that can nucleate the material upon which it was selected. Since selections result in clones that perform what is demanded by the screening process, there is no guarantee binding clones will work outside the display environment, in other buffer conditions, or with various surface treatments, let alone permit material growth. Also, the process of nucleation is more multivariate than simple adhesion and few quantitative metrics exist for validation. As a result, these complications confound the principles that can be taken from selections aimed at material growth.

An alternative to screening random combinatorial libraries for studying peptide-material interactions may be rational design. In this method sequences or mutations are pre-determined, which allows for direct hypothesis testing. Rational design is frequently used to explore active sites in enzymes [35, 116] or residues important for stability and affinity in proteins [53, 84]. Still, when studying less well characterized proteins or looking for improved functionality, rational design suffers due to the complexity of protein structures composed of many hundred amino acids. Short peptides, conversely, contain much less information due to their relative unstructured nature and limited number of amino acids. Most information can be captured in terms of peptide composition and sequence motifs. Carefully designed peptide variants will cover a greater diversity of total sequence space as compared to full proteins. Therefore, using rational design to explore peptide-material interactions should be much

more amenable to extracting out important binding principles.

A more systematic understanding of the interface between biomolecules and inorganic materials will have several advantages. Prior knowledge may preclude the need for time intensive genetic selections or lead to more intelligent library design. In addition, a clearer understanding of specificity and affinity will better define the possible applications, as well as hint at new ideas. The results within this work are aimed at tackling both the technical and methodological challenges in studying the underlying mechanisms in hope of realizing the full potential of inorganic binding peptides.

1.2 Specific Aims

1. Establish Yeast Surface Display (YSD) as a facile method for selection and study of peptides against inorganic materials

2. Interrogate peptide binding principles to II-VI semiconductors and metal oxides (synthetic sapphire) through a combination of random combinatorial selection and rational design

3. Develop assay for the facile quantification of peptide adhesion strength to inorganics

1.3 Scope of work

The work herein is based on the premise that a better understanding of peptide-material interaction will further discovery of novel interactions as well as increase potential applications. In this pursuit, the general approach was to first use combinatorial selection to hint at interaction principles and then use rational design to refine understanding. Specific Aim 1 is addressed in Chapter 2 by screening a human scFv YSD library against cadmium sulfide (CdS) and interrogating selected clones for regions necessary for binding. Addressing Specific Aim 2 concerns the majority of this

thesis. While in Chapter 2 we use combinatorial selection to hint at the importance of histidine residues to II-VI semiconductor CdS, Chapter 3 presents a rationally designed systematic approach to interrogate the important residues for a panel of II-VI semiconductors and gold. In addition, this chapter demonstrates how a mechanistic approach can have predictive power for the construction of novel peptide-material specificities. In Chapter 4, again combinatorial selection is used and selected clones interrogated to uncover the importance of basic amino acids at the binding interface of peptides and synthetic sapphire. Following the general approach, Chapter 5 then uses more rational design to investigate the importance of peptide sequence on the binding event. Specific Aim 3 is also addressed in Chapter 5, in which we develop an off-cell quantitative assay for the measurement of adhesion strength. Chapter 6 highlights three potential applications for material-binding peptides to assemble the protein-inorganic interface, as well as a general discussion on future directions and applications.

Chapter 2

Yeast Surface Display as a Tool for Studying Material Binding Biomolecules

2.1 Summary

This chapter establishes Yeast Surface Display (YSD) as a broadly applicable methodology for studying polypeptide-solid surface interactions. A YSD human repertoire antibody library was screened to identify rare-occurring scFv fragments as CdS-binding polypeptides. A semi-quantitative cell-surface binding assay, site-directed mutational analysis, and genetic engineering were used to identify short distal regions of the displayed polypeptides necessary and sufficient for CdS binding. Alanine scanning mutagenesis in combination with a series of engineered polyhistidine peptides elucidated a direct relationship between histidine number and binding strength, which appeared to be further modulated by arginine and basic residues. The minimum strength of interaction was established by competition studies using soluble synthetic peptide analogs, which showed half-maximal inhibition of yeast binding to CdS at $\sim$2 μM peptide. To demonstrate wide applicability, cells displaying material specific polypeptides formed self-healing biofilms and discriminated between fabricated heterostructure surfaces. In addition, the soluble peptides of selected CdS-binding sequences mediated aqueous synthesis of fluorescent CdS nanoparticles at room temperature.

2.2 Introduction

In the last few years there has been significant interest in identifying biomolecules with molecular specificity for inorganic materials that bind and/or direct the synthesis of various technologically and medically important materials [46, 128]. Methods employed to select or evolve such material binders include phage display [47, 87, 95, 96, 106, 152, 156], bacterial surface display [22, 23, 24, 78, 129], and monoclonal antibodies [21]. However, certain challenges arise using these display formats for identifying and characterizing inorganic material binding polypeptides. Beyond the difficulty in assaying the peptide-material interface mentioned in Chapter 1, Phage display suffers several inherent limitations during the biopanning process. First, the

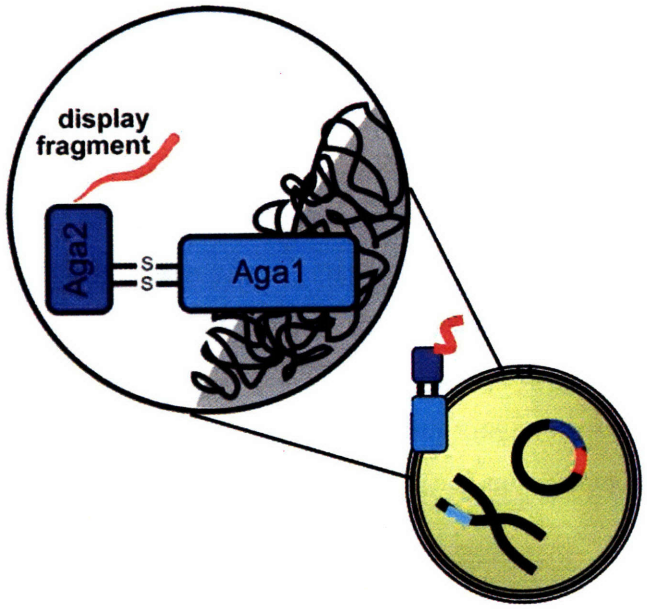

Figure 2-1: *Yeast Surface Schematic.* Diagram showing the c-terminally displayed fragment (red) on the surface of yeast cells as a fusion to the Aga2 protein (light blue). Aga2 is covalently linked to Aga1 (dark blue) by two disulfide bonds, which becomes covalently linked to the yeast cell wall polysaccharide. The Aga1 gene is integrated into the host chromosome of *S. cerevisiae* strain EBY100 while Aga2 is maintained on a plasmid. Expression of both proteins is regulated under the GAL1-10 inducible promoter and results in 10^3-10^5 surface expressed fragments per cell.

phage are propagated and amplified in bacterial cells that may induce display biases in the library. In addition, the phage bound during panning need to be eluted before bacterial propagation. This step may further the bias as elution depends on the interplay between eluent, peptide, and surface, and not just the peptide and surface. Bacterial surface display overcomes these selection disadvantages but may susceptible to natural biofilm formation on a several inorganic surfaces [89].

Yeast surface display (Fig. 2-1) may be a good alternative for both identifying and characterizing material binding polypeptides. Yeast surface display has successfully generated biomolecules with improved expression, stability, and high affinity for applications in protein therapeutics and drug discovery [50, 158]. *Saccharomyces cerevisiae* are ca. 4 μm spherical cells with a rigid cell wall, which are easily visualized and

quantifiable by conventional light microscopy. The relatively massive cell in comparison to phage or bacteria and the lack of cellular appendages allows for the application of mechanical forces to the particle-like cell body to quantitatively probe biomolecular interactions with surfaces [5, 15]. Advantageous in other cell display systems [22, 120], the ability to genetically regulate display in yeast [18] enables determination of background cell adherence and permits rescue of all surface binding clones. In addition, because organisms have evolved intricate systems to control inorganic materials as evident in biomineralization [7, 94], studies at a cellular/molecular level with an engineered system could possibly give insights into molecular mechanisms of natural biomineralization.

Herein, a detailed study of interfacial sequence-activity relationships between peptides and inorganic material surfaces using a new cell display method is reported. The method relies on living yeast cells to express and display on their surface a combinatorial library of proteins or peptides, which are then panned against a solid material surface. Subsequently, all cells bound to the material surface are rescued by turning off display and amplifying in culture. Single crystal CdS, a II-VI semiconductor material, was chosen to demonstrate this method due to its importance in optical devices and biological nanoparticle probes [160], although this method has also been applied to other materials such as CdSe, ZnS, ZnSe, Au, FePt, Al_2O_3, and GaN [119]. Importantly, using genetic engineering and biochemical techniques adapted to liquid-solid interfaces, we were then able to compare relative binding affinities of the CdS binding peptides. Further insights into the sequence-activity relationships of CdS binders and variants were gained through mutational analysis and alanine scanning mutagenesis. Finally, utility of identified peptides was demonstrated by engineered self-healing biofilms, cell adhesion to specific surfaces of material heterostructures, and peptide-dependent assembly of fluorescent CdS nanoparticles.

2.3 Results and Discussion

2.3.1 Panning for inorganic surface-binding biomolecules

Panning was performed against single crystal cadmium sulfide (CdS), a II-VI semiconductor, using a library of *S. cerevisiae* displaying 10^9 different human scFv antibodies and shorter polypeptides [44]. The general panning method is outlined in Fig. 2-2*A*. Sequential rounds of screening (d1-d7), were performed on a 1.0 cm^2 polished A-plate CdS single crystal to identify material binding clones (summarized in Table 2.1). The expression of library clones was induced by growth in galactose-based media (SG) [19] for 24 hours at room temperature. The CdS was exposed to the induced yeast library in an aqueous buffered environment for 1-24 h, washed in media, and visualized by light microscopy (Fig. 2-2*B*). The bound yeast were then permitted to "grow off the surface overnight by placing the CdS in glucose-based media (SD), which represses expression of the library clones (Fig. 2-2*B* inset). The grow off method ensures rescue of all clones bound to the material. Rounds d1-d4 were screened in SG-BSA while rounds d5-d7 were screened for shorter time periods in PBS-BSAT, which contains tween-20 and BSA, to increase the stringency of selection. In a control experiment, clones grown in SD (repressed expression) exhibited no binding (Fig. 2-2*C*) in comparison to identical cultures grown in SG (induced expression) (Fig. 2-2*B*). Even after attempting to grow off any bound cells by incubation of the CdS in media for 24 hours, the cultures remained clear (Fig. 2-2*C* inset). Thus, interactions with the surface of CdS were mediated through the displayed library members.

After round d7, a total of 36 yeast clones from the selected binding population were sequenced. DNA was isolated from each yeast clone, amplified in *Escherichia coli*, isolated and sequenced by common methods. Three unique CdS clones, D01, D07, and E01, were identified after grouping identical DNA sequences, and were represented 26, 6, and 4 times, respectively. The three sequences were translated and aligned with consensus IgG Fv domain sequences using IgG BLAST (*http://www.ncbi.nlm.nih.gov/igblast/*), and residues differing from the consensus were identified (Table 2.2). All three CdS clones were fragments of full-length scFvs,

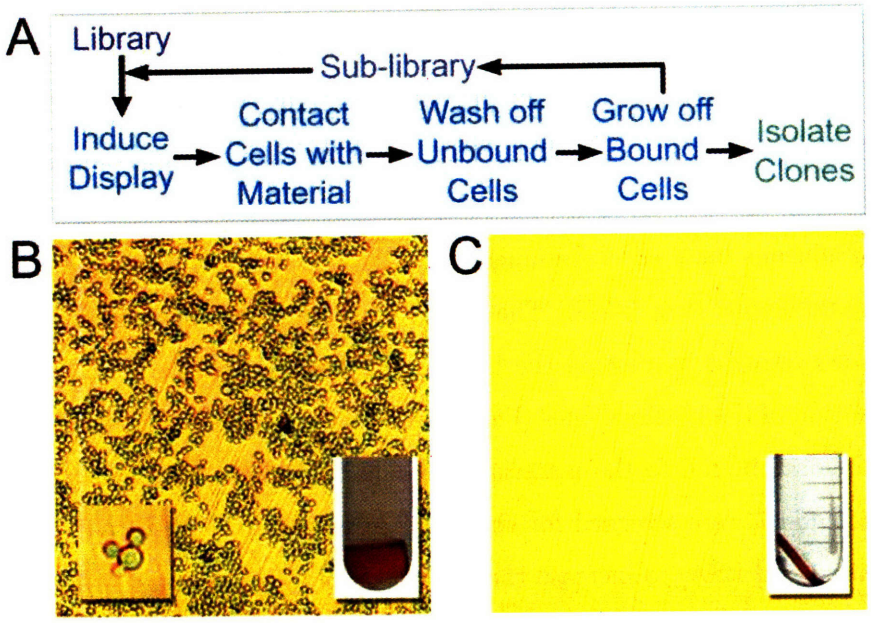

Figure 2-2: *Cell display panning method and library bound to CdS.* (A) General method used to identify material-specific yeast display library members that bind to a solid material surface. (B) Yeast library expressing surface-displayed scFv polypeptides bound to single crystal CdS during panning. (C) In contrast, the same yeast library grown in conditions that repress expression of the surface-displayed polypeptides exhibited zero background binding. Optical microscopy images show ca. 260 μm^2. Insets show a single budding yeast cell bound to CdS, and yeast cultures 24 h after the corresponding CdS crystals were incubated in SD, which allows the cells to detach from the material surfaces and grow.

Table 2.1: Summary of biopanning conditions

Round	Library used	Number of cells ($O.D._{600nm}$)[a]	Buffer[b] (Volume)	Screening Time (Hrs)
1	Naive scFv library	150	SG-BSA (50 mL)	24
2	Rnd. 1 sub-library	8	SG-BSA (8 mL)	24
3	Rnd. 2 sub-library	2	SG-BSA (4 mL)	6
4	Rnd. 3 sub-library	2	SG-BSA (4 mL)	2.25
5	Rnd. 4 sub-library	0.2	PBS-BSAT(0.1) (1.5 mL)	2.17
6	Rnd. 5 sub-library	0.1	PBS-BSAT(0.5) (1 mL)	1
7	Rnd. 6 sub-library	0.1	PBS-BSAT(0.5) (1 mL)	0.75

[a] 1 $O.D._{600nm}$ $\sim 2x10^7$cells.
[b] SG-BSA: SG media + 5 mg/ml PBS ;PBS-BSAT: 1xPBS + 5 mg/mL BSA + (v/v) % Tween20.

which upon analysis of DNA sequence appeared to have originated from frameshift mutations present in the natural antibody repertoire or introduced during PCR construction of the library. Feldhaus et al reported 68 % of the library to express the distal c-myc epitope [44], thus a maximum of about one-third of the library likely expresses scFv truncations. The resulting D01, D07, and E01 polypeptides are comprised of 47, 70, and 70 amino acids with 100, 91, and 90 % homology to class V_H6-1, V_H1-2, and V_H1-2 variable heavy chain domains, followed by 33, 13, and 13 amino acids, respectively, with no resemblance to the natural contiguous V_H sequences. The composition of the "frameshift amino acids was predominantly polar and charged residues, significantly enriched in histidine.

The DNAs corresponding to these clones were then transformed back into nave EBY100 yeast and clones were tested again for binding to CdS, to eliminate false positives due to host chromosomal mutations. All three CdS-binding sequences reconfirmed their original phenotype in a clonal verification binding assay (shown schematically in Fig. 2-3). The results are semi-quantitatively displayed in Fig. 2-4*A* as percent area coverage of the CdS surface (dark grey bars). The theoretical maximum for surface area coverage from the footprint of hexagonally packed perfect spheres was about 90.7 %. However, the yeast are not uniform, are randomly spaced, and lateral forces to move bound cells are insufficient to maximize their packing. The results show D01 covered 48 %, D07 covered 50 %, and E01 covered 40 % of the surface

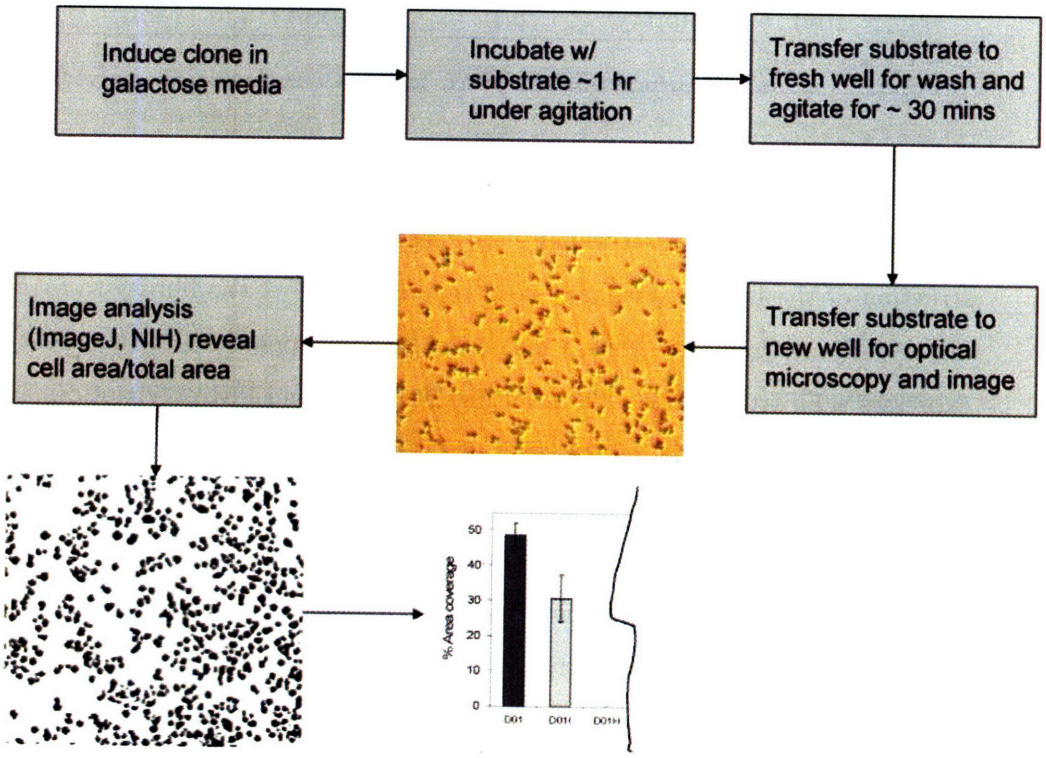

Figure 2-3: *Schematic of semi-quantitative cell binding assay.* See Experimental section 2.5.5 for details.

Table 2.2: Isolated CdS binding sequences and designed mutants

Clone	CDR1[a,b]	FRW2	CDR2[b]	FRW3[b]
D01	SNSAAWN	WIRQSPSRGLEWQG	**HDYRGHIHGHSQHGTEQP**	**DIRRHGRLLLCERCN***
D01I	SNSAAWN	WIRQSPSRGLEWQG	**HDYRGHIHGHSQHGTEQP**	**D***
D01H	SNSAAWN	WIRQSPSRGLEWQG	*	
D01pep[c]			**HDYRGHIHGHSQHGTEQP**	**D***
D07	GY**DL**H	WVRQAPGQGLEWMG	**R**INP**S**SGATNYAQ**R**FQG	RVTMTRDV**HHHGRHGAEHADI***
D07V	GY**DL**H	WVRQAPGQGLEWMG	**R**INP**S**SGATNYAQ**R**FQG	RVTMTRD*
D07R	GY**DL**H	WVRQAPGQGLEWMG	*	
D07pep[c]				DV**HHHGRHGAEHADI***
E01	**SYAIN**	WVRQAPGQGLEWMG	**R**INPNSGATNYAQ**R**FQG	RVTMTRDV**HHHGRHGAEQAEI***
E01V	**SYAIN**	WVRQAPGQGLEWMG	**R**INPNSGATNYAQ**R**FQG	RVTMTRD*
E01R	**SYAIN**	WVRQAPGQGLEWMG	*	
E01pep[c]				DV**HHHGRHGAEQAEI***

[a]Fused to FWR1 (not shown) followed by a -$(G_4S)_3$AS- linker at the C-terminus of Aga2.
[b]Residues in bold differ from contiguous V_H consensus sequences using IgBLAST.
[c]Fused directly to a -$(G_4S)_3$ASGGG- linker at the C-terminus of Aga2.

of the CdS. A previous calculation of adsorption, modeled as randomly placed disks on a surface, obtained a maximal surface coverage of 55 % [43]. Thus, D07 binding likely approaches the maximum surface coverage by a single monolayer of randomly adhered cells.

In this study, scFv fragments with C-terminal frameshift polypeptides were isolated over full-length scFvs despite their minority representation in the starting population (less than one-third) [44]. Not surprisingly, peptides were sufficient to mediate interaction with a flat material surface, as has been shown using peptides selected by phage display for a variety of materials [47, 156]. We hypothesize that since peptides have greater conformational freedom than the more structured scFv antibodies, there is a greater probability that a peptide will assume a configuration that results in an energetically favorable interaction with the flat crystalline surface. Panning a random peptide library displayed on the cell surface should serve to produce material specific peptides as well, complementary to phage panning, yet with ability to directly visualize binding and semi-quantitatively evaluate binding strength. We have created peptide libraries in yeast and are in the process of panning the library against

a variety of materials and will report results elsewhere.

We have also identified full-length clones from the scFv library by combining the panning method with alternating rounds of FACS, a powerful tool used extensively to screen this and other cell based libraries [34, 44], sorting for the presence of the C-terminal c-myc epitope tag. However, upon reconfirmation and comparison with our D01, D07, and E01 clones, these scFvs conferred a significantly lower adhesion ability, and therefore we focused our efforts on probing deeper into the mechanism of binding of the shorter polypeptide clones. This discrepancy between our identified scFvs and histidine-rich peptides may be explained by our results presented herein, which highlight the importance of sequence composition in determining binding strength.

2.3.2 Probing interfacial interactions between peptides and CdS

Peptides with inorganic material specificity have been reported previously [33, 156], however without a detailed study of the molecular basis of their surface interactions [55]. Characterization of the binding interactions between biomolecules and inorganic solid surfaces has proven difficult because many biochemical techniques to study binding phenomena require soluble or specially immobilized ligand/receptor pairs. By simple quantification of bound cell numbers, this system is amenable to identifying and further evaluating material specific polypeptide biomolecules. Here, we combine a semi-quantitative cell binding assay with genetic and biochemical manipulation to deduce peptide regions and specific amino acid side chains necessary for surface interaction with CdS.

First, truncation mutants derived from each CdS clone were genetically engineered (Table 2.2) and tested for binding to CdS (Fig. 2-4*A*) in order to determine regions necessary for binding. D01I, which removed only half of the C-terminal "frameshift amino acids from D01, bound to CdS. Removal of the entire frameshift region (clone D01H) abolished binding, which suggested that the frameshift region is necessary for mediating the yeast-material interaction. Similarly, D07V and E01V, which re-

moved all C-terminal frameshift amino acids from clones D07 and E01, respectively, did not show any ability to mediate CdS binding. As expected, further truncations that removed more of the antibody structure and C-terminal peptide region (D07R and E01R) did not exhibit ability to bind. Importantly, the expression levels of all clones were compared by immunofluorescent labeling of the proximal HA-epitope and flow cytometry [44], which showed no significant differences in expression. Thus we hypothesized that the short peptides attached at the C-terminus of the antibody framework fragments contributed much of the binding energy that held the yeast cells to the surface of CdS.

To test whether the peptides alone were sufficient to bind the yeast cells to the surface of CdS, we constructed Aga2 fusions of the peptides. Here the peptides were displayed without the antibody framework (Table 2.2), attached directly to the long flexible -$(G_4S)_3$AS- linker at the C-terminus of Aga2. These peptides were panned in parallel with the truncations and the original selected clones to determine relative binding efficiencies (Fig. 2-4*A*). Clones expressing D07pep were able to bind to CdS, clearly demonstrating the importance of the frameshift region in the original isolated D07 clone. E01pep and D01pep also repeatedly showed detectable binding, albeit at significantly lower adhesion strength even though their expression levels were similar to their parent clones and to D07pep. The decreased surface coverage of yeast expressing the peptides compared to the parent sequences suggested that the antibody framework may provide structural stability and thereby display the histidine rich peptides in a more optimal context.

These results also demonstrated that E01pep was a significantly weaker binder than D07pep, which was surprising since the peptides differed by only 2 of 15 amino acid residues (DVHHHGRHGAE[Q/H]A[D/E]I) with one change being conservative [D/E]. Under less stringent buffer conditions, the binding ability of E01pep improved, but remained significantly below D07pep. Again measured by flow cytometry, the two fusions were expressed at equivalent levels. Thus, the observed weakened binding of E01pep was hypothesized to result at least in part from the loss of histidine at position Q12, which was explored later in this report.

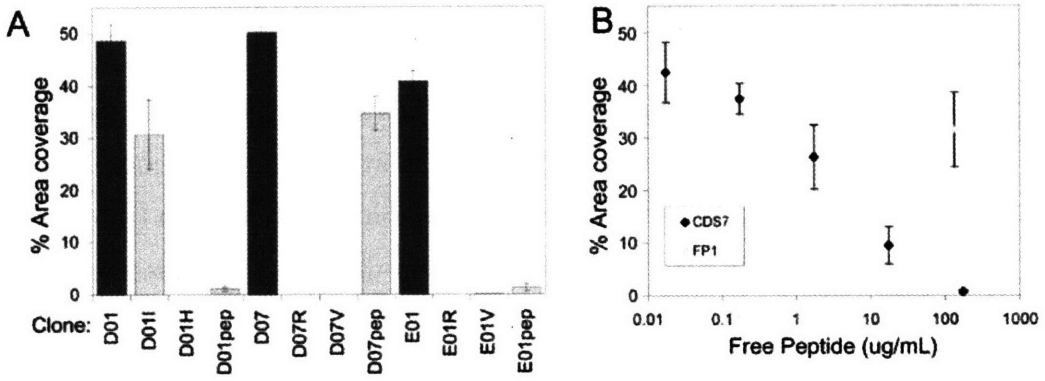

Figure 2-4: *Cell binding to CdS and competition with soluble peptides.* (A) Percent surface area covered by cells was calculated from images of isolated clones and engineered mutants (Table 2.2) bound to CdS. Parent clones (dark grey), mutants (light grey). (B) Binding of clone D07pep to CdS in the presence of soluble peptide CDS7 (derived from D07pep) or control peptide reported to bind FePt, FP1. See text for experimental details. All values listed are geometric averages from > 3 independent experiments $\pm$ std. error of the mean.

In order to test the off-yeast binding capability of the identified peptide sequences, competition studies with synthetic peptides CDS7 (n-GDVHHHGRHGAEHADI-c), corresponding to the sequence of D07pep, and FP1 (n-HNKHLPSTQPLA-c), identified by phage display to bind FePt [124], as a control, were performed against the binding of parent clone D07pep. The percent area coverage of CdS surfaces was used as a semi-quantitative metric for cell binding in the presence of the soluble peptides (Fig. 2-4*B*). Increasing concentrations of CDS7 from 17.45 ng/mL-174.5 μg/mL resulted in decreased binding of yeast clone D07pep to CdS up to 77 %. Further, 174.5 μg/mL CDS7 almost completely abolished binding (98 % calculated reduction) in contrast to an equimolar concentration of FP1 (134.3 μg/mL), which decreased binding by only 24 %. Thus, soluble CDS7 was able to effectively inhibit binding of clone D07pep with an estimated half-maximal inhibition achieved with ca. 3.5 μg/mL (2 μM) soluble peptide. This value should not be mistaken for an equilibrium dissociation constant (K_D) in a bimolecular reaction between CdS and the soluble peptide. The assayed phenomena were complex, with soluble peptide competing against a polyvalent bound cell for the solid surface of CdS. The half-maximal inhibition con-

centration of 2 μM may serve as a conservative upper-limit to a K_D value since it a concentration greater than the actual K_D of soluble peptide binding is expected to be necessary to overcome the avidity of the cell/material interaction.

Since relatively small peptide regions were shown to be both necessary and sufficient to cause binding between cell and material, a more detailed mutational analysis was performed within the peptide to arrive at residue level binding information. Selective alanine mutagenesis was performed on polar/charged residues along D07pep (Fig. 2-5*A*) and screened for binding against CdS (Fig. 2-5*B*). The polar/charged residues were chosen as a first order guess as to those responsible for the interaction. The Asp14 (D14) residue was not mutated due to a similar mutation in the clone E01pep. The non-polar residues may be important for spacing and/or structural specificity, which will be tested in future studies. Binding studies revealed that the histidine residues were those mainly responsible for binding since mutation of each individually to alanine substantially reduced the binding capacity of the peptide (Fig. 2-5*B*) without affecting expression level (data not shown). The binding levels of these histidine to alanine mutants correlated with that of E01pep (Fig. 2-4*A*), which also lacks one histidine compared to D07pep. These results suggested that binding interaction was one in which the histidine imidazole groups coordinate with cadmium on the crystal surface. Other work has demonstrated the importance of histidine for binding metal clusters and assembling inorganic materials [8, 138]. Because each histidine removal individually resulted in almost complete elimination of yeast binding under the conditions described, it further suggested that binding resulted from cooperative interaction of the five histidines on one or more ion in the CdS crystal. The four histidines remaining in the alanine scanning mutants, regardless of position, were not sufficient to reconstitute full binding under the assay conditions used.

Interestingly, mutation of the positively charged arginine (R07A) had a less dramatic decrease on the binding capacity and removal of the negatively charged aspartate (D01A) and glutamate (E11A) slightly improved binding. These results suggested a role of arginine in contributing to and of acidic side chains in down-modulating binding of these peptides to CdS, and that further random mutagenesis

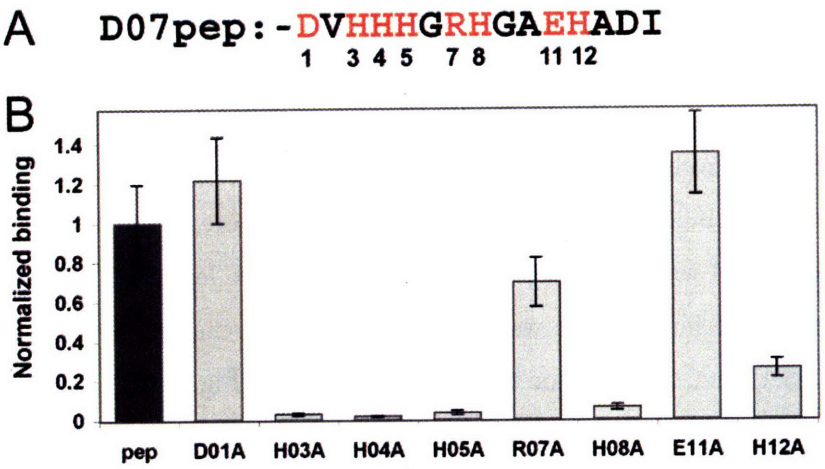

Figure 2-5: *Cell binding to CdS for engineered alanine scan mutants.* (A) The sequence on clone D07pep is shown with positions changed to alanine highlighted in red. Each mutation was made individually to result in eight variants of D07pep. (B) Binding of each alanine mutant clone to CdS is expressed as the percentage of the CdS surface covered by cells. See text for experimental details. All values listed are geometric averages from > 3 independent experiments $\pm$ std. error of the mean.

and rounds of selection may lead to identification of peptide variants with increased binding strength and/or specificity to materials. Instead, we chose an engineered approach to better understand the nature of these peptide-CdS interactions.

To examine further the role of histidine in binding to the CdS surface, we genetically engineered a series of yeast clones to express hexa-, penta-, tetra-, and trihistidine peptides as Aga2 fusions. Similar peptides expressed by cells have been used to chelate heavy metals free in solution [80, 140], but not to bind cells to the solid-material surfaces. Here we contacted our series of polyhistidine displaying clones with CdS and compared binding using our cell coverage assay (Fig. 2-6). Results clearly demonstrated histidine to be sufficient to mediate cell binding, and the number of histidines to be directly related to cell binding ability. Analysis of other reports showed that histidine appears in almost all CdS/ZnS selected peptides [47], FePt selected peptides [124], and iron oxide adhering polypeptides [22], however, peptides binding other material surfaces need not contain histidine [22, 23, 146, 156], suggesting an importance for a wider variety of side chains or motifs. Further, detailed study on

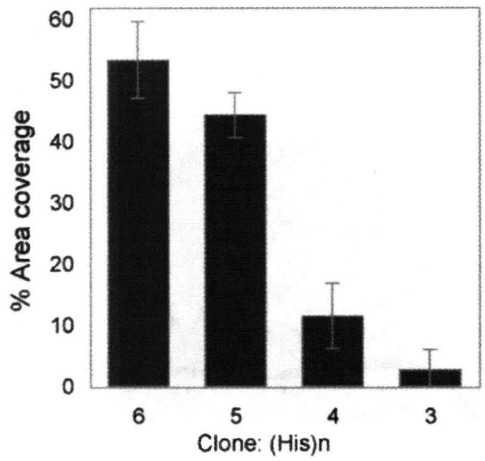

Figure 2-6: *Cell binding to CdS for displayed polyhistidine peptides.* Sequences were engineered with 6, 5, 4, or 3 histidines and displayed by yeast as fusions to Aga2. Binding of each clone was evaluated with the cell coverage assay. All values listed are geometric averages from 2 independent experiments ± std. deviation.

the basis of GaAs (100) binding over Si (100) highlighted the need to understand relationships between chemical composition and spatial structure in elucidating the basis of adhesion specificity [51]. Our current studies are aimed at elucidating the role of other amino acid side chains in modulation of material specific interactions.

2.3.3 Materials applications of cell display

Yeast displaying scFvs and fragments were used to demonstrate potential application of cell-material specific interactions (Fig. 2-7). CdS clone D07 was contacted with the CdS surface forming a multi-layer living coating, or biofilm, that was able to grow into regions cleared by disturbance, thus was self-healing (Fig. 2-7*A*). Even after over three weeks in SG, when the biofilm was removed by application of fluidic sheer, the bottom layer of cells remained bound to CdS and able to regenerate into a complete coating. Selected peptides transposed to other cell types such as pseudomonas might be useful as self-healing biofilms for corrosion prevention, bioremediation, medical [79], or other applications [125].

We also demonstrated use of the selected clones to aid in detection and identifica-

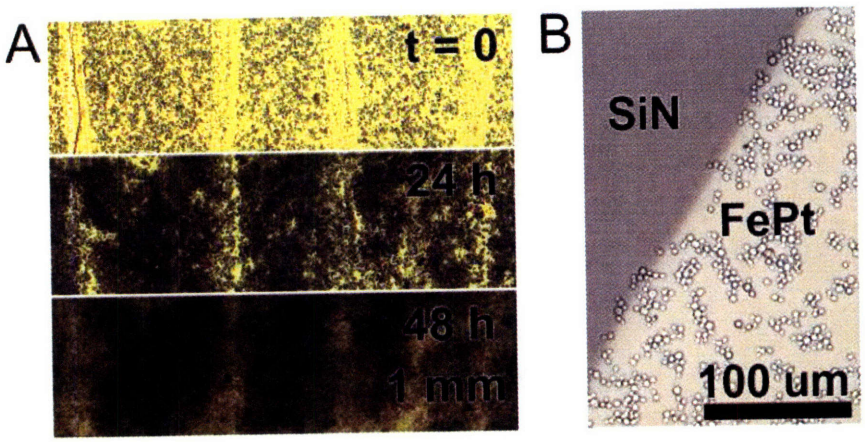

Figure 2-7: *Applications of yeast displaying novel material interacting polypeptides.* A selected portion of bound cells expressing CdS clone D01 were cleared from the surface of CdS at t = 0. After 24 h growth, cells were observed to bind to the cleared areas and by 48 h, the biofilm completely self-healed. (B) Labeling of a metal-insulator heterostructure with material specific yeast. An isolated FePt-clone binds selectively to FePt over SiN and SiO_2. Scale bars shown.

tion of regions of a surface with particular compositions. For example, we used a FePt binding clone to detect FePt over SiN/SiO_2, as seen using light microscopy by cells covering the region of the heterostructure containing of Fe and Pt, and not on the Si containing region (Fig. 2-7*B*). Similarly phage and bacterial displayed polypeptides have shown specificity between material types [146, 156], using fluorescence based imaging.

The utility of these selected biomolecules is not limited to display on yeast cells. It is of interest to display such material binding polypeptides on other eukaryotic cell types to mediate cell-material interaction. For example, current methods used to attach neurons or engineered cells to electrodes require exogenous adhesion molecules and results in imprecise cell localization [31, 141]. Material-specific polypeptides, displayed by human neurons, may enable direct attachment to an Au electrode, or other device, resulting in a direct interface between cell and device. These and similar biomolecular bridges may be used in implants, tissue engineering scaffolds, biosensors, medical diagnostics and therapeutics.

2.3.4 Application of biomolecules for material assembly

To further demonstrate the versatility of isolated material specific reagents identified with our system, we used CDS7 peptide to assemble fluorescent semiconductor nanoparticles in aqueous solution at room temperature (Fig. 2-8). In brief, aqueous $CdCl_2$ was added to various concentrations of CDS7 peptide dissolved in water and incubated at room temperature. Subsequently, aqueous Na_2S was added dropwise until equimolar concentration with $CdCl_2$ was reached. Fluorescence ranging from blue-green to yellow was immediately observed upon exposure of the CDS7 nanoparticle solutions to a UV source, examples of which are shown in Fig. 2-8*A*. The broad fluorescence emission above the band-edge wavelength was thought to originate from many surface-state hole-pair recombinations, which can dominate emission as nanoparticle size decreases and surface area/volume ratio increases. The nanoparticles were then characterized by TEM (Fig. 2-8*B*), which showed relatively uniform particles with an average diameter of ca. 3.2 nm for 1:10 molar ratio of CDS7 peptide: salts. Although nanoparticles were seen with both peptides, the CdS-specific peptide produced nanoparticles with significantly better optical properties over the FP1 control across a broad range of concentrations, as shown in Fig. 2-8*A*. Here, even the control peptide may serve to lower the activation energy of nucleation such that many nucleation sites compete for limited precursor salts. Tuning of growth conditions of the peptide-mediated process and/or changing the peptide sequence may lead to quantum dots with characteristics resembling current commercialized organic high-temperature methods.

The inherent bioconjugation ability of aqueous peptide grown nanoparticles may be attractive for many emerging quantum dot biotechnologies [117]. In addition, engineered cells, especially yeast, can function as biomolecular factories for proteins and peptides [29, 126]. It may be possible to couple this synthesis potential of cells to the production of high value materials using material-specific biomolecules to direct the assembly of the materials.

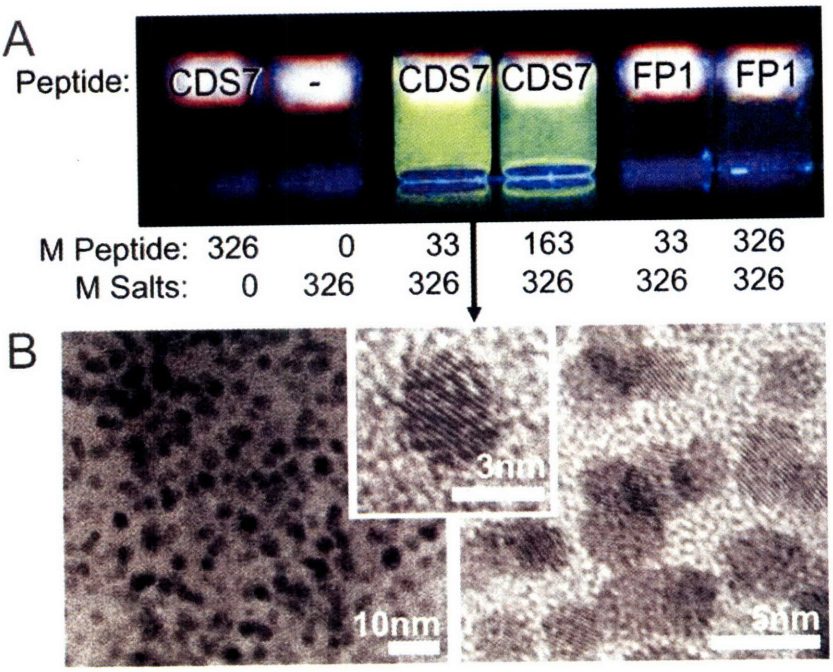

Figure 2-8: *Fluorescent nanoparticles assembled by material-specific peptides.* (A) Solutions of CdS nanoparticles were formed at room temperature in aqueous conditions by mixing material specific peptides with aqueous solutions of $CdCl_2$ then Na_2S. Intense fluorescence was observed from the CDS7 peptide mixed with the metal salts (center), but not from control solutions with CDS7 peptide alone or the metal salts alone (left). The FP1 peptide mixed with the metal salts (right) only resulted in marginal fluorescence. The samples shown were representative of near-optimal fluorescence achieved across a broader range of concentrations. (B) TEM image of CdS nanoparticles from solution indicated by arrow. Lattice images were visible indicating crystalline structure of the nanoparticles with average diameter of 3-4 nm.

2.4 Conclusions

We have shown that contacting yeast-displayed peptides, site-directed mutants, and engineered peptides leads to semi-quantitatively different, reproducible cell coverages. Using this yeast display platform, we found that binding strength to CdS was directly proportional to the number of histidines present in displayed peptides and influenced by neighboring residues. We also demonstrated the importance of peptide sequence in aqueous, room-temperature synthesis of fluorescent semiconductor nanoparticles. The next chapter focuses on further insights into peptide interfacial interactions to enable development of a complete set of design rules for engineering novel material-specific biomolecules.

2.5 Experimental

2.5.1 Yeast strain and library

S. cerevisiae engineered to display a human repertoire single chain antibody (scFv) library [44] was maintained as previously described [20]. The scFvs fused to the C-terminus of Aga2 are encoded on 2-micron plasmids downstream of a Gal-based promoter, and maintained in yeast strain EBY100 which has Aga1 under control of a Gal-based promoter integrated in its genome [20].

2.5.2 Materials

Polished single crystal CdS, A-plate (Cleveland Crystal) and FePt thin film on SiN wafer (gift of T. Thomson, IBM, Almaden, CA) were cleaned by brief aqueous sonication in a bath sonicator (Fisher Scientific), rinsed in 70 % ethanol and stored dry.

2.5.3 Panning procedure

In general, selection was carried out by exposing the material to a culture of induced yeast cells in synthetic dropout media supplemented with galactose (SG) [20] or phosphate buffered saline (PBS) based buffers, washing the material in fresh buffer for 1 h, then rescuing bound cells by growing cells off the material in synthetic dropout media supplemented with glucose (SD) [20]. Panning rounds d1-d7 were performed at RT under the following conditions. Round d1: 150 OD cells in 75 mL SG + 5 mg/mL Bovine serum albumin (SG-BSA), 24 h incubation; d2: 8 OD cells in 8 mL SG-BSA, 24 h incubation; d3: 2 OD cells in 4 mL SG-BSA, 6 h incubation; d4: 2 OD cells in 4 mL SG-BSA, 2.25 h incubation; d5: 0.2 OD cells in 1.5 mL PBS + 5 mg/mL BSA + 0.1 % tween20 (PBS-BSAT), 2 h incubation; d6: 0.1 OD cells in 1 mL PBS-BSAT, 1 h incubation; d7: 0.1 OD cells in 1 mL PBS-BSAT, 45 min incubation.

2.5.4 Genetic engineering of mutants

Truncation mutants of selected scFv clones and Alanine scan mutants of D07pep were constructed using Quickchange mutagenesis (Stratagene) to add stop codons or change codons to alanine at the desired locations, using plasmid DNA isolated from clones D01, D07, and E01 as templates. Mutants corresponding to distal frameshift peptides lacking the V_H regions were cloned by generating dsDNA inserts from oligonucleotides for D01pep (5' CCCGGGGCTAGCGGTGGCGGCCATGATTACA-GAGGTCATATTCATGGTCATTCTCAACATGGTACTGAACAACCAGATTAGG ATCCGATCAG 3'), D07pep (5' CCCGGGGCTAGCGGTGGCGGCGATGTTCAT-CATCATGGTAGACATGGTGCTGAACATGCTGATATTTAGGATCCGATCAG 3'), and E01pep (5' CCCGGGGCTAGCGGTGGCGGCGATGTTCATCATCATGGTA-GACATGGTGCTGAACAAGCTGAAATTTAGGATCCGATCAG 3') annealed to a primer (5' ATCCCGGGGCTAGCGGTGGCGGC 3') using Expand Enzyme (Roche Diagnostics). Inserts digested *NheI/BamHI* were cloned into *NheI/BamHI* digested pCTCON, resulting in fusion of the peptides at the end of a $(G_4S)_3$ flexible linker in the same context as the scFvs. Similarly, polyhistidine clones were engineered by

annealing oligonucleotides to create ligatable sticky ends and inserting the dsDNA directly into digested vector. Sequenced plasmid DNAs harboring these cloned mutants and peptides were transformed into EBY100 using the Geitz transformation kit (Tetralink).

2.5.5 Cell Binding Assay

Cells transformed with plasmid DNA including truncation, peptide, and alanine scan mutants, were grown to mid-log phase in SD at 30 ^{o}C then induced in SG for 18 to 24 h at RT. 2 OD_{600} units of cells were resuspended in 1.5 mL SG-BSAT in 2 mL microcentrifuge tubes. 0.5 cm^2 CdS was placed into each clone culture and rocked 1 h, washed in SG-BSAT in new tubes for 30 min, and imaged by optical microscopy in 6-well culture plates. Digital images were collected with AxioCam MR on a Axioplan optical microscope (Carl Zeiss), and percent area coverage was measured using ImageJ v1.3 developed by Wayne Rasband, NIH. Briefly, images were thesholded to define cell vs. background areas, and the ratio of cell area to total image area was calculated. Values for each clone were derived from 675 μm x 535 μm areas and averaged from 3 images taken from each of 2-4 independent experiments.

Competition assay with soluble peptide. CdS was contacted with clone D07pep, as described in the clonal verification binding assay, in the presence of soluble synthetic peptides CDS7 (n-GDVHHHGRHGAEHADI-c) and FP1 (n-HNKHLPSTQPLA-c) (MIT Biopolymers). CDS7 peptide is the same sequence expressed as a fusion by clone D07pep. FP1, selected by phage display to bind FePt, was used as a control. 10X solutions of peptide in water were added to final concentrations ranging from 17.45 ng/mL-174.5 μg/mL (0.01-100 μM) during binding and wash steps. Cell binding was measured as described above.

2.5.6 Biofilms

On CdS: A 0.5 cm^2 polished CdS single crystal was incubated with 1 OD_{600} / mL pre-induced clone D07 for 1 h at RT on a rocker. The CdS was then placed into a

6-well plate with fresh SG-BSAT. A pattern of cells was cleared from the surface using a pipette tip and 5X images taken at t = 0, 24, and 48 h. On FePt: FePt binding clone (Aga2-linker-QVQLVKSEAEVKEPGASVKVSCKASGYTFTGHYMHWLRHAPGQ GLEWMGRFNPYSDKLCTEVSGQGHHDRGHVHQNSLHGAEKAEI) was contacted with the FePt/SiN wafer hetero-surface under identical conditions used in CdS binding assays.

2.5.7 Nanoparticle assembly and TEM

RT aqueous $CdCl_2$ (5.05 mM; 37 μL) was added dropwise to a stirring solution of peptide in H_2O (37.4, 187, or 374 mM; 500 μL) and equilibrated 12 h at RT. Then Na_2S solution (5.05 mM; 37 μL) was added to the vigorously stirring peptide/cadmium solution and stirred 1 h at RT before characterization. Particles in solution were exposed to long wavelength UV light and imaged with a digital camera (Sony). 10 μL of sample was dropped onto a copper-coated carbon grid and dried in a vacuum desiccator then imaged by TEM using a JOEL 2010 electron microscope.

Chapter 3

Compositional Influence on Binding Specificity Studied with Rationally Designed Peptides

3.1 Summary

This chapter reports on a systematic study of peptide sequence-activity relationships for II-VI semiconductor (CdS, CdSe, ZnS, ZnSe) and Au binding using a yeast surface display system and define criteria for tuning peptide affinity and specificity for these material surfaces. First, homo-hexapeptides of the 20 naturally occurring amino acids were engineered, expressed on yeast surface, and assayed for the ability to bind a material surface in order to define functional groups sufficient for binding. Histidine (H_6) was able to mediate binding of yeast to the five materials studied while tryptophan (W_6), cysteine (C_6), and methionine (M_6) exhibited different levels of binding to single crystalline ZnS and ZnSe and polycrystalline Au surfaces. The ability of neighboring amino acids to up- and down-modulate histidine binding was then evaluated using interdigitated peptides (X-H-X-H-X-H-X). While the 20 amino acids exhibited a unique fingerprint of modulation for each material, some general trends emerged. With neutral defined by alanine, up-modulation occurred with glycine, basic amino acids, and the previously defined binding amino acids histidine, tryptophan, cysteine and methionine, and down-modulation generally occurred with acidic, polar, and hydrophobic residues. We conclude that certain amino acids directly bind the material surface while neighboring amino acids locally modulate the binding environment for the materials we studied. Finally, by employing the compositional and spatial criteria developed herein, it was possible to predictively design peptide sequences with material specificity including a multi-material binder, a Au-specific binder, and a ZnS-specific binder, that were verified as such in the context of yeast display.

3.2 Introduction

Published reports on selected peptides have provided preliminary insights as to how selected peptides may interact with materials [24, 30, 78, 122, 146], but general principles relating chemical composition and spatial arrangement to interfacial function and specificity are needed [51, 55]. The aim of this chapter is to develop principles

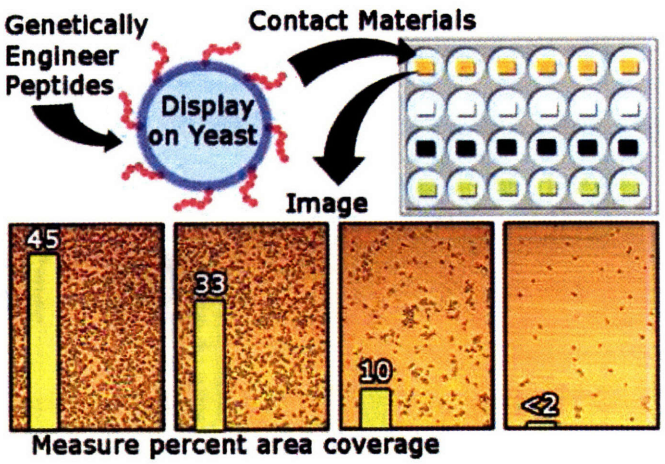

Figure 3-1: *Workflow of assaying designed peptide-mediated binding to solid material surfaces using yeast display.*

governing the peptide-inorganic material interaction at the level of amino acid functional groups, focusing on II-VI semiconductors CdS, CdSe, ZnS, and ZnSe and Au. Work presented in the previous chapter on selected peptides binding CdS suggested that composition and context primarily determine the relative strength of peptide binding to material surfaces. Herein we broaden the scope and potential applicability of our findings through experiments directed at answering the following questions: 1) Which amino acid functional groups are sufficient for binding short peptides to these five inorganic material surfaces? 2) How do neighboring amino acid functional groups and their spatial arrangement in a peptide sequence modulate binding strength? 3) Can our results be used to predictively design peptides specific for these different material surfaces?

To answer these questions, compositionally simple peptides were genetically engineered, displayed on the surface of yeast, and rapidly evaluated for binding to the inorganic material surfaces using a cell-based system (Fig. 3-1) modified for higher throughput and sensitivity from previous methods [122]. Four II-VI semiconductors, single crystalline CdS, CdSe, ZnS, and ZnSe, and a poly-crystalline Au film were chosen due to their importance in optical and electronic applications, and because closely related materials presented the greatest challenge for engineering material specificity.

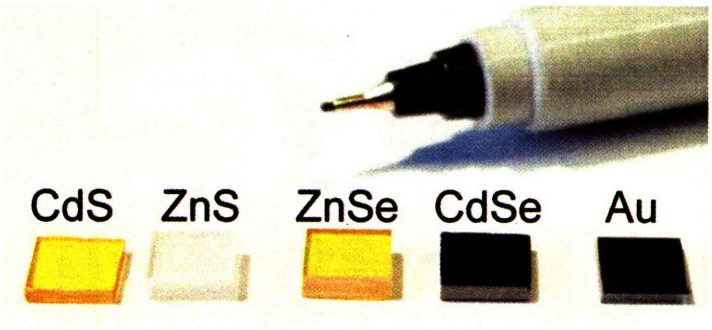

Figure 3-2: *Image of respresentative II-VI and Au substrates used in this study.* Each substrate is approximately 0.5 x 0.6 cm.

Through systematic study we defined a hierarchal set of compositional and spatial parameters for binding, which enabled predictive-based design of material-specific peptides. Further these principles were applied to understanding reported sequence-activity relationships of genetically selected material binding peptides.

3.3 Results and Discussion

3.3.1 Homopeptdies reveal residues sufficient for binding

First we were interested in determining the minimal amino acid[1] compositional diversity sufficient to constitute peptide-inorganic material interactions. Genetically engineered peptides consisting of each of the 20 natural amino acids were displayed as homo-hexamers on the surface of yeast as fusions to Aga2 and individually contacted with a panel of inorganic materials, including CdS, CdSe, ZnS, ZnSe, and Au following scheme in Figure 3-1. The materials represent 4 semiconductors (CdS/CdSe; wurtzite, ZnS/ZnSe; zinc-blend) and a metal (Au), chosen to potentially find principles dependent upon material properties. Figure 3-2 shows representative substrates used in this study. The relative binding affinities of each amino acid versus each material were measured using our previously developed semi-quantitative cell-based

[1]Amino Acids. Key- A: alanine, C: cysteine, D: aspartate, E: glutamate, F: phenylalanine, G: glycine, H: histidine, I: isoleucine, K: lysine, L: leucine, M: methionine, N: asparagine, P: proline, Q: glutamine, R: arginine, S: serine, T: threonine, V: valine, W: tryptophan, Y: tyrosine.

binding assay [122], which was based on the percentage surface area covered by bound individual and budding yeast cell bodies. In the plate format used herein, values for cell area coverages ranged from zero to an average maximum of ca. 35 %. All peptides expressed well on the yeast surface as measured by immunostaining and flow cytometry and did not promote yeast aggregation (data not shown). The results presented in Figure 3-3 clearly show that homo-hexamers composed of residues containing side chain functional groups with an aromatic secondary nitrogen, (H, W), or a sulfur, (C, M), were sufficient for binding to the materials under study. Interactions of (H), (C), and (M) with heavy metals and materials are well known [70, 91]. However, direct binding by (W) alone was surprising, even though it was reported to be enriched in genetically selected metal oxide binders [146]. Other amino acids with known metal coordination capabilities [91] (E, D, Y, S, T, K, R) were unable to confer binding when displayed individually in our system. Interestingly, (H) bound all five materials, yet (C), (M), and (W) exhibited selectivity. This implied that peptides with (H) would be the most promiscuous, that is unless additional compositional, spatial, or structural constraints were added that enabled discrimination between materials. We explored compositional and spatial constraints later in this report.

All peptides identified through genetic selection against Au, CdS, and ZnS in published reports and earlier work were found to contain residues that bound as homo-hexamers: 10 of 10 Au-selected peptides [24, 139] have (H, C, M, or W), 5 of 6 CdS-selected peptides [47, 122] have (H) and the other has a (W), and 9 of 9 ZnS-selected peptides [47] have (H) and/or (M). In addition, 37 reported peptides selected for a wide variety of other materials (PbS [47]; Fe_2O_3 [22]; FePt [124]; ZnO [78]; MnO_2 [129]; Zeolites [112]; SiO_2 [106]; $CaCO_3$ citegaskin2000-1211) all contained at least one (H, C, M, or W) residue. However, other selections against materials (GaAs [156]; ZnO [146]; Cu_2O [146]; Cr_2O_3 [129]; CoO [129]; PbO_2 [129]) resulted in a minority of peptides (12 of 40) that did *not* contain these residues. Therefore, although selected peptides are enriched in the binding residues found in this study, this analysis suggested that other amino acids or combinations thereof may be capable of binding to material surfaces. Interestingly, the motifs (RR), (PR), or (RP) are

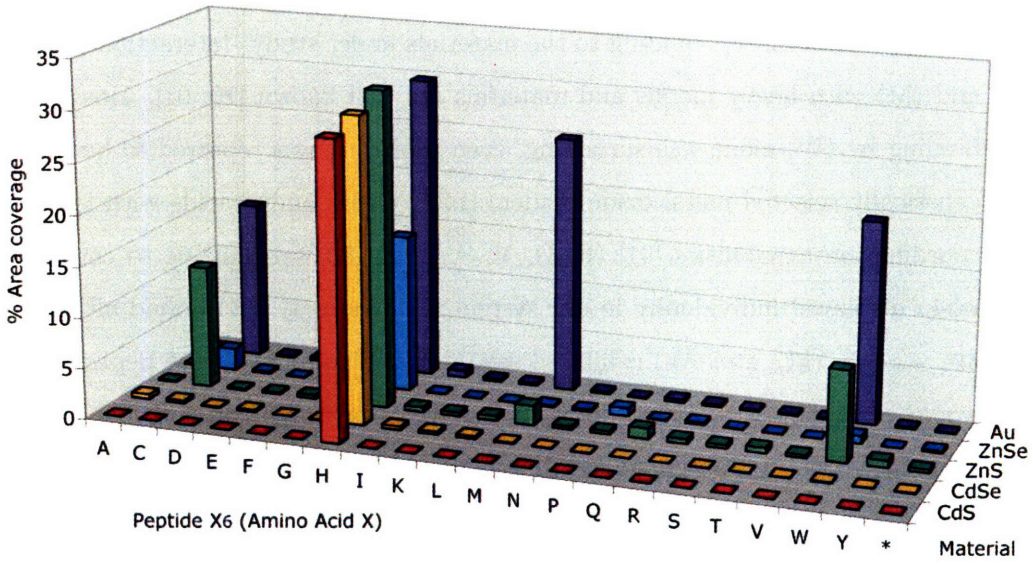

Figure 3-3: *Compositional specificity with X6 peptides.* Each of the 20 natural amino acids was tested for binding to five inorganic materials- single crystalline CdS, CdSe, ZnS, and ZnSe and poly-crystalline Au film. The peptides were displayed as homo-hexamers on the surface of yeast as fusions to Aga2 and contacted with each solid material. Binding of each clone was expressed as the percentage of the material surface covered by cells averaged from > 3 independent experiments. For each average value shown, $\pm$ std error of the mean was less than one quarter of the bar height. No peptide control (*). See text for experimental details.

present in 6 of the 9 phage or bacterial selected metal oxide binders that lack (H) and (W). Whether these and other motifs are sufficient for binding in our system is currently under study. Mechanistically, binding may depend on the relationship between the material-specific electronegativity and the acidity of the peptide side chains, as proposed by Goede and coworkers[51], or by matching electrostatic attractions with lattice spacing parameters, although apparently not the case for one unconstrained peptide studied[51].

3.3.2 Modulation of binding strength with neighboring amino acids

Since genetically selected peptides are diverse in overall composition and exhibit variable binding characteristics, we were motivated to understand the potential roles of individual amino acids in contributing to material specificity and/or binding affinity. Our experimental approach was to identify and evaluate residues that modulated the binding strength of a known binding residue. Since hexa-histidine bound all five materials, we used (H) as a common binding residue to enable comparisons across these materials. Interdigitated peptides, of the general form XHXHXHX (X = one of the 20 natural amino acids), were genetically engineered for display on the surface of yeast and measured to express equally well [119].

The 20 interdigitated amino acids were ranked by their ability to influence binding of the three (H)s to CdS, ZnS, and Au, and results were normalized to AHAHAHA in Figure 3-4. In our cell-binding assay, binding of AHAHAHA was intermediary in comparison to the other 19 clones for all materials but relatively low in absolute terms for CdS and Au (Percent area coverages- CdS; 4 $\pm$ 2.1, ZnS; 18 $\pm$ 2.5, Au; 4.5 $\pm$ 1.7). Clearly, neighboring residues had significant effects on adhesion; Results show that in general (K) and (W) up-modulated relative to (A) and acidic and hydrophobic residues without a nitrogen tended to down-modulate binding relative to (A), which has only a methyl side chain. Side chains with oxygen as hydroxyl and carboxyl functional groups– although important in chelating soluble metals[91]– were

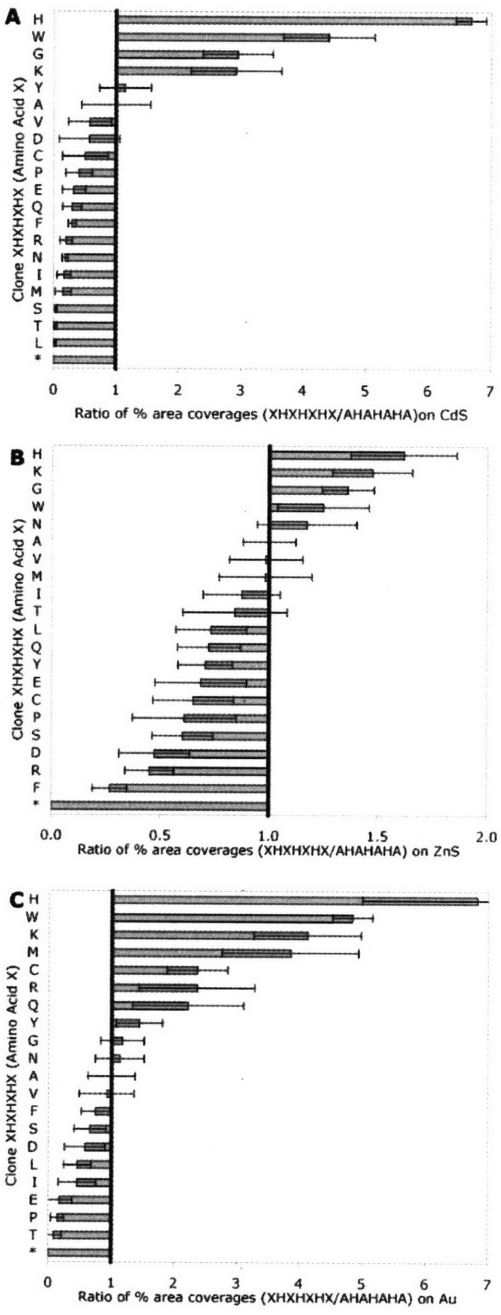

Figure 3-4: *Contextual influence on binding strength.* Up- and down-modulation of histidine binding by all other amino acids versus alanine was evaluated using interdigitated hexapeptides (XHXHXHX, X = one amino acid per clone) displayed on yeast, for (A) single crystalline CdS, (B) single crystalline ZnS, and (C) poly-crystalline Au film. Values shown represent the percent area coverage for each clone normalized to the percent area coverage of AHAHAHA for CdS (4 ± 2.1), ZnS (18 ± 2.5), Au (4.5 ± 1.7) $\pm$ std error of the mean for ≥ 3 independent experiments. No peptide control (*).

also down-modulators in the context of cell display, which correlated with statistical studies[146] and the inability to bind in homo-hexamer form (Fig. 3-3). Yet each material had different modulation fingerprints, which were exploited later in this report to design material-specific peptides. Spatial positioning effects on the modulation of histidine binding to CdS, ZnS, and Au were studied using two approaches. In the first, interdigitated clones from Figure 3-4 (XHXHXHX) were compared with heptamers of identical composition but rearranged sequence (XXHHHXX). Results showed that the order of (G) or (E) had negligible effects on binding of the three (H)s within statistical error for materials CdS, ZnS, and Au (Fig. 3-5). However, a statistically significant difference was observed with placement of (R) residues: RRHHHRR > RHRHRHR. Whether these observations are yeast display system-dependent or related to proposed arginine-rich motif-based effects on binding [78, 146] is uncertain.

In the second approach, a spacer residue (G) was added between paired (E)'s flanking three (H)'s in a series of peptides of the formula (EEG_nHHHG_nEE, where n = 0-3). From Figure 3-4, (E) was seen to down-modulate binding relative to (G). Spatially separating (E) from (H) improved binding sequentially for the materials tested: CdS, ZnS, and Au (Fig. 3-6). In fact, binding increased almost linearly with the number of (G)'s added, until binding was roughly equivalent to GGHHHGG binding to CdS (at n = 2) and ZnS (at n = 3). Trends for Au were the same, yet at n = 3 binding was still significantly below GGHHHGG possibly due to (E)'s apparently greatest aversion to Au. Extrapolation of these results implies that contributions of individual modulating residues are locally restricted in unconstrained peptides, likely due to peptide deformation upon interaction with solid material surfaces [105]. Further, peptide affinity apparently improved with increased peptide conformational flexibility since (G) > (A) > (P) was seen in Figure 3-4. Conversely, material specificity may be improved by adding structural constraints that promote formation of favorable bond angles with specific lattice parameters. Taken together, in general, the binding of unconstrained peptides to these inorganic surfaces required certain binding residues, which were significantly modulated by spatially proximal functional groups.

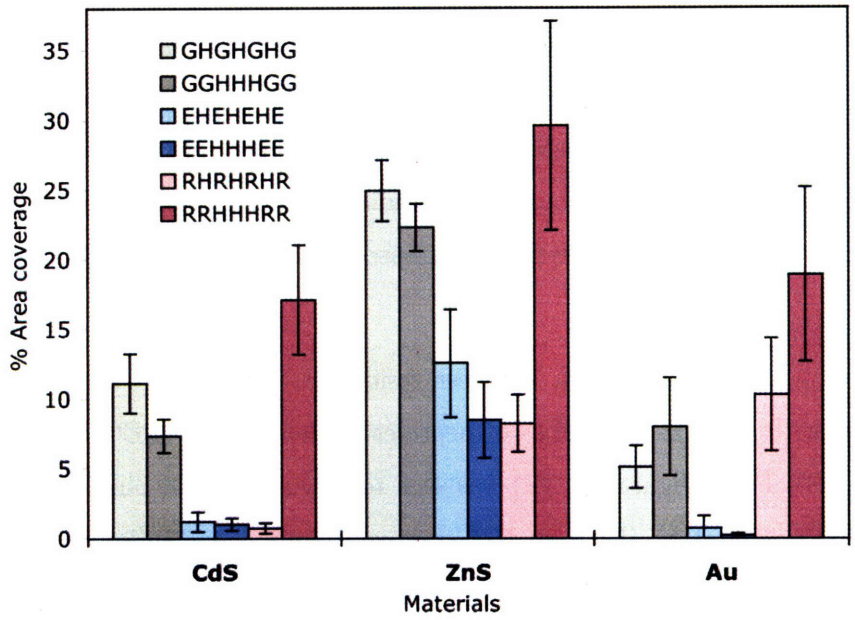

Figure 3-5: *Influence of primary sequence on modulation of histidine binding.* The influence of spatial positioning on peptide-mediated binding was studied by creating variants of identical chemical composition but varied sequential order. Interdigitated peptides (XHXHXHX) and flanking peptides (XXHHHXX), where X = (E, G, or R), were displayed on yeast as Aga2 fusions. Binding of clones to CdS, ZnS and Au was measured as a percentage of the material surface covered by cells, averaged from 3 independent experiments ± std error of the mean.

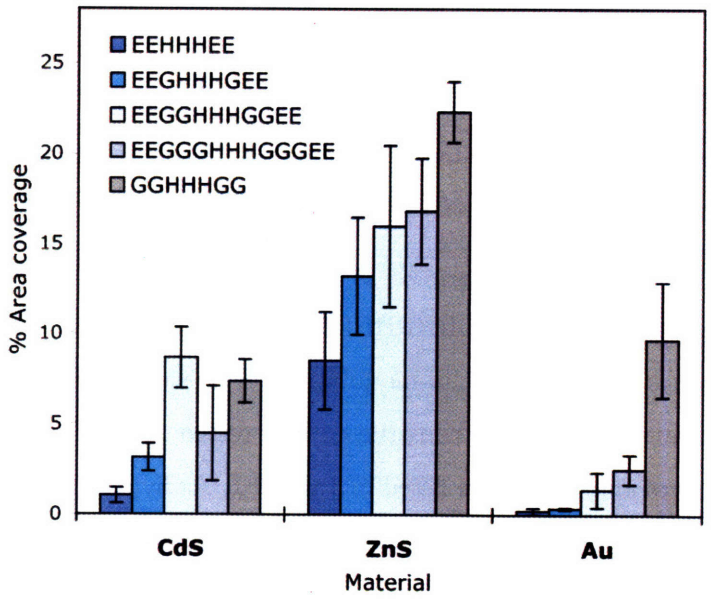

Figure 3-6: *Spatial separation effects on the modulation of histidine binding.* The down-modulation of histidine (H) binding by glutamate (E) was evaluated as a function of sequential proximity using glycine (G) as a spacer. A series of four clones, EEG_nHHHG_nEE (where n = 0, 1, 2, 3), were displayed on yeast as Aga2 fusions. Binding of clones to CdS, ZnS and Au was measured as percentage of the material surface covered by cells, averaged from 3 independent experiments ± std error of the mean.

3.3.3 Analysis of library-selected CdS binding peptide

A potential strength of rational peptide design is the ability to help understand the binding principles between more compositionally diverse peptides. To test this capability, a CdS-binding peptide was extracted from a YSD peptide library and designed variants analyzed for binding. A dodecamer peptide library was constructed as described in ref. [119] and biopanned for six rounds against single crystalline CdS. Sequencing ten clones from round 6 sub-library revealed seven unique clones, of which five reconfirmed binding to CdS after phenotype transfer. One reconfirming clone, A08, was selected for further mutational analysis due to its compositional simplicity (five unique amino acids out of 12 positions).

The rationally-designed peptide study suggests the binding capability of clone A08, with a sequence of RSGRRRHHHRL, would result from the presence of three (H) residues along with five up-modulating (R) residues. To test this hypothesis, several variants of A08 were constructed and tested for binding the CdS, ZnS, and Au. Sequences and results are listed in Table 3.1. As hypothesized, replacing the (H) residues with (A) abolished binding to all three surfaces, and only was restored slightly on ZnS surface by replacement with more charged residues (A08H-R, A08H-PRP), and on Au surfaces by charged residues and (M) and (W), two amino acids shown to directly mediate cell adhesion to Au (Fig. 3-3). The modulation capacity of the five (R) residues in A08 was tested by several mutational variants (A08R-X). Overall, results were consistent with the modulation fingerprints found from the interdigitated peptides (Table 3.1). Replacement of the arginines with up-modulators (K) or (W) retained the strong binding capability seen in A08, while replacement with down-modulators (E), (S), (A), (Q), all diminished binding to varying degrees depending on the substrate.

As a simple test of peptide sequence on the binding behavior, peptide A08 was randomly scrambled (A08Scr) and tested against the same three substrates. The scrambled peptide retained binding levels equivalent to the A08 peptide. Although not proof that sequence is unimportant in peptide adhesion, it strongly suggests that

Table 3.1: Binding of CdS-peptide A08 variants

Name	Sequence[a]	CdS binding[b]	ZnS binding[b]	Au binding[b]
A08 /wt	RSGRRRSHHHRL*	+++	+++	+++
A08H-A	RSGRRRSAAARL*	–	–	–
A08H-R	RSGRRRSRRRRL*	–	+	+
A08H-PRP	RSGRRRSPRPRL*	–	+	+
A08H-M	RSGRRRSMMMRL*	–	–	+
A08H-W	RSGRRRSWWWRL*	–	–	++
A08R-K	KSGKKKSHHHKL*	+++	+++	++
A08R-W	WSGWWWSHHHWL*	+++	+++	+++
A08R-Q	QSGQQQSHHHQL*	++	++	–
A08R-E	ESGEEESHHHEL*	–	–	–
A08R-L	LSGLLLSHHHLL*	–	++	+
A08R-S	SSGSSSSHHHSL*	–	+	–
A08R-A	ASGAAASHHHAL*	–	++	–
A08Scr	HRGRRLSRSHRH*	+++	+++	+++

[a]Fused directly to a -$(G_4S)_3$ASQGGG-linker at the C-terminus of Aga2.
[b]+++: > 20 %; ++: 10-20 %; +: 2-10 %, –: < 2 % area cell coverage on substrates. n ≥ 2.

peptide composition is of greater importance. The consistency in results between the rationally-designed peptides and the mutational variants shows the power of simple rational design in understanding and predicting the binding behavior of slightly more compositionally diverse peptides. One caveat is that all studies were carried out in using yeast-display and therefore were biased by the same display-based effects. It is an open question how universal these finding are when transported outside the cell-display format, although we address below how our findings might apply to peptides selected from other display formats.

3.3.4 Testing binding principles with predictive peptide design

As a proof of principle for predictive-based design of material-specific peptides, we engineered three peptides predicted to be a CdS, ZnS, and Au multi-material binder (Z1; KHKHWHW), Au-specific (Z2; RMRMKMK), and ZnS-specific (Z3; PHPH-

THT). Data from both the homo-hexamer study (Fig. 3-3) and the interdigitated peptide study (Fig. 3-4) provided basis for peptide design. The following rationales were used in programming specificity: The strongest general binder, (H), was interdigitated with strong general up-modulators, (K, W), to form the multi-material binder, Z1. Residues (M), which was sufficient to bind Au, and (R), which showed unique up-modulation ability for Au over CdS and ZnS, were combined with the general up-modulator (K) to promote Au-specific binding by Z2. Finally, ZnS-specific Z3 was designed by choosing residues that strongly down-modulated binding of (H) to CdS and Au but only minimally affected binding to ZnS; As seen in Figure 3-4, residue (T) eliminated binding only on Au and CdS, and on an absolute scale (P) was significantly less down-modulating for ZnS. All three peptides performed as predicted by our design criteria in our cell coverage assay when expressed by yeast, as shown in Figure 3-7. The small amount of material cross-reactivity may be overcome by adding additional compositional or structural constraints to such sequences. We hope to further refine rules for material binding using more precise metrics for binding, studying increasingly complex peptide compositions, including structural constraints on peptide presentation, and addressing a wider array of materials.

Our design criteria also appear applicable in improving understanding of the basis for material specificity observed with selected peptides identified by other groups. For example, Thai and coworkers observed highly variable affinities in their ZnO binders for Au[146]. Applying our findings, it appears that CN120 (PASRVEKNGVRR) and CN111 (PAGLQVGFAVEV) do not bind Au because they lack (H, C, M, and W) residues, and CN185 (RTDDGVAGRTWL) is unable to confer binding due to its single (W) placed between two strong down-modulators for Au, (T) and (L). Also, the ranking of their ZnO sequences that bound Au- CN146 (MRHSSSGEPRLL) > CN179 (RIGHGRQIRKPL) > CN155 (VRTRDDARTHRK)- may be explained by composition and context as well; CN146 contains two binders (H) and (M), CN179 has one binder (H), and CN155 has one binder (H) next to one strong down-modulator (T). Of course experimental mutational analysis would be necessary for verification of these hypotheses.

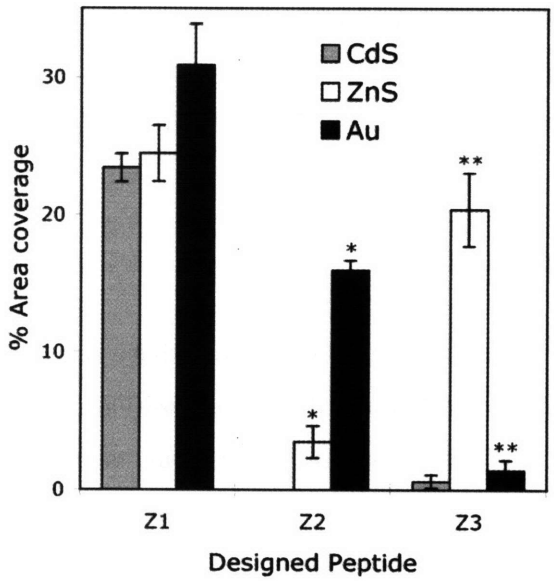

Figure 3-7: *Predictive-based design of material-specific peptides.* Three peptides engineered to be a multi-material binder, Z1 (KHKHWHW), Au-specific Z2 (RMRMKMK), and ZnS-specific Z3 (PHPHTHT) were displayed by yeast as Aga2 fusions. Binding of clones Z1-Z3 to CdS (grey bars), ZnS (white bars), and Au (black bars) was expressed as % of the material surface covered by cells, averaged from 2 independent experiments ± std. error of the mean. Material specificity was shown to be statistically significant using a student t-test with $p < 4x10^{-8}$ (*) and $p < 2x10^{-5}$ (**).

Extending and validating our studies with other peptide-based systems are required to identify system-dependencies and establish robust universal design rules to aid molecular engineers. Specifically, further systematic studies are needed to elaborate on design criteria to include structural relationships and possible multi-amino acid motifs. Another critical issue is that of the material itself; the exact nature of the bonds, crystal structure, orientation, surface composition, and polarization of the inorganic materials, we expect, will influence binding events. Through greater mechanistic understanding of interfacial interactions more complex inorganic hybrid architectures may be realized through bio-directed self-assembly.

3.4 Conclusions

From systematic study of peptide sequence-activity relationships, we conclude that interfacial binding depends primarily on composition; For the II-VI semiconductors CdS, CdSe, ZnS, and ZnSe and Au studied, only residues from the group of histidine, tryptophan, methionine, and cysteine appeared sufficient for significant binding. Additionally, each of these materials had a unique fingerprint of binder-modulator relationships, where spatially proximal amino acids tuned the binding strength of binder-residues/motifs in unconstrained peptides. From the composition and contextual principles investigated, predictive-based design of material-specific binders was realized. Further studies, focusing on compositional, spatial, structural, and material-dependent rules may eventually lead to formulas for calculation of binding specificity and affinity from peptide sequence and structure.

3.5 Experimental

3.5.1 Yeast Surface Display

Peptides were displayed as fusions to the C-terminus of Aga2, which is encoded on a 2-micron plasmid downstream of a Gal-based promoter. The expression vectors

were maintained in *S. cerevisiae* strain EBY100, which has Aga1 under control of a Gal-based promoter integrated in its genome, as previously described [20].

3.5.2 Genetic Engineering of Yeast Displayed Peptides

The yeast expression vector was constructed by removing the BstXI site of pCTCON [44] by silent mutagenesis at Val97 of TRP1 using Quickchange Kit (Stratagene) and inserting a 1.5 kB DNA stuffer fragment at the C-terminus of Aga2s $(Gly_4Ser)_3$ linker with NheI/BamHI. The resulting vector, pBPZ, has non-identical BstXI sites flanking the stuffer enabling efficient cloning of DNA-encoded inserts. Engineered peptide expression vectors (X_6 and XHXHXHX clones) were generated from annealed oligonucleotides (i.e. G_6 peptide oligos: 5' GTGGCGGTGGTGGTGGTG-GCGGATAGCCAGTAGC and 5' CTGGCTATCCGCCACCACCACCACCGCCAC-CGCC) with BstXI compatible sticky ends ligated into BstXI sites of pBPZ. The complete list of oligonucleotides used is listed in ref. [119]. No peptide control (*) has an encoded stop. All vectors were amplified, sequenced, and then transformed into EBY100.

3.5.3 Materials

Polished A-plate single crystal CdS and CdSe (Cleveland Crystal), polished single crystal ZnS and ZnSe (Electronic Space Products International), and Au coated slides (Evaporated Metal Films Corporation) were cut into 0.5 cm x 0.6 cm pieces for use in binding experiments, cleaned by brief aqueous sonication in a bath sonicator (Fisher Scientific), rinsed in 70 % ethanol, and stored dry. Surface integrities of CdS, CdSe, ZnS, ZnSe were monitored by low angle XPS with a Kratos AXIS Ultra Imaging X-ray Photoelectron Spectrometer.

3.5.4 Cell coverage assay

Evaluation of material binding was carried out as described previously [122], modified to a plate format for increased throughput and performed in buffer lacking BSA,

both of which improved the assay sensitivity for evaluating weak binders. In short, material samples were contacted with 1 OD_{600} of induced yeast cells in 1 mL PBS 0.1 % tween-20 (PBST) in wells of 24-well culture plates under fluidic sheer provided by rocking at a steady 2 cycles/sec for 1 hour, then washed in fresh PBST for 30 min. Digital images were collected with AxioCam MR on a Axioplan optical microscope (Carl Zeiss), and percent area coverage was quantified using ImageJ v1.3 developed by Wayne Rasband, NIH. Concurrently, expression levels of all induced clones were measured by staining for the proximal HA-epitope tag as described [18], and analyzed using FlowJo (TreeStar Software). All clones expressed efficiently and at comparable levels.

3.5.5 Biopanning of YSD peptide library against CdS

A yeast surface display dodecamer peptide library was constructed as detailed in ref. [119] (Ch. 3). Library BP12, constructed by an Anneal-Extension method was used for biopanning against single crystal CdS. The general panning process against single crystal CdS was as described in Chapter 2. Briefly, peptide-expressing yeast mixtures (nave library, round 1; rescued cells, subsequent rounds) were panned against CdS, washed to remove loosely adherent cells, and placed in growth media to rescue and amplify bound clones. Six panning rounds, g1-g6, were performed at RT under the following conditions; round g1: 8 OD cells in 4 mL SG + 5 mg/mL bovine serum albumin + 0.1 % tween 20 (SG-BSAT(0.1)), 8 h incubation; g2: 1 OD cells in 1.5 mL SG-BSAT(0.1), 4.3 h incubation; g3: 1 OD cells in 1.5 mL PBS-BSAT(0.1), 1 h incubation; g4: 0.2 OD cells in 1.5 mL PBS-BSAT(0.5), 1 h incubation; g5: 0.1 OD cells in 1.5 mL PBS-BSAT(0.5), 1 h incubation; g6: 0.01 OD cells in 1.5 mL PBS-BSAT(0.5), 1 h incubation. Ten clones were sequenced from the g6 sub-library and analyzed for binding to CdS using the cell coverage binding assay described above.

3.5.6 Mutational analysis of CdS clone A08

Variants of CdS-selected clone A08 were created in a yeast display format with complementary oligos in an identical fashion to the creation of X_6 peptides (Sec. 3.5.2). After transformation into yeast EBY100, clones were tested for binding to CdS, ZnS, and Au as described in Sec. 3.5.4.

Chapter 4

Metal-Oxide Binding Peptides, Part I: Combinatorial Yeast Surface Display Libraries for Selection of Sapphire Binding Peptides

4.1 Summary

In order to better address the nature of peptide binding to metal oxides, peptides were identified from a dodecamer peptide yeast surface display library that bound a model metal oxide material, the C, A, and R crystalline faces of synthetic sapphire (α-Al_2O_3). Seven rounds of screening yielded peptides enriched in basic amino acids compared to the naive library. Retesting of each unique clone against all three faces sapphire reaffirmed sequencing results that the C-face was the most permissive, often binding yeast even without peptide expression, while the R-face bound only those yeast expressing multiply-charged positive peptides. Cell binding to the A-face was highly sensitive to buffer excipients, with non-specific binding eliminated primarily with bovine serum albumin and restored only by expression of basic peptides. Cell detachment assays showed that cell adhesion strength correlated positively with increasing basicity of expressed peptides. Cell adhesion was also shown to be sensitive to buffer ionic strength as well as incubation with soluble peptide (with half maximal inhibition of cell binding at $\sim$5 μM peptide). This result suggested mainly an electrostatic binding mechanism between positively charged peptides and negatively charged sapphire surfaces.

4.2 Introduction

The difficultly of observing the material-biological interface has slowed the understanding of how selected peptides undergo material recognition [128]. Recently, there have been attempts to study peptide-mediated binding mechanisms. Goede et al. suggest peptide adhesion to certain semiconductors can be explained by electronegativity and the acidity of amino acid side chains [51]. In an earlier study, we investigate the importance of metal-coordinating amino acids in the binding of yeast displayed peptides to II-VI semiconductor substrates [121]. A single molecule study on an unnatural amino acid, dopa, (a post-translationally modified tyrosine prevalent in marine mussel adhesion proteins) shows that it adheres strongly to titanium oxide

surfaces through metal-oxygen coordination [85]. Although promising for a variety of applications, the challenge of incorporating dopa into expressed peptides make their use as protein affinity tags less straightforward. Other recent studies have suggested the importance of charged amino acids in the specific adhesion between peptides and material surfaces [58, 146, 157]. Since adhesion most likely depends of the properties of the peptide and the local environment of the interface, further studies are needed to help clarify and catalogue how peptides interact with material surfaces in order for this approach to be applicable to emerging technologies.

Because most materials undergo oxidation in aqueous environments, studies of peptide-material interactions (naturally in aqueous environments) need to address adhesion to oxide surfaces. Metal oxides materials, such as alumina (Al_2O_3) or silica (SiO_2), are often used as substrates for biological assays due to their strength and chemical compatibility with aqueous environments. Recently, transition metal oxides have been exploited as sensitive gas sensors [32] and have promise for novel biosensors [144]. Uncovering if and how peptides of natural amino acids adhere to metal oxide materials should facilitate the design of peptides for use in many biological applications, including specific protein and cell deposition without the need of additional chemical processing steps.

Single crystal alumina, or synthetic sapphire (α-Al_2O_3), serves as a good test metal oxide due to its strength, stable oxide layers, high optical transparency, and availability in many crystalline orientations. Commonly used as a substrate in epitaxial growth of semiconductors, α-Al_2O_3 is also widely used as a model oxide in the study of environmental adsorbents [92, 145, 150]. For the study of peptide adhesion herein, three surface orientations (C, A, and R) of synthetic sapphire were chosen. In addition to testing simple adhesion, discrimination among various surface planes serves as a stringent test of peptide specificity. Unlike the II-VI semiconductors, preliminary studies with sapphire using the rational peptide approach described in the Chapter 3 did not result in any obvious adhesion or specificity rules. Alternatively, combinatorial selection from random libraries, as established in Chapter 2 and consisting of a more diverse sequence pool, may be used to potentially uncover more subtle adhesion and

Table 4.1: Summary of biopanning conditions

Round	Library used	Number of cells ($O.D._{600nm}$)[a]	Buffer[b] (Volume)	Screening Time (Hrs)
1	Naive PL12	100	PBST (50 mL)	8
2	Rnd. 1 sub-library	1	PBST (1 mL)	13
3	Rnd. 2 sub-library	2	PBS-BSAT (1 mL)	2.5
4	Rnd. 3 sub-library	1	PBS-BSAT (1 mL)	1
5	Rnd. 4 sub-library	0.2	PBS-BSAT (1 mL)	1.5
6	Rnd. 5 sub-library	0.1	PBS-BSAT (1 mL)	1.5
7	Rnd. 6 sub-library	0.05	PBS-BSAT (1 mL)	1.5

[a] 1 $O.D._{600nm}$ ~$2x10^7$cells.
[b] PBST: 1xPBS 0.1 % Tween20 (v/v); PBS-BSAT: PBST + 5 mg/mL BSA.

specificity principles. Therefore, this chapter concerns the creation of a yeast surface displayed dodecamer peptide library and subsequent biopanning against the three surface orientations of α-Al_2O_3. After a panning, selected peptides were analyzed and interrogated under different binding conditions to investigate the importance of ionic charge interactions in the peptide-mediated cell adhesion process.

4.3 Results and Discussion

4.3.1 Biopanning and sequence analysis

Peptides that mediate cell binding to sapphire crystal faces were selected from a pool of approximately 10^7 random twelve amino-acid peptide clones. This pool, denoted the PL12 library, was created by cloning oligonucleotides with twelve repeating NNK codons onto the N-terminal of Aga2p in the yeast display plasmid. After creation, the yeast library was biopanned through seven rounds against the C, A, and R face of sapphire to enrich for binding peptides. Biopanned cells, each expressing a unique peptide, were agitated in the presence of sapphire surface, and then loosely bound cells were removed by surface washing. The adherent cells were then grown off the surface to create a subpopulation used in the subsequent round of biopanning.

Stringency of binding was increased through subsequent rounds by decreasing cell concentrations and the time for cells to interact with substrate, as well as increasing

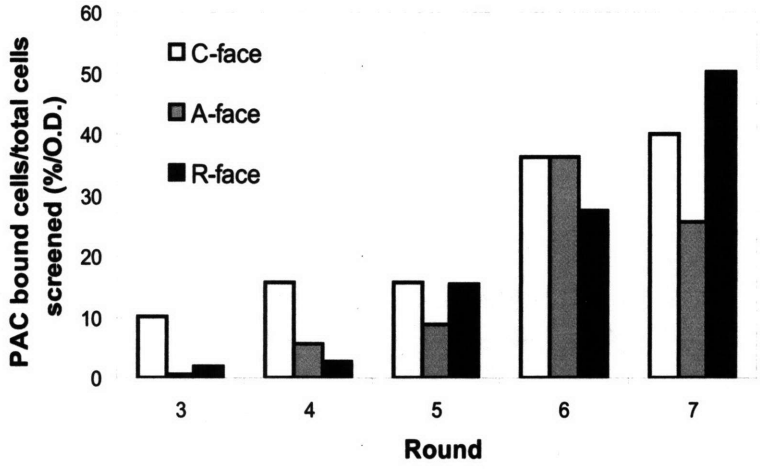

Figure 4-1: *Enrichment of sapphire binding clones.* Cell coverage measured between washing step and grow-off step in the biopanning process and divided by the total number of cells screened.

the excipients (Tween20 and BSA) in the screening buffer (Table 4.1). In an attempt to enrich for face specificity of binding peptides, a subtraction method was used in rounds three through seven, in which cells binding from a previous round (e.g. grown from the A-face) were incubated with all three faces, but only cells attached to surface of interest (e.g. the A-face) were grown off for subsequent rounds.

After the third and all successive rounds of panning, the bound cells were visualized with optical microscopy to check for the enrichment of bound clones. Enrichment, which was approximated by the number of bounds cells (Percent cell Area Coverage on substrates) divided by the total cells screened, increased steadily from rounds three through seven on all surface orientations (Fig. 4-1). Even so, the greatest enrichment most likely occurred during the first three rounds when the total number of screened cells was much larger. After Round 7, rescued sub-libraries and uninduced cells were tested for binding against each of the sapphire faces and images are shown in Figure 4-2. A marked increase in cell binding after induction of peptides is clearly visualized for all three sub-libraries. Specificity for each orientation, conversely, was more subtle with each sub-library binding well to each surface orientation. The clear-

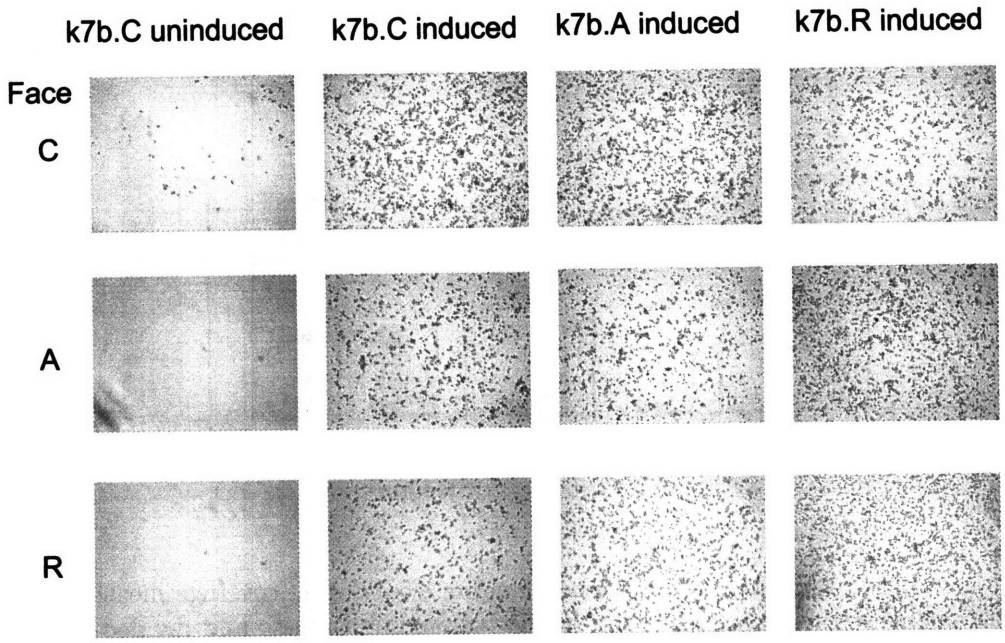

Figure 4-2: *Binding of Rnd. 7 sub-libraries against the three orientations of sapphire.* Cells screened in 0.5 mL PBS-BSAT at 2 O.D./mL and washed for one hour in a fresh 0.5 mL PBS-BSAT.

est differences included the preference of the C sub-library for the C-face, and the R sub-library preference for the A- and R- face over the C-face (Fig. 4-2).

Next, twenty four clones from each round seven sub-library were sequenced and the results are presented in Table 4.2. Seven of the unique sequences appeared in more than one sub-library, suggesting a similar mechanism for peptide binding on the varying faces. The C-face proved most promiscuous with 21 unique peptides out of 23 sequenced candidates, while the A and R-face sub-libraries contained significant enrichment with only 8 and 12 unique sequences, respectively.

Sequencing statistics are summarized in Table 4.3 along with data from the nave PL12 library. Compositional analysis of sequences revealed a strong bias for positive amino acids (~3-fold for C library, ~4-fold for A and R library) and against negative and hydrophobic amino acids (~2-fold for C library, ~4-fold for A and R library) versus the unselected PL12 library. The average unselected clone contained approximately 10 % positive amino acids and 40 % hydrophobic amino acids whereas the

Table 4.2: Sequencing data from Round 7 sub-libraries

Name	Sequence	Net charge[a]	Sub-library origin (representation)
A11	RCRPGRIKSKHL	+5	C(2), A(3)
A02	AGRRRGCRAFHQ	+3	C
A03	RVRHRRVQSRCR	+6	C
A07	KPKKCFTGNRHD	+3	C(2)
A06	VCHREAFYMKT	+1	C
A08	VCGGRHRPWHAN	+2	C
A09	RLRSPWSKGGCA	+3	C
A10	RRGKTCRKESPK	+4	C
A12	RRGKPRRMGKHY	+6	C
B01	RRKPWRGRDRHI	+5	C
B02	INTSRRHRKTRT	+5	C, R
B03	VCGAKRRRKKPR	+7	C
B04[b]	KMRAWGHPIWNW	**+2**	C
B05	CARWHAVGANRD	+0	C
B06	AWLRGCAMHVRG	+2	C
B07	RRKPKTCGR	+5	C
B08	WVVRSVSACRTK	+3	C
B09	TKHGKRSRCYNL	**+4**	C
B10	RIWCRVRRGRRCS	+6	C
B11	CTKWGCWFLWSD	+0	C
D01	HRARKKGCAYTK-t[c]	+5	C, A(8), R(3)
C02	ARRPKTRTRCHS	+5	A
C03	RSICQSKRRGRN	+5	A(2)
D09	RKLKPPHRHNHH	+4	A(3), R(7)
C12	NRCLTRRKKKKN	+7	A, R
D02	RTAKRKWKHTRD	**+5**	A(5), R(3)
D12	ARKKGRKRRHQH	+7	A, R
E07	RCCRKKETHRHG	+4	R
E09	KPKRCRKHACRN	+6	R
E11	RVKSGRKHKGRG	+6	R(2)
F02	KRHKQKTSRMGK	**+6**	R(2)
F05	GRQARKCSKHHA	+4	R
F12	KRSKKCLRKNGS	**+6**	R

[a]at neutral pH.

[b]clones in bold characterized by centrifugation assay.

[c]-t = ELARPVAWGRIRTKAYF (frameshifted framework region).

Table 4.3: Statistics from Round 7 sequencing results

Sub-library	Total Sequenced (#)	Unique Sequences (#)	Percent positive[a] amino acids (%)	Percent negative[b] amino acids (%)	Percent hydrophobic[c] amino acids (%)
Naive	45	45	10	7	40
C	23	23	35	3	21
A	24	8	44	2	14
R	24	12	43	1	11

Amino acids [a]K,R,[b]E,D,[c]W,F,I,A,L,V.

average A and R-face selected clone contained about 40 % positive amino acids and 10 % hydrophobic amino acids. With no other significant compositional trends or motifs discovered, this result suggests that basic amino acids are crucial for peptide-mediated yeast binding to sapphire.

4.3.2 Testing individual sapphire clones

After phenotypic transfer into new yeast hosts, each of the 33 unique sequences was tested for binding against the three faces of sapphire. Binding experiments were carried out a 1xPBS buffer with Tween20 added as an excipient, similar to rounds one and two during biopanning. Results are shown in Figure 4-3, in which cell binding is plotted against the relative basicity/hydrophilicity (two properties significantly enriched for during screening) of each peptide. Binding on the C-face and A-face did not correlate with increasing basicity/hydrophilicity (Fig. 4-3*A*, *B*) as opposed to binding on R-face, which showed greater binding to basic and hydrophilic peptides (Fig. 4-3*C*). No correlations were seen between any other physiochemical property of the peptides and binding capacity. The trends for binding capacity to the C-face were unsurprising since peptides from the C-face sub-library did not show significant enrichment for basic peptides. Conversely, the A-face sub-library had significant enrichment for basic peptides but retesting did not preferentially favor those clones. Surprisingly, the A-face showed large endogenous (non-induced) cell binding in these experiments (Fig. 4-3*B*, hatched area), which was not seen during post screen imaging (Fig. 4-2).

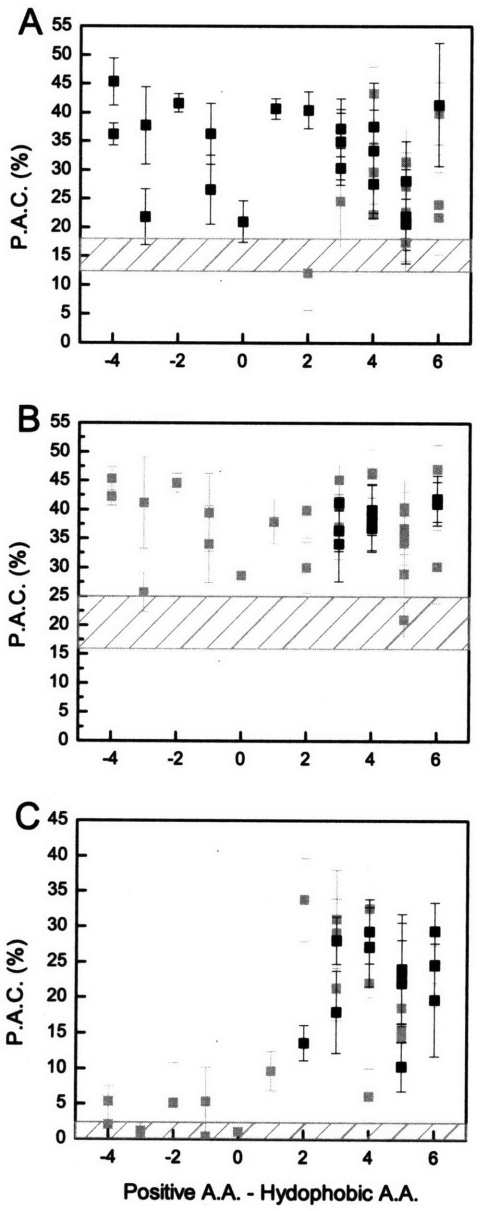

Figure 4-3: *Individual binding tests on all 33 unique clones against the (A) C, (B) A, and (C) R-faces of sapphire.* Binding was performed in PBST and each data point represents the average and standard deviation of Percent Area Cell coverage (P.A.C) measured from three images on each of three independent substrates. Each clone is ranked by the number of positive amino acids (A.A.) minus hydrophobic amino acids and black points represent binding of clones found from the corresponding sapphire face. Hatched grey regions represent a standard deviation ± mean of exogenous cell binding.

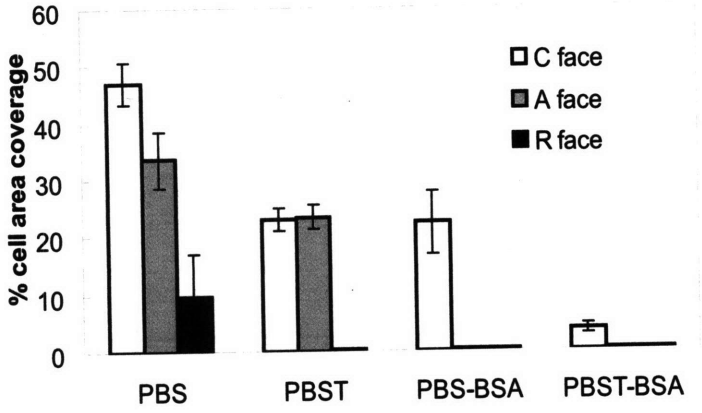

Figure 4-4: *Binding of non-induced cells in the presence of various non-specific binding excipients.* Data represents values and standard deviations from two independent substrates.

To explore further, the endogenous cell binding was tested in 1xPBS buffers with a variety of excipients (Fig. 4-4). The C-face bound yeast endogenously regardless of excipient added and binding was reduced appreciably only with both BSA and Tween20 in the screening buffer. This endogenous binding would reduce selection pressure for peptide-enhanced cell binding and therefore explains the lack of a highly enriched pool of peptides during screening (in PBS-BSAT) and during retesting (in PBST). The R-face, conversely, did not bind yeast endogenously, regardless of the excipient in the screening buffer, and therefore explains both the highly enriched pool of basic peptides from screening, and the correlation between peptide basicity and binding seen during retesting. The binding behavior of the A-face exhibited intermediary characteristics: endogenous binding only when BSA was absent from the screening buffer, such as those used during retesting. Therefore, an enriched pool of peptides was expected during screening since BSA was present, but during retesting without BSA large endogenous cell binding precluded any correlation between peptide basicity and yeast binding capacity.

Although the underlying reason for this endogenous cell adhesion is unknown, structural studies of a hydrated C-face [40] show a completely hydrated surface of

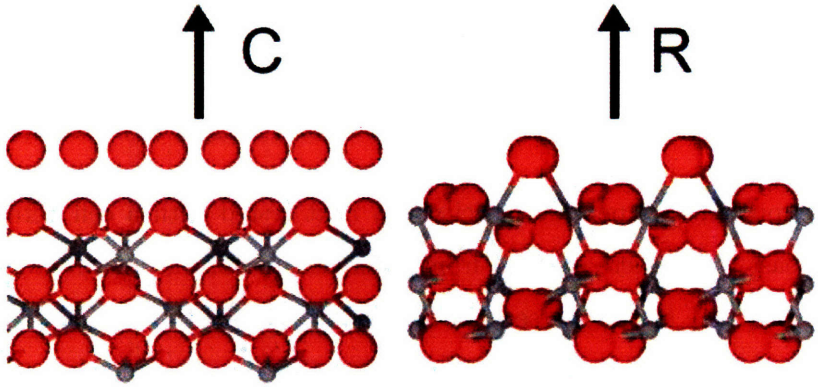

Figure 4-5: *Models of the synthetic sapphire (α-Al_2O_3) crystalline orientations.* Crystals of the hydrated C-face (left) and R-face (right) generated from X-ray diffraction. Oxygen is represented by red spheres and aluminium by gray spheres. Non-bonded oxygen atoms on the C-face represent a close-packed water layer with hydrogen atoms not shown. Models recreated from refs. [40, 148].

doubly coordinated oxygen atoms (Fig. 4-5). The authors suggest this will lead to surface passivated with hydroxyl groups that will be highly reactive towards metal ions. Therefore, endogenous cell binding to the C-face might occur through divalent metal ion bridging (from endogenous calcium or magnesium ions) between cell surface biomolecules and the sapphire surface. Conversely, the A and R-face showed less endogenous cell binding in the buffers utilized in this study (Fig. 4-4). Structural studies of the hydrated R-face predict a more complex surface with a mix of singly, doubly, and triply coordinated oxygen [148] (Fig. 4-5). The singly and triply coordinated oxygen are predicted to have greater basic and acidic character, respectively, than doubly coordinated oxygen, but the ionic interactions are thought to occur mainly through exposed singly coordinated groups [28]. Although structural studies of the hydrated A-face have not been reported, modeling of the bulk crystal structure suggests a surface of character intermediate of C and R. In the remaining studies, binding experiments are carried out on the A and R substrates in a PBS-BSAT buffer to reduced endogenous cell binding and better assay the peptide-sapphire interaction.

4.3.3 Centrifugal cell detachment assay

The importance of peptide basicity was next tested with a cell detachment assay. Five yeast clones were selected from different sub-libraries and represent a range of physiochemical properties seen in sequencing (Table 4.2) . As a control, a yeast clone stop was created that was identical to the other clones except for termination of the Aga2 display construct at the beginning of the peptide coding sequence. By locking the substrates in wells and applying a centrifugal force, this assay allowed for quantitative detachment forces to be applied to cells so that adhesion strength between clones could be compared. Figure 4-6 shows the detachment of yeast clones on the A and R-face of sapphire. Tests on the C-face resulted in significant binding with the stop clone control throughout the range of forces tested.

Again, this demonstrates the high level of endogenous yeast binding to the C-face that prohibits the ability to selectively assay for peptide-mediated yeast binding on this face. The A- and R-faces, conversely, demonstrated significant peptide-mediated adhesion with more basic peptides binding with increasing strength. Yeast clone B04, with a net +2 charge at neutral pH, bound slightly better then the stop clone. The slightly more basic clone B09, with a +4 charge, mediated a stronger adhesion while the most basic clones bound with the greatest adhesion. The significant increase in binding strength with basic amino acids suggests their importance in mediating cell binding. The similarity in trends between the A and R-face (Fig. 4-6*A* vs. Fig. 4-6*B*) also suggests a related binding mechanism between the two surfaces. Prior studies on the crystal planes of sapphire reveal a point of zero charge around pH $\sim$ 4-6, which would lead to negatively charged surfaces at neutral pH [45, 48]. These negatively charged surfaces, most likely from surface coordinated oxygen, would attract positively charged groups on the basic amino acids leading to a favorable energetic interaction.

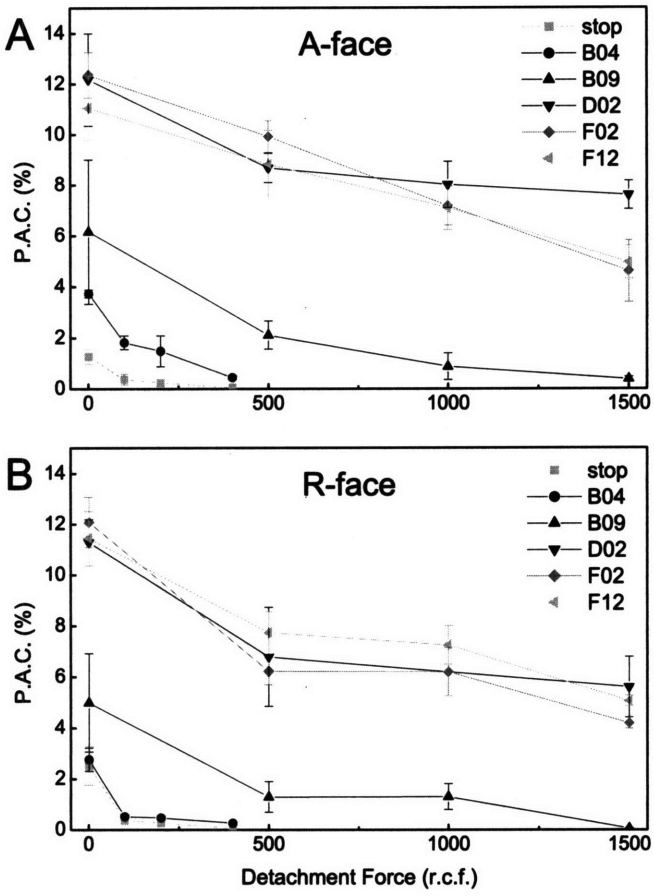

Figure 4-6: *Centrifugal force cell detachment of selected yeast clones.* The adhesion of peptide-expressing cells measured in Percent cell Area Coverage (P.A.C) as a function of various detachment forces against the (A) A-face and (B) R-face of sapphire. Each data point represents the average and standard deviation of binding from three independent substrates.

4.3.4 Physiochemical testing of the binding event

To further test the possibility of an electrostatic mechanism between the basic peptides and negatively charged sapphire surfaces, clone F02 (Table 4.2) was tested in varying ionic strength buffer. The stop clone was used as a negative control. The clones were tested at various dilutions of PBS buffer (10 mM phosphate buffer, 2.7 mM potassium chloride, 137 mM sodium chloride, pH 7.2), with both Tween20 and BSA as excipients. The 166 mM ionic strength corresponds to the PBS-BSAT buffer used during the later biopanning rounds. Results show that clone F02 bound maximally at intermediate ionic strengths while the stop clone bound little throughout the range of ionic strengths (Fig. 4-7*A*).

The biphasic binding of clone F02 with increasing ionic strength is characteristic of bridging two like-charged surfaces with an oppositely charged molecule. The yeast cell wall consists of a skeletal layer of -glucans and a diverse matrix of glycoprotein [99, 167] that confer a net negative charge on the yeast. Zeta-potential measurements confirmed both non-expressing and basic peptide expressing yeast retain a net negative surface charge at neutral pH (data not shown). Sapphire plates, unlike alumina particles, have also been shown to have a net negative charge a neutral pH [45, 48]. A schematic of the proposed mechanism is shown in Fig. 4-8. At low ionic strength, the force of repulsion between like-charged yeast and sapphire limit the binding interaction. In fact, screening yeast in water eliminated any noticeable binding regardless of expressed peptide or sapphire face chosen. At intermediate ionic strength, charge screening is increased and the repulsion between yeast and sapphire weakens, allowing the bridging of yeast and sapphire surface with a positively charged peptide. At high ionic strengths, short range ionic interactions are screened by ions in the buffer, thereby eliminating the ionic peptide bridge between yeast and surface. The fact that the stop clone does not bind to the A and R-face throughout the range of ionic strengths tested suggests that other surface forces between the yeast and sapphire surface are not predominant in binding.

To confirm that peptide is solely responsible for the adhesion of yeast, it is im-

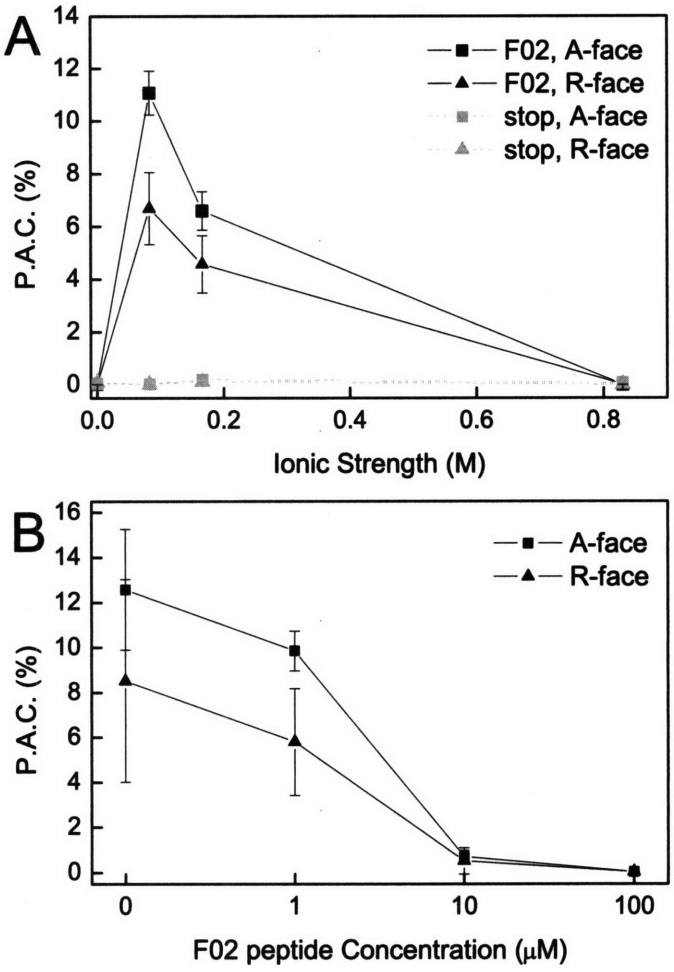

Figure 4-7: *Physiochemical investigation of the cell binding event.* (A) The effect of ionic strength on the peptide induced cell binding (measured in P.A.C.) to sapphire. Binding of clones F02 (black, solid) and stop (grey, dashed) against A (■), and R-face (▲), under various dilutions (0x, 0.5x, 1x, 5x) of 1xPBS (166 mM, pH 7.2). The excipients of 0.1 % Tween20 and 5 mg/mL BSA remained constant for each dilution. (B) Competition of yeast clone F02 with various concentrations of soluble F02 peptide. Binding of F02- induced yeast to the A- (■) and R-face (▲) was measured in the presence of soluble F02 peptide in PBS-BSAT buffer. Each data point represents the average and standard deviation of binding from two independent experiments.

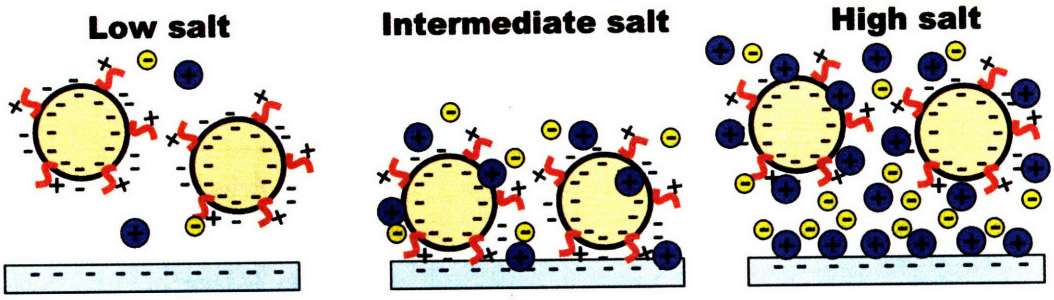

Figure 4-8: *Schematic of charge-charge interactions at the yeast-sapphire interface in various ionic strength buffers.* Interaction between peptides and surface occur only at intermediate ionic strength where long-range electrostatic interactions are screened while short-range interactions are still permissible.

portant to show that soluble peptide (outside the context of cell display) can inhibit the binding of peptide-expressing yeast. Figure 4-7*B* shows the inhibition of F02-expressing yeast by increasing concentrations of soluble F02 peptide. Representative images from the R-face are shown in Figure 1. The half-maximal inhibition of yeast occurred between 1 and 10 μM, demonstrating at least micromolar level binding of soluble peptide to the sapphire surfaces. Again, similar inhibition of the yeast on each faces suggests similar binding affinities to both surfaces. The binding of soluble peptide most likely occurs at lower concentrations but higher ones are necessary to inhibit the binding of multivalent yeast cells.

Several recent publications have implicated the importance of charge interactions with adhering polymer and peptides to inorganic materials. Polycationic polymer poly-L-lysine has been shown to electrostatically adsorb negatively charged metal oxide surfaces TiO_2, Nb_2O_5, Ta_2O_5, SiO_2, and ITO [10, 63, 74]. In a similar method to the one presented herein, Thai et al. suggest small motifs of lysine and arginine are responsible for binding peptides to Cu_2O and ZnO, though detailed interrogation of those sequences for direct cause and effect are not presented [146]. Studying fluorescently-labeled homopeptides of all 20 amino acids against a variety of inorganic surfaces, Willett et al. found large binding only among charged peptides [157]. Further, in the interrogation of a titanium binding peptide with adhesion force microscopy, Hayashi et al. suggests the importance of charge interactions for adhesion

to Ti as well as surfactants for eliminating non-specific binding [58]. In a study of peptides binding to II-VI semiconductors, we show the ability of lysine to increase the binding of histidine containing peptides relative to other amino acids[121]. Interestingly, after selection of a random dodecamer phage library against thermally grown SiO_2, Eteshola et al. find a prevalence of histidine residues in their binding peptides [41]. Although the imidizole of histidine can be titrated around neutral pH, it is unclear if charge plays a role in peptide binding, and the authors do not provide further experimental insight into the binding mechanism. Although expanding our affinity tags to other materials will covered in the next chapter and also the focus of future research, the simplicity of the electrostatic mechanism and findings from recent publications suggests they will be applicable on other materials that have a net negative surface charge.

4.4 Conclusions

Binding peptides were identified from a dodecamer peptide yeast surface display library against a model metal oxide material, the C, A, and R crystalline faces of sapphire (α-Al_2O_3). Through a variety of physiochemical binding tests, peptides were shown to interact with sapphire through multiple basic amino acids that mediate local electrostatic interactions with surface anions. The next chapter will focus on using rationally designed peptides to give greater insight into the binding mechanism and interaction strength.

4.5 Experimental

4.5.1 Materials

Synthetic sapphire (α-Al_2O_3) windows were purchased from Crystal Systems (Salem, MA). The three orientations obtained were the C-plate (0 0 0 1), A-plate (1 1 -2 0), and R-plate (1 -1 0 2). The sapphire was produced by a heat exchanger method, cut with a tolerance of 2^o, polished to an 80/50 scratch/dig and a flatness of 10 waves per

inch, as quoted by the manufacturer. Al_2O_3 substrates were refurbished for multiple experiments by HCl acid rinses, followed by brief sonication in distilled water, and 70 % (v/v) ethanol in water.

4.5.2 Yeast Strain and PL12 Library construction

A yeast display peptide library was created from a degenerate oligonucleotide pool encoding random 12-mer peptides with a NNK bias. Peptides were displayed as fusions to the C-terminus of Aga2, which is encoded on a plasmid downstream of a Gal-based promoter. The expression vectors were maintained in *S. cerevisiae* strain EBY100, which has Aga1 under control of a Gal-based promoter integrated in its genome, as previously described [20].

Vector construction

The yeast expression vector was constructed by removing the BstXI site of pCT-CON22 by silent mutagenesis at Val97 of TRP1 using Quickchange Kit (Stratagene) and inserting a 1.5 kB DNA stuffer fragment at the C-terminus of Aga2s $(Gly_4Ser)_3$ linker with NheI/BamHI. The resulting vector, pBPZ, has non-identical BstXI sites flanking the stuffer enabling efficient cloning of DNA-encoded inserts.

DNA inserts and library construction

Oligonucleotides used in library construction were obtained from Oligos, Etc. The degenerate oligonucleotide pool encoding the random 12-mer peptide library (PL12BstXI) 5'-pGTGGCGGTAGCGGC $(NNK)_{12}$ TAGCTAGCTAGGCCAGTAGC, synthesized with an NNK bias in order to reduce the stop codon frequency, was annealed to two short primers (5'BstXIanneal) 5'-pGCCGCTACCGCCACCGCC and (3'BstXI-anneal) 5'-pCTGGCCTAGCTAGCTA. The resulting hybrid DNA library containing duplexed BstXI sticky ends was directly ligated into the BstXI sites of pBPZ, and electroporated into E. coli Electromax DH10B (Invitrogen, Carlsbad, CA) for amplification on plated LB Amp+ media.

Scale-up of DNA

For large-scale libraries, electroporation rescue cultures were pooled together, and diluted in LB before plating. PL12 Library was spread onto 100, 500 cm^2 square plate tissue culture dishes (Corning) containing LB Amp+ agar media. Each square plate is capable of growing greater than 2 million individual colonies, however we typically plated these peptide libraries at a density of $2x10^5$- $1x10^6$ colonies per square plate. After growth overnight at 37 ^oC, all colonies were scraped from the plates using LB media and cell spreaders, pooled into a single flask, mixed thoroughly and aliquotted into 250 mL conical tubes. After centrifugation and decanting of media, cell pellets were either frozen for long-term storage, or prepped using a Qiafilter Maxi-prep kit (Qiagen, Valencia, CA). Final library contained a diversity of greater than $2x10^7$ clones.

Yeast Transformation

Yeast transformation in general was performed following the Gietz 60X large-scale transformation protocol with Gietz Transformation Kit reagents (Genomics One, Buffalo, NY) and EBY100 was prepared according to Gietz recommendations. Yeast transformed with peptide library DNA were passaged in 4 L then 2 L of SD media in order to amplify transformed cells out of the background of non-viable EBY100, mixed, and frozen down in 50 % glycerol/50 % SD media as 150 OD_{600nm} aliquots at -80^oC.

4.5.3 Biopanning PL12 yeast display library against Al_2O_3 surfaces

Biopanning rounds are summarized in Table 4.1. *Round 1.* 100 O.D. of PL12 yeast (1 O.D. $\equiv$ 1 Abs. Unit at 600 nm; $\sim 2x10^7$ cells) were induced overnight in select galactose (SG) induction media. 100 O.D. of cells from the induction culture were isolated and resuspended in 50 mL phosphate buffered saline, 0.1 % Tween20 (PBST, pH 7.2). Cells were incubated at room temperature under agitation for $\sim$8 hours

with three 1-inch diameter Al_2O_3 wafers, one of each different orientation (C-plate, A-plate, and R-plate). Wafers were washed separately in 5 mL PBST under agitation for 1 hour and then combined into one flask with 30 mL select dextrose (SD) growth media for expansion of bound cells, termed *k1*. *Round 2.* For the selection of C-plate binders, one 0.5 cm x 0.5 cm C-plate Al_2O_3 substrate was placed in a 24-well plate and incubated with 1 O.D. of induced *k1* cells suspended in 1 mL PBST and agitated for ~13 hours. Similar selections were done in parallel with A and R-plate substrates. The substrates were washed in 1 mL fresh PBST for 2 hours and then transferred to 4 mL SD media to grow off bound cells. Cell sub-populations from the C-plate were called *k2.C*, from the A-plate were *k2.A*, and from the R-plate were called *k2.R*. *Round 3.* First round of subtraction screening: Each induced sub-population from round 2 was incubated at 2 O.D in 1 mL PBST + 5 mg/ml bovine serum albumin (PBS-BSAT), which was added to limit non-specific interactions and increase binding stringency, with all three faces of Al_2O_3 for 2.5 hours under agitation. Substrates were washed for 1 hour in fresh PBS-BSAT under agitation and select substrates then transferred to 4 mL SD media to grow off bound cells. For screening sub-population *k2.C*, the C-plate was transferred for grow off and recovered cells were termed *k3.C*. Corresponding procedures were followed for A and R-plate screening. *Round 4.* Identical procedures to that of Round 3 except 1 O.D. of *k3* sub-populations were screened for only 1 hr. *Round 5.* Identical procedures to that of Round 4 except 0.2 O.D. of *k4* sub-populations were screened in 0.5 mL PBS-BSAT for 1.5 hrs. *Round 6.* Identical procedures to that of Round 5 except 0.1 O.D. of *k5* sub-populations were screened with substrates. *Round 7.* Identical procedures to that of Round 6 except 0.05 O.D. of *k6* sub-populations were screened with substrates. DNA was isolated from *k7* sub-populations and transformed into E. coli. Transformants were plated out and DNA prepped for sequencing of individual clones. Twenty four clones from each of the three sub-populations were sequenced.

4.5.4 Individual clone binding assay

Plasmid DNA from sequenced clones were transformed back into parent yeast strain EBY100 using the Geitz Transformation Kit (Genomics One, Buffalo, NY). For each independent experiment, the following procedure was performed. Yeast clones were induced overnight in 4 mL SG induction media. Al_2O_3 of size 0.5 cm x 0.5 cm were rinsed in 10 % (w/w) aqueous HCl for approximated two hours, followed by brief sonication in distilled water and 70 % (v/v) ethanol in water. In a single well of a 48-well plate, 0.25 O.D. cells were incubated with a single Al_2O_3 substrate in 0.5 mL PBST, under constant agitation for 1 hour. The substrates were washed for 1 hour by transferring to a new well with 0.5 mL PBST under constant agitation. The substrates were then transferred to new wells for optical imaging. Three digital images from each substrate were collected on an Axioplan optical microscope (Carl Zeiss), and percent cell area coverage (P.A.C) was quantified using ImageJ v1.3 developed by Wayne Rasband, NIH. Each of the 33 clones was tested against the C, A, and R-plates of Al_2O_3 in greater than two independent experiments.

4.5.5 Centrifugal force cell detachment assay

Forces necessary to detach yeast cells from substrates were tested by a modified centrifugal detachment assay. Yeast cultures were induced and substrates cleaned as in the clone binding assay. Substrates were anchored to the bottom of a 48-well cell culture dish by two silicon gaskets (height: 10 mm, i.d.: 4.76 mm, o.d.: 11.1 mm). Induced cells where diluted to 0.1 O.D./mL in PBS-BSAT and carefully added to the substrates. After settling for 20 minutes at 1 x g, the gaskets were sealed with clear adhesive tape and the plates oriented in a Beckman SPINCHRON tabletop centrifuge to apply a set detachment force to cells for 10 minutes. For the lower limit, 1 x g of detachment force was applied to cells by flipping over the plates for 10 minutes. The upper limit of detachment force was set by centrifuge and rotor specifications at 1500 x g. After applying the force, the upper gasket was removed followed by the addition of buffer to refill the well with fluid. Three digital images from each substrate were

collected and analyzed as mentioned above.

4.5.6 Varying ionic strength assay and soluble peptide competition

Varying ionic strength

To test the effect of ionic strength of cellular adhesion, 0.25 O.D. of induced cells suspended in various ionic strength buffers were incubated with an Al_2O_33 substrate in a 48-well plate under constant agitation for 30 minutes. The substrates were washed for 1 hour in new wells with similar buffer under constant agitation before transferring again for optical imaging. Three digital images from each substrate were collected and analyzed in terms of cell area coverage as mentioned above. Various ionic strength buffers were made from dilutions of PBS (5x, 1x, 0.5x, distilled water) each containing 0.1 % Tween20 and 5 mg/mL BSA.

Soluble peptide competition

A soluble peptide (ac-CGGKRHKQKTSRMGK-cooh) containing the F02 clone sequence was synthesized (Genscript Corp., Piscatway, NJ) and dissolved to 10 mM concentration in distilled water containing 1 mM EDTA (to prohibit disulfide bridge formation). Various dilutions of peptide in PBS-BSAT buffer were added to the sapphire surfaces with 0.25 O.D. cells for a final volume of 0.5 mL PBS-BSAT. The substrates were washed and imaged for cell binding as described above.

Chapter 5

Metal-Oxide Binding Peptides, Part II: Rationally Designed Peptides and Affinity Determination

5.1 Summary

In this chapter, rationally designed peptides were used to (1) gain more insight into the binding mechanism with sapphire, and (2) determine the strength of interaction though affinity measurements. First, peptides cloned into yeast showed that lysine led to stronger interactions than arginine, and that charge distribution affected adhesion strength. Taken together, we postulated that binding arose from peptide geometries that allowed maximal alignment of basic amino acids towards the surface so that the charged groups can undergo local electrostatic interactions with the surface oxide. Next, peptides were cloned onto the c-terminus of maltose binding protein (MBP) for quantification of binding affinities in a modified ELISA. Peptide K1 (-$(GK)_6$) showed a half-maximal binding at $\sim 10^{-7}$ M, which marked a >1000-fold binding improvement to sapphire as compared with wild-type MBP. Doubling peptide K1 (termed 2K1) led to nanomolar affinities (an ~100-fold improvement in binding over K1). Peptide 2K1 was also shown to bind a variety of oxide surfaces at high affinity and in a manner which can be selectively inhibited by high salt conditions. Targeting proteins to metal oxide surfaces with peptide tags such as 2K1 may provide a facile one-step alternative coupling chemistry for the formation of protein bioassays and biosensors.

5.2 Introduction

In the previous chapter, it was shown that positively charged residues were sufficient for mediating yeast adhesion to single-crystalline sapphire. Herein, we take a closer look at how arrangement and connectivity of those positive charges affects peptide adhesion. Using rational design principles described in Chapter 3, it was possible to design peptides that adhered yeast cells at strengths equivalent to biopanning-enriched peptides while exhibiting much lower compositional complexity.

Due to the difficulties of study the peptide-material interface as discussed in Chapter 1, two additional properties of inorganic-binding peptides are severely underreported. First are the ability peptides to function in multiple environments. Display

constructs, such as phage or yeast cells, can significantly influence binding behavior of peptides. Since most applications require the peptide outside the original display construct, additional testing is necessary. The second issue is determination of a quantitative binding affinity. The affinity of a peptide is a crucial metric for assessing utility in downstream applications. Oftentimes, researchers are more interesting in the nucleating properties of their inorganic-specific peptides and therefore do not attempt to determine binding affinities. Even so, only a few options are readily available for affinity measurements, including surface plasmon resonance (SPR), quartz crystal microbalance (QCM), and ellipsometry, which all suffer from a lack of material versatility and low-throughput experimental runs.

The second half of this chapter addresses both of these issues with a focus on using sapphire binding peptides as affinity-tags for facile protein immobilization. Rationally designed sequences were transferred from yeast to a model protein and the specificity of peptides was proven out of the context of yeast display. The model protein, maltose binding protein (MBP), was also used for the development of a modified ELISA that allowed for the facile determination of binding affinity. The results from this chapter demonstrate the potential of these peptide tags to be used as a protein immobilization tool.

5.3 Results and Discussion

5.3.1 Effect of peptide sequence on yeast binding

As the importance of positively charged peptides has been demonstrated for mediating yeast adhesion to sapphire, we next considered the effect of charged residue placement along the peptide sequence. To this end, dodecamer peptides were designed and cloned onto the c-terminus of the Aga2 yeast display construct. Each designer peptide, listed in Table 5.1, contained six positively charged amino acids but varied either in type of residue (lysine or arginine) or the grouping of these residues along the peptide. Testing the peptides against A and R-face sapphire revealed two clear trends (Fig. 5-

Table 5.1: List of interrogated rational designed peptides

Name	Sequence[a]	Net charge[b]	Construct[c]
stop	*	-	Aga2, MBP
X1	GXGXGXGXGXGX*	+6	Aga2, MBP
X2	GGXXGGXXGGXX*	+6	Aga2
X3	GGGXXXGGGXXX*	+6	Aga2
cK1	CGKGKGKGKGKGKC*	+6	Aga2
K1P	GKPKGKPKGKPK*	+6	Aga2
2K1	$(GK)_6AS\ (GK)_6$*	+12	MBP
H6	HHHHHHA*	+0	MBP
K6	GGGGGGKKKKKK*	+6	MBP

[a]X denotes either Lysine (K) or Arginine (R); '*' denotes a stop codon.
[b]at neutral pH.
[c]Aga2: yeast surface display fusion; MBP: N-terminal maltose binding protein.

1*A*): first, lysine peptides bound better than identically constructed arginine peptides (e.g. K1 > R1), and second, grouping charged residues decreased peptide binding (e.g. K1 > K2 > K3). No clear preference for the A or R-face of sapphire was seen. Cell coverage results on the A and R-face were similar for the K1 peptide and clone F02 under comparable assay conditions (Fig. 4-7*A*, 0.17 M ionic strength versus Fig. 5-1*A*), suggesting similar binding affinities between K1 and biopanned clones.

Two more peptide variants of K1 were designed and tested against the A-face of sapphire (Fig. 5-1*B*). The first, cK1, is the K1 peptide flanked by cysteine residues that form a disulfide linkage in the oxidizing environment outside the cell and therefore constrain the alternating lysine residues into a loop. This peptide showed binding comparable, if not slightly better, than the unconstrained K1 peptide. The second peptide, K1P, in which the second, fourth, and sixth glycine residues of K1 were replaced with proline, showed a significant decrease in cell binding over K1.

Although our cell-based experiments cannot resolve the detailed molecular interaction, they provide empirical evidence for the proposed interaction. From cell detachment assays (Sec. 4.3.3), a clear trend is noticed between the basicity of the peptide and the interaction strength, which suggests the importance of multiple charge interactions. The importance of electrostatic interaction strength between peptide and surface is shown empirically by two experiments. First, altering the ionic strength, which modulates electrostatic interactions by charge screening, was shown to affect

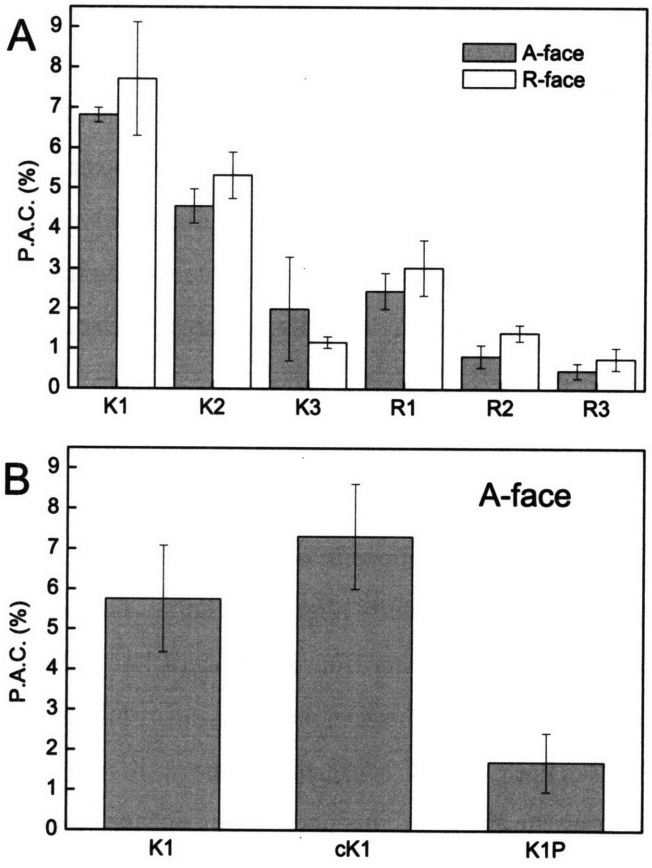

Figure 5-1: *Designer dodecamer peptides (Table 5.1) against sapphire.* (A) Yeast clones with peptides of various residue grouping bound in PBS-BSAT to the A- (grey) and R-face (white) of sapphire. Each data point represents the average and standard deviation of binding from two independent experiments. (B) Variant forms of the K1 peptide bound in PBSBSAT to the A-face of sapphire. Each data point represents the average and standard deviation of binding from three independent experiments.

peptide mediated-cell binding (Sec. 4.3.4). Second, the difference between lysine and arginine binding in designed peptides may result from difference in the localization of charge on the side-chain group. The positive charge in lysine is confined to a primary amine while in arginine it is delocalized in the guanidinium group. This delocalization may weaken salt bridges with anions on the sapphire surface as compared to lysine and therefore result in a weaker binding interaction. The guanidinium group can also become oxidized, which would eliminate the positive charge, and disrupt electrostatic interaction with the surface. In addition, access of the positively charged groups to the surface may be greater in lysine than arginine due to a longer alkyl chain connecting the peptide backbone to the charged moiety, as well as having a smaller charged moiety (amine versus guanidinium) in order to access surface specific grooves.

The importance of side chain access to the surface is given empirically by binding experiments with the designed peptides. In a linear peptide chain, alternating amino acid side chain groups orient in opposite directions. Therefore, in neighboring amino acids it is energetically unfavorable to align side chains. Grouping of charged residues into neighboring amino acids, going from sequence K1 to K2 to K3, would decrease the ability of peptides to align charged residues and result in the observed decrease in binding. As the basic amino acids are grouped, it also leads to a decrease in charge coverage over the surface. This decrease in surface coverage is not believed to be a factor because constrained peptide cK1 bound on the order of K1 while being constrained to a smaller net surface area. Additional evidence for the importance of charge alignment is seen by introducing rigid kinks in the peptide backbone with proline residues, with clone K1P, and the resulting decrease in peptide mediated cell binding. Even so, From an engineering perspective, these results are encouraging because it suggests the ability to tune the affinity of the peptide by simply changing the number of charged groups or the flexibility of the backbone. In addition, the binding could be modulated simply by altering the ionic strength of the buffer. These effects were explored later in this chapter with peptides expressed as affinity tags on maltose binding protein.

5.3.2 Peptide mediated adhesion of maltose binding protein (MBP) to sapphire

In order to demonstrate applicability of these peptides as affinity tags in protein bioassays, we engineered two forms of the maltose binding protein (MBP): with and without a c-terminal K1 peptide. Engineering and purification of MBP, a good model protein because its stability in E. coli leads to large expression and high yield purifications, was accomplished using the pMAL expression kit from New England Biolabs. Binding to sapphire was measured by the activity of HRP conjugated to an anti-MBP antibody. Figure 5-2*A* shows the significantly improved binding (over several orders of magnitude) of K1 peptide equipped with MBP (MBP-K1) over the nave MBP (MBP*) to the A-face of sapphire. The binding of MBP-K1 was significantly more than background at $\sim$ nanomolar concentrations and bound in similar quantities to MBP* at 500-1000 fold lower concentrations. Half-maximal binding for MBP-K1 occurred between $\sim 10^{-7}$-10^{-6} M, which is slightly lower in concentration than the half-maximal inhibition found from soluble F02 peptide (Fig. 4-7*B*). Deriving a dissociation constant from this assay, however, is difficult for a couple reasons. First, endpoint measurement of absorbance was prone to saturation non-linearities and therefore limited the dynamic range of the signal. Second, assays were carried out in plastic wells that also had intrinsic binding to tested proteins and therefore skewed quantitative results. A modified ELISA was developed to address these issues and results were presented in Sec. 5.3.3.

Figure 5-2*B* shows the selectivity of each crystal face for MBP-K1 over MBP* at an incubation concentration of 10 μg/mL ($\sim$0.23 μM). All three faces demonstrate similar affinities for the protein, again suggesting the lack of geometric specificity of the peptides towards each surface. Interestingly, although the C-face binds MBP* better than the other faces, it also shows a significant improvement in binding with the MBP-K1 protein. Such specificity could not be demonstrated with the yeast as endogenous yeast binding to the C-face masked any potential peptide-specific binding.

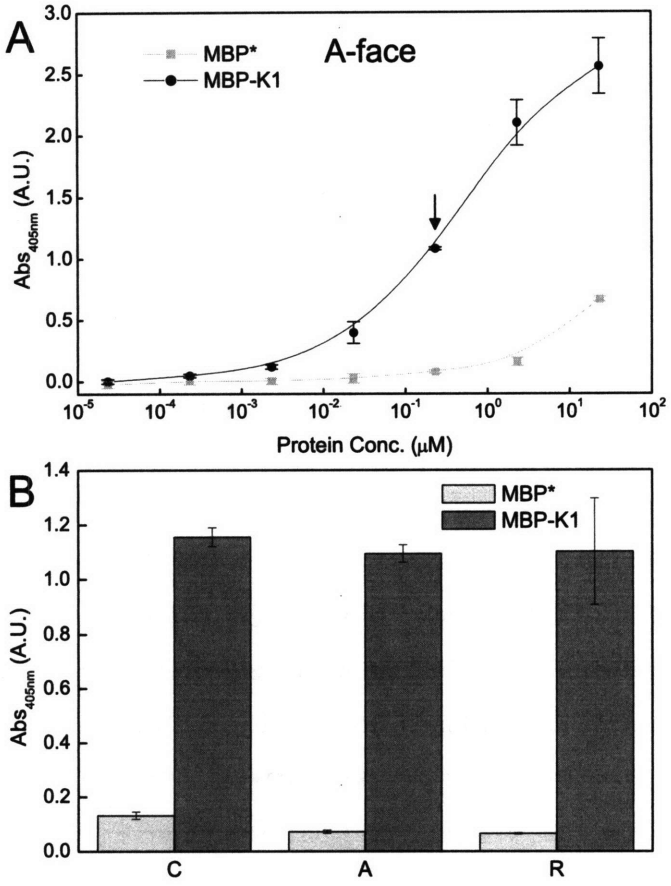

Figure 5-2: *Measurement of maltose binding protein adhesion to single crystalline sapphire.* Adhesion was performed in PBST buffer. Protein MBP-K1 contains the K1 peptide (Table 5.1) at the end of linker at the c-terminus. Protein MBP* is the same construct minus the twelve-amino acids of K1. Adhesion is measured through a chromogenic reaction with horse radish peroxidase, which is conjugated to an anti-MBP antibody. Absorbance is measured at 405 nm and subtracted from absorbance of no protein controls. (A) Adhesion of MBP-K1 and MBP* to A-face sapphire at serial dilutions of the incubation concentration. Arrow represents the peptide concentrations used in part (B). (B) Adhesion of MBP-K1 and MBP* to C-, A-, and R-face of sapphire with an incubation concentration of 10 μg/mL (0.23 μM). Each data point represents the average and standard deviation of binding from at least two independent experiments.

5.3.3 Determination of equilibrium Dissociation constants with a modified ELISA

In order to obtain more quantitative affinity information, the MBP binding assay further was modified. First, sapphire substrates were incubated with protein in 96-well untreated polystyrene plates. Control experiments showed minimal background binding of proteins assayed to untreated polystyrene (unlike plasma treated polystyrene, which was explored quantitatively below). Second, the amount anti-MBP-conjugated HRP adsorbed onto the surface was measured by the enzymatic turnover rate rather than endpoint analysis, which greatly expanded the dynamic range of the assay. With these changes, modified MBP concentrations ($[P]_o$) were titrated over several orders of magnitude, and along with enzymatic rate ($[R]$), were used to find equilibrium Dissociation constants (K_D) by fitting a simple two paramter hyperbolic equation

$$[R] = \frac{[R]_{max}[P]_o}{K_D + [P]_o} \tag{5.1}$$

where $[R]_{max}$ is the other free parameter representing the enzymatic rate at saturating levels of binding. Equation 5.1 represents a Langmuir model that assumes first-order, reversible kinetics in which available protein is not significantly depleted upon binding.

This analysis was used to determine the K_D of K1 to sapphire and tissue culture treated polystyrene (TCT-ps). TCT-ps, created by exposing polystyrene to oxygen plasma or UV/ozone to leave a net negatively ionized surface [ref], is a common surface treatment in tissue culture due to its ability to promote cell adhesion [ref]. In this study, it was used as control amorphous surface to contrast the structured crystalline sapphire. Equilibrium binding curves are shown in Fig. 5-3 and parameters listed in Table 5.2. MBP-K1 bound sapphire at $K_D \sim 80$ nM, which was in fairly close agreement to values estimated from early binding analysis (Fig. 5-2A). MBP-K1 bound TCT-ps at $K_D \sim 360$ nM, an approximately five fold lower affinity than sappire.

The effect of increasing positively charged amino acids on binding affinity was tested by linking two K1 sequences together between an alanine-serine spacer. This

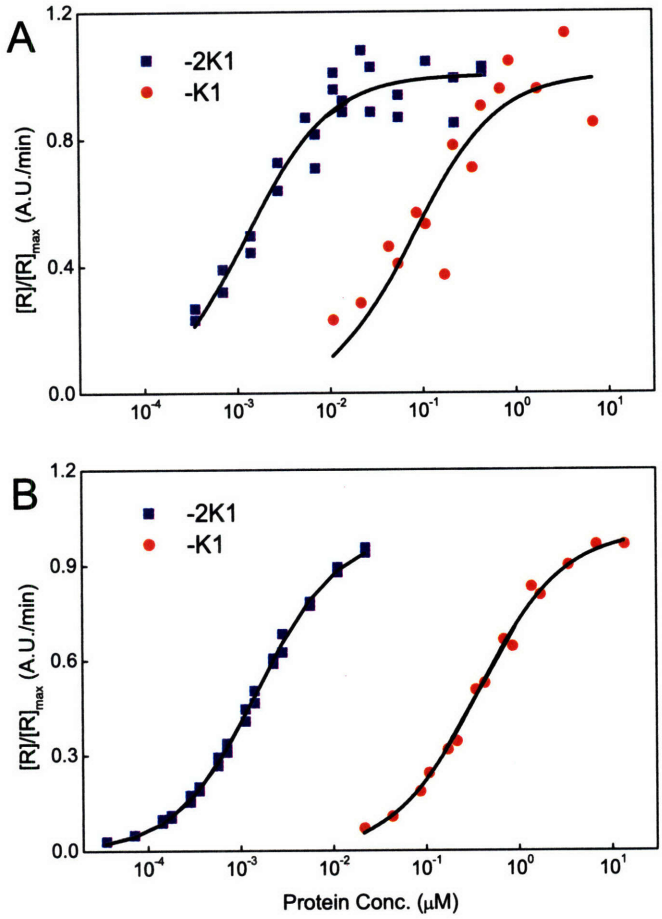

Figure 5-3: *Modified ELISA assay results for peptides K1 and 2K1 against sapphire and tissue culture treated polystyrene (TCT-ps).* Peptides K1 and 2K1 (Table 5.1) were attached to the c-terminus of MBP an data gathered as described in Sec. 5.5.4. MBP-K1 (●) and MBP-2K1 (■) are tested against (A) sapphire and (B) TCT-ps. Enzymatic rates ($[R]$) are normalized to parameter ($[R]_{max}$) of Eq. 5.1 and best fits (Table 5.2) represented by the solid lines.

new peptide (2K1) was cloned onto the c-terminus of MBP and tested for binding to sapphire and TCT-ps (Fig. 5-3). Doubling the length of K1, increased the affinity towards sapphire 50 to100-fold, with an apparent K_D of 1.3 nM. Similarly, binding to TCT-ps was dramatically increased with apparent K_D of 1.47 nM for MBP-2K1. These results demonstrate that it was possible to modulate the affinity of these peptides by altering the number at basic amino acids. Increasing the multiplicity of peptides to increase affinity had been also demonstrated by Tamerler et al., who report that tripling a selected gold-binding peptide into a 42 amino acid peptide increases equilibrium dissociation constants to 10^{-7}-10^{-6} M, with binding energies on the order of self-assembled monolayers [142]. The nanomolar affinities demonstrated by K1 and 2K1 are even greater than the 42 amino acid gold-binding peptide, and are on par with many antibodies.

By creating a His-tagged MBP clone (Table 5.1), it was possible to compare the affinity of designed sapphire binding peptides to a commonly used affinity tag for protein purification and immobilization, His-tag and nickle-NTA, under identical assay conditions. Results are presented in Table 5.2. With a K_D of approximately 30 nM, the His-tag Ni-NTA interaction was between 2K1 and K1. In fact, concentrations of MBP-K1 at $\sim 10^{-6}$ M that exhibited clear binding to sapphire were similar to concentrations used for capture of His-tagged proteins onto Ni-NTA covered plates [61]. Therefore, it should be possible to use the sapphire affinity tags for similar protein immobilization applications as His-tags. An advantage of the sapphire tags over His-tags is the lack of surface chemistry necessary to modify substrates. A disadvantage, conversely, is that the electrostatic mechanism of binding is less specific and more sensitive to buffer ionic strength. In fact, using the strategy of increasing the number of basic amino acids to increase affinity may lead to a trade-off between affinity and specificity, as a more basic peptide will have increased interaction with all electronegative surfaces.

In order to look more closely at the specificity of peptides towards sapphire, two more peptides were cloned onto the c-terminus of MBP: R1 and K6 (sequences in Table 5.1. Expressed on yeast, R1 showed a significantly lower binding affinity towards

Table 5.2: Best fit parameters to Eq. 5.1 from modified ELISA

Name	Substrate	K_D (nM)	$[R]_{max}$ (A.U./min)
K1	sapphire[a]	80 ± 45	0.34 ± .05
	TCT-ps[b]	360 ± 4	1.14 ± .04
2K1	sapphire	1.3 ± 0.3	0.34 ± .01
	TCT-ps	1.47 ± 0.07	1.54 ± .03
R1	sapphire	460 ± 395	0.22 ± .05
	TCT-ps	130 ± 34	1.29 ± .06
K6	sapphire	320 ± 127	0.38 ± .05
	TCT-ps	101 ± 23	1.23 ± .05
H6	Ni-NTA[c]	30 ± 3	1.48 ± .06

[a]The A- and R-face combined.
[b]Tissue Culture Treated-polystyrene by vacuum gas plasma.
[c]Qiagen Ni-NTA HisSorb plates.

A and R-sapphire (Fig. 5-1*A*), while K6 did not bind under similar assay conditions (data not shown). Consistently, each peptide expressed as MBP fusions also showed a reduced affinity (~4-10 fold relative to K1) so sapphire (Table 5.2). Interestingly, specificity to TCT-ps was reversed as both K6 and R1 showed a greater affinity to TCT-ps (~3-4 fold) than K1. These results suggest that lysine preferentially interacts with the structurally organized sapphire surface anions (K1 vs. R1) and that the ability to orient all basic groups in one directions is more important for crystalline surfaces than amorphous materials (K1 vs. K6). In order to validate these hypotheses, further molecular based simulations for peptides against sapphire are being done.

5.3.4 Non-equilibrium association and dissociation of peptide 2K1 on TCT-ps

Determining the time for the peptides to reach equilibrium and then the time for it to be removed from the surface is important for downstream application development. For this reason, association and dissociation assays were performed with MBP-2K1 binding to TCT-polystyrene (Fig. 5-4). Three concentrations of MBP-2K1 (22 nM,

4.4 nM, and 0.9 nM) were chosen to bracket the previously calculated K_D of 1.5 nM, and then incubated with TCT-ps for various times up to twenty minutes. Figure 5-4*A* shows that all three concentrations neared equilibrium after twenty minute incubations. Fitting the data to a rising exponential function gave time constants for association of 0.0024 s^{-1}, 0.0042 s^{-1}, and 0.022 s^{-1}, for each respective higher concentration. Making the pseudo-first order approximation of non-depleting protein concentrations, the kinetic rate parameters k_{on} and k_{off} were estimated from the slope and intercept, respectively, from a linear fit of assoc. time constant versus concentration. This resulted in a k_{on} of 9.7×10^5 $M^{-1}s^{-1}$ and a k_{off} of 0.0008 s^{-1}. From these values, it was possible to calculate a non-equilibrium estimate of K_D of 0.8 nM, which was approximately one-half of the the equilibrium measured value of 1.5 nM.

Figure 5-4*B* shows the dissociation of MBP-2K1 from TCT-ps at the same three concentrations as above. Surprisingly, after 24 hours of washing, only about 20-30 % of protein was removed from the surface. Decay time constants of 1.8×10^{-6} s^{-1}, 2.2×10^{-6} s^{-1} , 4.6×10^{-6} s^{-1}, for each respective higher concentration, were fit to the data and corresponds to a decay half-life of approximately 60 hours. This data suggests that peptide 2K1 is suitable for applications of protein surface labeling that last up to a few days. Interestingly, the decay constants from the dissociation experiment are almost three orders of magnitude slower than the estimated k_{off} from the association experiment. This discrepancy might be explained by a two-step binding event in which a loosely associated state transitions to a more tightly bound state. Physically, the loosely bound state might represent the protein domains interacting with the surface and the 2K1 peptide only partially bound, while the tightly bound state would represent a rearrangement so that the protein domains are now oriented away from the surface and the 2K1 peptide fully complexed with the surface. The assays above would only measure the tightly bound protein, as the loosely associated state would either by removed or transitioned to tightly bound during the numerous rinses or 20 minute antibody incubation. Therefore, the dissociation experiment (Fig. 5-4*B*) measures the detachment from the tightly bound state (slow k_{off}), while the

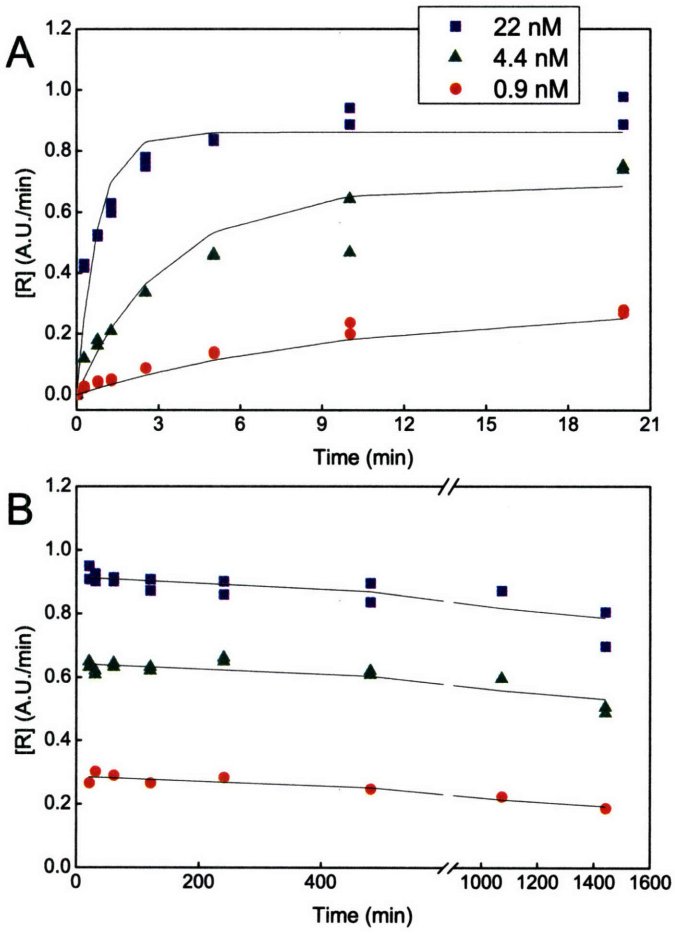

Figure 5-4: *Timecourse experiments of MBP-2K1 on tissue culture treated polystyrene (TCT-ps).* (A) Association of MBP-2K1 to TCT-ps at three separate concentrations (■: 22 nM; ▲: 4.4 nM; ●: 0.9 nM) measured by enzymatic rates ($[R]$) of HRP conjugated to anti-MBP antibody. (B) Dissociation of the same concentrations of MBP-2K1 from TCT-ps after a 20 minute association time. Solid lines represent best fits of the data to simple exponential rise and decay functions for association and dissociation graphs, respectively. See Sec. 5.3.4 for discussion of values.

association experiment concerns the flux between the unbound, loosely bound, and tightly bound protein, and hence a faster estimated k_{off}. Further experimentation with varying incubation times followed by dissociation timecourses would be necessary verify the two-step model and parse out the individual rate parameters.

5.3.5 Versatility of peptide 2K1 as a general protein affinity tag towards oxide materials

Peptide 2K1 was characterized further to determine its utility as a general affinity tag. Figure 5-5*A* shows 2K1 binding to TCT-ps at various ionic strength solutions. Binding resembled the biphasic behavior seen with peptide F02-mediated yeast adhesion to sapphire (Fig. 4-7*A*). In this case, the decrease in binding at low ionic strength may be explained by the repulsion of net negative MBP protein (pI~5 with -11 net charge at neutral pH) and negatively ionized TCT-ps surface. Maximal binding occurs near the ionic strength of 1 x PBS (166 mM), which makes the tag suitable for bioassays performed at physiological conditions. At ionic strength greater than 350 mM, binding is almost eliminated due to charge screening between peptide and surface. This property is advantageous in that it should allow for easy refurbishing of substrates and sensors by incubation with high salt buffers.

In this study, synthetic sapphire was chosen as a model metal oxide material. However, many applications will require different oxide based materials, so it is important to consider how general this technique will be to other oxide materials. Peptide 2K1 was tested for binding to a panel of silicon oxide substrates (Fig 5-5*B*). Affinity of the peptide varied greatly on the various materials with a general trend of more structured substrates leading to more binding. Binding was similar between A-face of sapphire and the C-face of single-crystalline quartz (represented by Z in the figure), both highly ordered oxide surfaces. Binding to a less ordered oxide, thermally grown silicon dioxide on a Si wafer (T) was approximately half of quartz. Binding to amorphous silica, in the form of a borosilicate microscope slide (S), was reduced to almost background levels. It is uncertain whether binding was directly related to

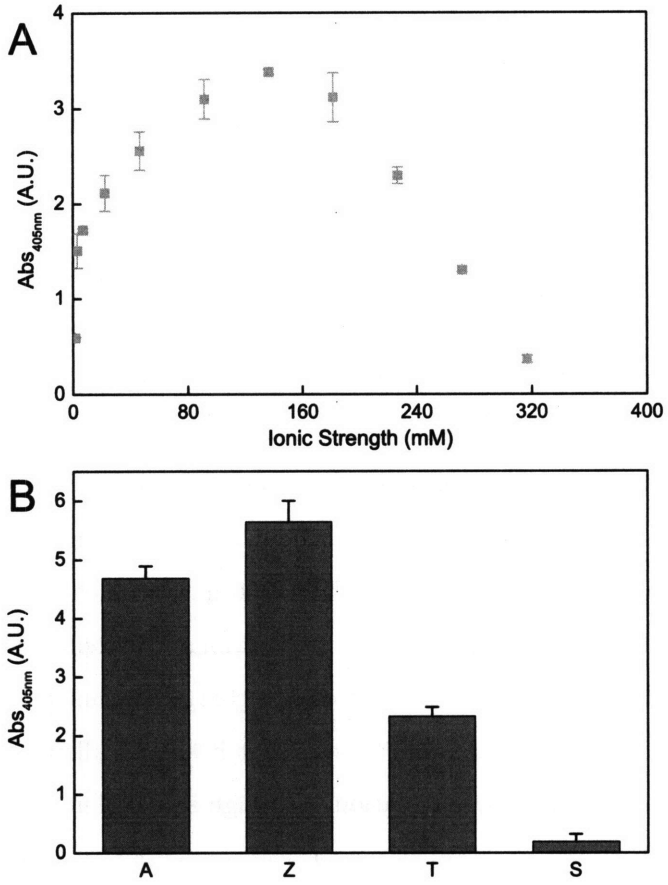

Figure 5-5: *Characterization of peptide 2K1.* (A) Effect of ionic strength on the binding of MBP-2K1 to TCT-ps. Protein incubated at a final concentration of 0.1 μg/mL in 0.1xPBST supplemented with various concentrations of NaCl. (B) Binding of MBP-2K1 to various oxide substrate. A: A-face sapphire; Z: Z-cut quartz (single-crystal SiO_2); T: Thermally grown 100 nm SiO_2 layer on Si wafer; S: standard microscope slide (borosilicate glass). Protein incubated at a final concentration of 1 μg/mL in 1xPBST For both experiments, absorbance at 405 nm was measured after a 10 minute incubation period in an ABTS reaction mix. Each data point represents the average and standard deviation of binding from two independent substrates.

atomic order, or whether the atomic structure in these substrates just increased the level of surface anions (oxygen). We propose the latter since amorphous TCT-ps did not exhibit long-range atomic order but bound peptides with high affinity. In either case, the ability of 2K1 to bind a variety of oxide materials increases its value as a general protein affinity tag. This value is demonstrated in the next chapter as peptide 2K1 is used to functionalized a SiO_2 mass sensor.

5.4 Conclusions

Through a variety of physiochemical binding tests, peptides were shown to interact with sapphire through multiple basic amino acids that mediate local electrostatic interactions with surface anions. The best rationally designed peptides were able to adhere yeast cells at strengths equivalent to biopanning-enriched peptides while exhibiting much lower compositional complexity. To show applicability towards directed protein targeting of surfaces, peptides were cloned onto maltose binding protein (MBP) and shown to bind oxides with affinities similar to common peptide affinity tags. Targeting proteins to surfaces with peptide tags may provide a facile one-step alternative to covalent coupling chemistry in the assembly of protein biosensors. The next chapter will focus on preliminary efforts to demonstrate the utility of these tags in a variety of biochemical assays.

5.5 Experimental

5.5.1 Materials

Synthetic sapphire (α-Al_2O_3) windows were purchased from Crystal Systems (Salem, MA). The three orientations obtained were the C-plate (0 0 0 1), A-plate (1 1 -2 0), and R-plate (1 -1 0 2). The sapphire was produced by a heat exchanger method, cut with a tolerance of 2^o, polished to an 80/50 scratch/dig and a flatness of 10 waves per inch, as quoted by the manufacturer. Al_2O_3 substrates were refurbished for multiple

experiments by expose to fresh piranha solution (3:1 H_2SO_4: 30 wt% H_2O_2), followed by brief sonication in distilled water, and 70 % (v/v) ethanol in water.

5.5.2 Yeast displayed rationally designed peptide variants

Designed dodecamer peptide were prepared by genetically engineering oligos into the yeast display vector. Briefly, complementary oligos encoding the desired sequence and BstXI overhangs were annealed and then ligated into a BstXI digested pBPZ vector. Following electroporation into E. coli Electromax DH10B (Invitrogen, Carlsbad, CA), colonies were grown and DNA extracted for sequence confirmation. Correctly constructed vectors were than transformed into EBY100 yeast using the Gietz quick transformation protocol and maintained on SD media. Binding of clones to sapphire was tested as those in the ionic strength assay (Sec. 4.5.6) but with 1xPBS-BSAT buffer.

5.5.3 Modifying Maltose Binding Protein (MBP) with peptides and measuring affinity towards sapphire

Cloning peptides onto the c-terminus of MBP

The pMAL-c2x vector (New England Biolabs, Beverly, MA), which encodes for the cytoplasmic expression of MBP, was digested with EcoRI and HindIII to allow for insertion of oligonucleotides on the c-terminus. Complementary oligos with EcoRI and HindIII compatible ends, encoding sequences listed in Table 5.1, were annealed and ligated into the digested pMAL-c2x vector. Ligation reactions were transformed into chemically competent TOP10 E. coli (Invitrogen, Carlsbad, CA) and cloning success was verified through sequencing. Next, DNA from successful clones was transformed into chemically competent TB1 E. coli for protein expression.

Protein expression and purification

The procedures for expression and purification were taken from the pMAL Protein Fusion and Purification Kit (New England Biolabs, Beverly, MA). Briefly, TB1 E.

coli harboring the modified pMAL vectors were grown to mid-log phase in Glucose-Rich Media plus ampicillin before induction with IPTG to a final concentration 0.3 mM. After two hours of induction, cells were harvested by centrifugation and frozen overnight at -20 degrees. The cells were then thawed in cold water and lysed by probe sonication. The crude extract was separated from the insoluble cell mater by centrifugation and applied to an amylose resin column. The bound MBP constructs were then eluted from the column with 20 mM maltose in 1x column buffer (20 mM Tris HCl, 1 mM EDTA, 200 mM NaCl) and concentrated in 10000 MWCO Centricon Plus-20 centrifugal filtration devices (Millipore, Billerica, MA). Purification steps were monitored by SDS-PAGE and the final concentration of protein was calculated by absorbance at 280 nm and referenced with a known MBP standard from New England Biolabs.

Purification of peptide 2K1 was carried out exactly as above with noted exceptions. First, pelleted cells were resuspended and lysed in 1x column buffer supplemented with 1 M NaCl (CB-high salt). Branched, 2000 kDa Polyethyleneimine (PEI) was then added to the crude extract at a final volume ratio of 0.1 %, in order so elute and precipitate protein-bound nucleic acid. The crude extract was then washed over an amylose column with CB-high salt before eluting as mentioned above.

Measuring MBP bound to sapphire substrates

Purified protein stocks were serially diluted to the appropriate concentration in 1xPBS containing 0.1 % Tween20 (PBST). 250 μL of protein solution were added to clean sapphire substrates in 48-well plates and incubated for three hours under constant agitation on an orbital shaker. Substrates were washed twice, each time transferring to new wells containing 400 μL PBST and agitating for 15 minutes. Substrates were then transferred to wells containing a 2000-fold dilution of stock HRP conjugated anti-MBP monoclonal antibody (New England Biolabs, Beverly, MA) in PBS containing 5 mg/mL BSA (PBS-BSA) and agitated for 30 minutes. The substrates were washed two times as before with PBS-BSA then transferred to a 96-well plate. Next, 200 μL of chromogen solution (0.5 mg/mL ABTS (2,2'-Azino-di-(3-ethylbenz-thiazoline

Sulfonic Acid), 0.03 % hydrogen peroxide in 0.1 M citrate buffer, pH 4.2) was added to the sapphire substrates under agitation. After 15 minutes, the substrates were removed and the absorbance of each well was measured at 405 nm (A405) on a 96-well UV/Vis plate reader (SpectraMAX 250, Molecular Devices, CA). Raw absorbance values were then subtracted from a background reading taken from substrates exposed to no MBP (~0.2 AU).

5.5.4 Obtaining equilibrium Dissociation constants with modified ELISA

Modified ELISA were carried out in standard 96-well plates. Nickel-tri-nitroacetic acid binding was tested in Ni-NTA HisSorb plates (Qiagen). Tissue culture treated polystyrene binding was tested in BD-Falcon plates 35-3072. Sapphire binding was tested in untreated polystyrene plates (Corning 3651) with results averaged from both the A- and R-face. Protein stocks were serially diluted in PBST and 200 μL were added to the wells followed by a 30 minute incubation. During all incubation steps, plates were agitated at 400 rpm on an orbital shaker. Wells were rinsed three times with PBST and exposed to 200 μL of 1:2000 dilution of HRP conjugated anti-MBP monoclonal antibody as above. Following a 30 minute incubation with antibody, wells were again rinsed three times with PBST. In the case of sapphire binding, substrates were then transferred to new wells. Next, 20 μL of 5 mg/mL ABTS was combined with 160 μL of 0.1 M citrate buffer, pH 4.2, in each well. 20 μL of 0.3 % hydrogen peroxide was then added and absorbance measurements were immediately taken every twelve seconds for four minutes to observed color production at 405 nm. The slope of raw absorbance versus time were used to obtain rates of color production (Abs_{405nm}/min) and used as a metric for the amount anti-MBP antibody in the wells. The equilibrium Dissociation constant (K_D) was obtained by fitting rate values to a simple two-parameter hyperbolic equation (Eq. 5.1) using the NLS fitting tool in OriginPro (OriginLab, Northhampton, MA). 95 % confidence intervals were quoted for each parameter based on the standard error times the critical value from the

t-distribution at the given confidence value.

5.5.5 Timecourse experiments with modified ELISA

Experiments were carried out using protein MBP-2K1 on Tissue culture treated polystyrene 96-well plates (BD-Falcon plates 35-3072). For association experiments, protein stocks were diluted in PBST and 150 μL were added to the wells and incubated for a set period of time (from 20 minutes to 15 seconds). During all incubation steps, plates were agitated at 400 rpm on an orbital shaker. Wells were then rinsed two times with PBST and exposed to 150 μL of 1:2000 dilution of HRP conjugated anti-MBP monoclonal antibody as above. Following a 20 minute incubation with antibody, wells were again rinsed two times with PBST. The amount of HRP in each well was quantified as described in Sec. 5.5.4. Approximate kinetic rate parameters k_{on} and k_{off} was determined by fitting to a rising exponential using non-linear least squares regression. Dissociation experiments were performed in a similar manner except that a 20 minutes protein incubation was followed by washing that varied in time over a 24 hour period. Following a 20 minute incubation with antibody, protein that remained bound was measured through HRP enzymatic turnover and approximate values for k_{off} was determined by fitting to a decaying exponential function.

Chapter 6

The Application of Peptides as Versatile Affinity Tags

6.1 Summary

The ability to coat surfaces with functional protein is a major challenge in the construction of biosensors and bioassays. This chapter highlights various methods of using peptide 2K1 to create protein-functionalized oxide surfaces. First, two methods of micro-scale patterning 2K1-tagged MBP are described using standard soft-lithography techniques. Next, a method to selectively inhibit tagged-protein from electronically-biased indium tin oxide electrodes is described. Lastly, the utility of 2K1-tagged MBP in functionalizing a novel mass-based biosensor is demonstrated. The chapter closes with a prospectus on the future of peptides for inorganic materials covering topics from discovery and interrogation, to future applications.

6.2 Introduction

Protein-based biosensors (the integration of proteins and signal transducers) have long been utilized in applications for basic research, food science, and medical diagnostics. Similarly, protein-based arrays, the multiplexed linking of proteins to a solid support, are sought for the high-throughput study of proteins. Unfortunately, both devices are limited by the challenges of interfacing proteins with the solid-support, including loss of activity upon immobilization due to unfolding [111] and the complex chemistries necessary for efficient coupling. Current approaches typically utilize covalent schemes such as thiolylation [109] and silanization [6] for direct conjugation, or adsorption to functionalized layers that act as an intermediary between the surface and protein [52]. Ideally, the linking of protein to a surface would be facile, with high chemical and spatial specificity, non-denaturing, and reversible. Although conjugation schemes have been proposed to address some of these issues [64, 166], a more simplistic approach is desirable.

An alternative to chemical coupling may be peptide affinity tags that are genetically incorporated onto the protein genetically and can direct it to the solid support without the need for further chemistry on the surface or the protein. Additionally,

these peptide tags have the potential to control protein orientation, be highly specific, and provide reversibility. Affinity tags, such as the oligo-histidine (his-tags), have been widely used for binding proteins to solid nickel-NTA resins for protein purification. His-tags have also been used for protein conjugation to quantum dots [98], Ni-NTA functionalized self-assembled monolayers [86], and polymer surfaces [166]. Unfortunately, his-tags are not suitable for adhering with high affinity to all surfaces of interest. Inspired by biomineralization [94] and the templating of inorganics on biological surfaces [12, 136], an alternative approach is the selection of material-binding biomolecules from a random biological library [22, 23, 122, 156].

While many material-binding peptides have been reported and more research has recently gone into the study of these material-binding peptides (including work described in earlier chapters) there have been relatively few published examples of using these peptides as protein affinity tags [118]. Since oxide surfaces, such as SiO_2, or plasma-treated polymers, are common substrates in biological applications, an oxide-binding peptide, such as 2K1, with its ability to adhere proteins with nanomolar affinity, may be a good candidate as a versatile protein affinity tag. This chapter highlights three unique ways in which 2K1 may be used to immobilize protein to oxide-surfaces and closes with a broad overview of the future for material-selective peptides.

6.3 Results and Discussion

6.3.1 Micropatterning of affinity tagged proteins on oxide surfaces

The ability to functionalize surfaces on the micro-scale with biologically active molecules has shown utility in areas ranging from stem cell biology [75] and neurobiology [131], to immunology [38, 76]. Most biological micro-scale patterning techniques utilize a form soft lithography termed micro-contact printing (μCP). Initially developed for patterning self assembled monolayers by George Whitesides group [104], it was first

applied to direct protein patterning in 1998 [14, 67]. In general, this approach involves (1) creating polydimethylsiloxane (PDMS) elastomer "stamps" from a photolithographically patterned silicon wafer, (2) adsorbing a biomolecule on the PDMS stamp, then (3) transfer of the biological to a desired substrate by contact stamping. [71]. This general procedure was used to guide the development two schemes for micropatterning affinity tagged proteins on oxide surfaces (Fig. 6-1).

The first scheme, termed microscale Plasma-Initiated Patterning (μPIP), involves first patterning the surface with plasma, and then incubating it with a protein that selectively binds the plasma-treated surface [83]. This method (depicted in Fig. 6-1 left) was used to bind MBP-2K1 to O_2-plasma treated regions of a polystyrene substrate. Briefly, a PDMS mold was used to mask a polystyrene (PS) surface. Next, the layers were treated with an O_2-plasma, which oxygenates exposed regions into a highly electronegative hydrophilic surface [39, 69, 114]. The PDMS mold was then removed to expose both PS and plasma-treated polystyrene (PT-PS). MBP-2K1, which has nanomolar affinity toward oxygenated PS (Table 5.2), was then incubated with the substrates. Figure 6-1*A* shows adhesion of immuno-stained MBP-2K1 to a PT-PS region and not an untreated PS region.

As described, this method could still benefit from some optimization. First, using a PDMS mold as a simple mask does not allow for facile patterning on the microscale as the short-lived plasma-induced reactive species cannot penetrate into microchannels under the mold. Fortunately, simple lithographic techniques have been described to patterned PT-PS features into PS [88, 100]. Also, the pre-patterning method is somewhat limited to materials that can be selectively oxygenated with plasmas or UV/ozone treatment, which consist of mainly carbonaceous polymers. Still, given the inherent cell adhesion properties of plasma-treated polymers, specifically PT-PS over PS [36, 37, 149], adding the ability to selectively target proteins to the PT-PS with affinity tags should greatly increase the functionality of these systems.

The second patterning scheme (Fig. 6-1 right) is much closer to traditional μCP and was used to pattern MBP-2K1 onto TCT-PS (tissue-culture-treated polystyrene by UV/ozone exposure). Briefly, a PDMS stamp is activated by exposure to O_2-

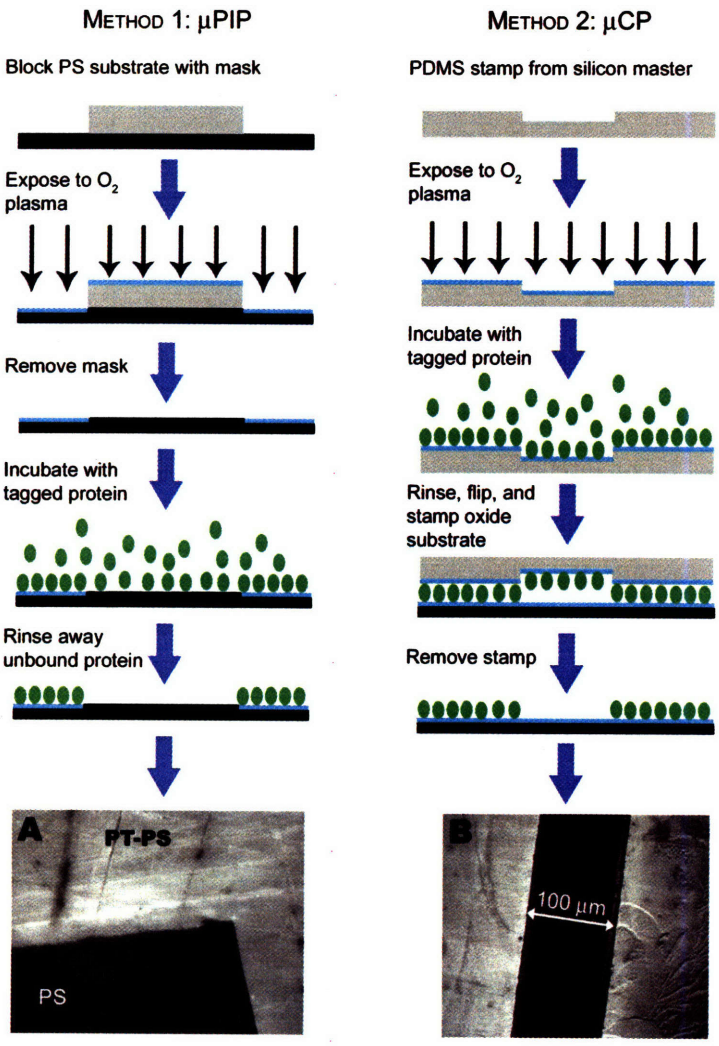

Figure 6-1: *Surface patterning of tagged proteins.* Two methods for patterning peptide tagged proteins onto oxide surfaces. (Left) μPlasma-Initiated Patterning (μPIP). A hydrophobic organic surface, such as polystyrene (PS), is masked in a desired pattern and selectively oxidized (represented with light blue surface) with O_2 plasma. The mask is then removed and the proteins preferentially bind to the oxidized surface. (Right) μContact Printing (μCP). Protein is first bound to an oxidized polydimethylsiloxane (PDMS) stamp that is micro-patterned with standard soft-lithography techniques [165]. The protein is then transferred to an oxide surface with direct μ-contact stamping. (A) Immuno-labeled MBP-2K1 selectively bound to plasma-treated polystyrene (PT-PS) over polystyrene (PS). Imaged with 40x objective. (B) Immuno-labeled MBP-2K1 transferred to tissue culture treated polystyrene using the μ-contact stamping technique.

plasma and loaded with MBP-2K1. After incubation with protein and subsequent washes, the stamp is pressed onto TCT-PS to transfer the protein at the regions of contact. Figure 6-1*B* depicts a TCT-PS surfaced immuno-stained for MBP. Two regions of protein deposition are clearly visualized flanking a protein deficient 100 μm channel. Variations of the procedure showed that both the peptide 2K1 on MBP and the PDMS activation step are necessary for the efficient stamping of MBP onto TCT-PS (data not show). Using a similar procedure, it was shown that laminin could be micro-patterned onto plasma-treated PMMA for the alignment and growth of Schwann cells [130, 151].

In general, printing methods involving plasma treatment are simpler, more cost effective, less labor intensive, and more environmentally friendly than wet chemical methods [130]. In addition, plasma activation of the PDMS stamp greatly decreases the protein equilibration time over the more common hydrophobic PDMS surfaces [14]. Hydrophobic adsorption to the stamps may also lead to unwanted denaturing of the protein of interest [4]. The additional functionality of the peptide affinity tag, such as 2K1, for selectively adhering to plasma-treated surfaces should greatly expand the repertoire of proteins suitable for μCP, including extremely soluble proteins like MBP, without the requirement for long incubation times as required with hydrophobic surfaces.

6.3.2 Electronic removal of affinity-tagged proteins

As highlighted above, there has been considerable recent success with spatial patterning at molecular interfaces. Adding temporal on surfaces is another highly desired means of increasing functionality [81]. These strategies commonly involve functionalizing surfaces with molecules that respond to environmental stimuli such as light [66], temperature [65], and pH [97]. Of particular interest are surfaces that respond to electrical stimulus due to the potential for facile integration with well established microelectronic devices and the superior temporal resolution they provide. Most examples of electrochemically active surfaces involve specially functionalized self-assembled monolayers (SAMs) that either, reversibly change surface wettability [73, 82, 153], or

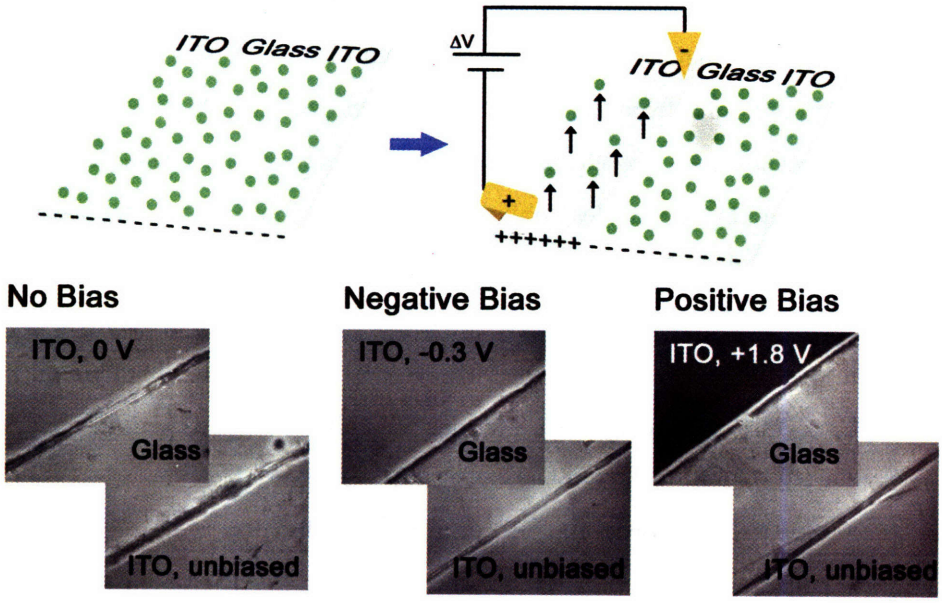

Figure 6-2: *Electronic removal of tagged proteins from patterned ITO.* Schematic of tagged protein binding to patterned ITO electrodes (top left) and selective binding inhibition with an applied positive bias (top right). (Bottom left) Immuno-labeled MBP-2K1 on patterned ITO electrodes with a 5 minute incubation and no applied bias. (Bottom middle) Immuno-labeled MBP-2K1 with a 5 minute incubation under -0.3 V bias. (Bottom right) Immuno-labeled MBP-2K1 with a 30 second incubation under -1.8 V bias. All Images taken with a 10x objective.

change surface reactivity [162].

A conceptually simpler approach, but not inherently reversible, is to use electrochemical desorption of surface adhered molecules to expose the underlying surface. This method was first shown by oxidative desorption of hydrophobic thiols on gold to change surface wettability [1], and later used to control cell migration [68]. More recently, it was shown the poly-L-Lysine-grafted-polyethylene glycol (PLL-g-PEG) could be electrochemically desorbed from indium tin oxide (ITO) surfaces. The bare ITO surfaces were then backfilled with functionalized PLL-g-PEG for the selective assembly of protein microarrays [143]. ITO surfaces are good candidates for biologically sensors due to their low electrical resistivity and high optical transparency [54].

Given the good oxide binding properties and similarity of multiple lysine residues

in both PLL and the affinity tag 2K1, we wanted to test whether it was possible to perform similar electrochemical desorption from ITO of 2K1-MBP. Figure 6-2 depicts the setup and results from 2K1-MBP desorption experiments. Briefly, ITO films on glass were etched into two electrically isolated electrodes. Proteins were then incubated with the ITO electrodes, while simultaneously biasing one electrode. The bias was then removed, and after washing and immuno-staining, the surfaces were imaged for the presence of MBP-2K1. As shown in Figure 6-2, applying a 0 V and -0.3 V bias for 5 minutes to the ITO did not alter the of MBP-2K1 versus the unbiased ITO electrode. Conversely, applying a +1.8 V bias for only 30 seconds significantly inhibited binding as compared to the unbiased electrode. Similar conditions were used by Tang et al. to selectively remove PLL-g-PEG from ITO electrodes, although they reported significant electrolysis of water at a +1.8 V, which wasnt seen in our experiments. The discrepancy might be attributed to the differences in electrochemical cells used. Conversely, electrolysis and destruction of the ITO electrode was seen at similar negative potentials and therefore large negatives bias could not be tested. Although the mechanism of protein removal with applied positive bias is not currently understood, it has been hypothesized to be due to either, accumulated positive surface charge repelling positively adsorbed molecules, or oxygen generated from electrolysis that reacts with adsorbed molecules and changes the physiochemical properties leading to adsorption [143].

The ability to selectively adsorbed proteins onto electrode surfaces may be important for the facile construction of protein arrays. An obvious advantage of using affinity-tagged proteins over PLL-g-PEG-biotin/Ni-NTA, is that fewer processing steps are involved to deposit proteins. For applications requiring large arrays, cutting the number of steps in one deposition cycle would significantly decrease the overall processing time. Another advantage is the possibility for lower applied potentials, due to the smaller size of affinity tags like 2K1 versus PLL. Advantages of the PLL-g-PEG system over affinity tags is the inherent anti-fouling properties of PEG, as well as the potential to functionalize one PLL-g-PEG chain many times and therefore increase protein packing density. Although more optimization is necessary, a combination of

affinity-tagged proteins and PLL-g-PEG may provide faster and more reliable protein array construction.

6.3.3 Functionalization of a mass sensitive suspended mass resonator (SMR)

With advances in microfluidic and microfabrication techniques, there has been a recent trend towards miniaturization of biosensors [123]. Advantages of these systems include high sensitivity, label-free sensing, small handling volumes, and parallelization. Recently, Burg et al. developed a microfabricated mass sensor using a fluid-filled cantilever with reported mass sensitivities down to approximately 300 attograms [25]. A schematic of the sensing mechanism is shown in Fig. 6-3*A*. Briefly, the suspended mass resonator (SMR) is driven to vibrate at its resonance frequency and monitored optically with a laser. As molecules are flowed into the cantilever, changes in effective mass of the cantilever are monitored as a change in resonance frequency. The increase in mass due to accumulation of adsorbed molecules on the walls, or the presence of large dense particles, dampens the resonance frequency of the cantilever. In this manner, SMR was shown suitable for measuring adsorbed antibodies as well as single gold and bacteria particles [25].

Although a highly sensitive and versatile technique, a constant challenge for SMR, and other surface sensing techniques such as surface plasmon resonance (SPR) and quartz crystal microbalance (QCM), is the ability to perform facile and specific surface functionalization. Traditional techniques utilize covalent bonding methods, such as thiol linkages to gold or silanization of oxide surfaces. Although forming highly stable surfaces, these methods are typically irreversible and therefore limit the versatility and lifetime of the device, especially for many microfabricated sensors, such as the SMR, in which the sensing surface is directly integrated into the whole apparatus. Therefore, the SMR is best suited for a reversible functionalization scheme that could be continually changed to meet the application. Ideally, the functionalization would be stable over the course of an experiment, non-fouling, versatile in conferring

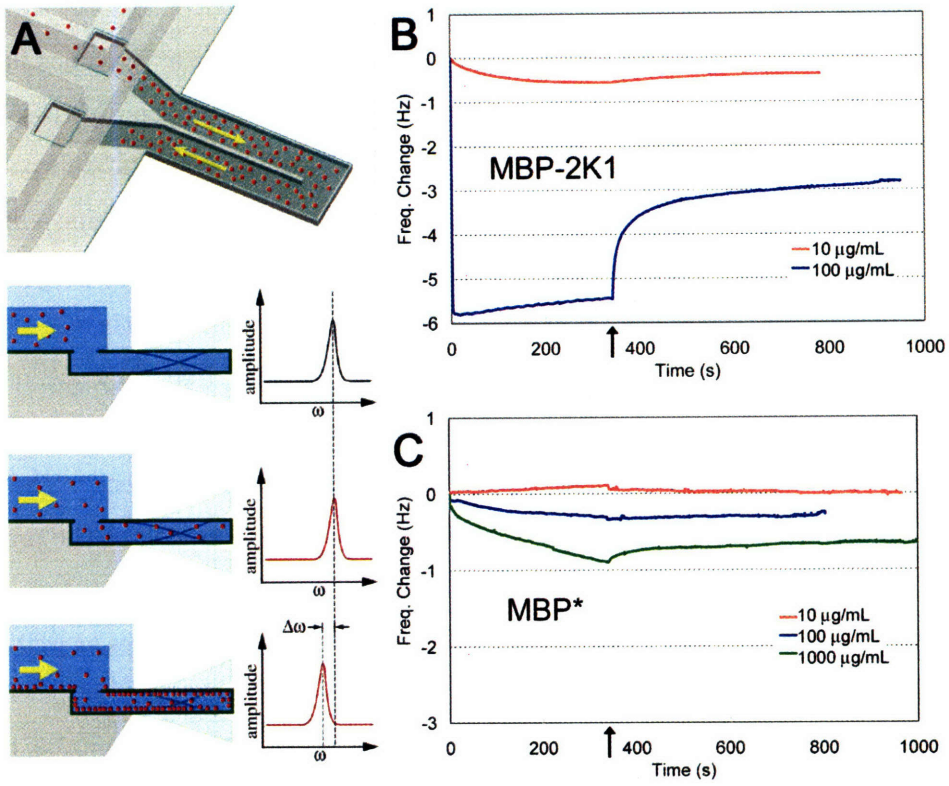

Figure 6-3: *MBP binding in Surface Mass Resonance (SMR) Sensor* (A) Schematic of SMR function upon the introduction and accumulation of molecules in the cantilever. Borrowed from ref. [26]. Dose response curves of (B) MBP-2K1 and (C) MBP* (MBP without 2K1 peptide), binding to SMR in 1xPBS. Protein introduced at time zero and flushed with buffer after 6 minutes (arrows).

specificity, and facile in preparation. A successful candidate has been the PLL-g-PEG-biotin polymers mentioned above, where the highly positively charged nature of PLL binds to the native surface oxide of the silicon cantilever in the SMR. This polymer was used to adhere biotinylated antibodies through a neutravidin intermediary layer [25]. Unfortunately, this process involves multiple steps that can be both time consuming and hard to standardize. An alternative may be functionalization with a protein layer that contains a genetically encoded surface affinity peptide.

Since affinity tag 2K1 directed protein binding to SiO_2 (Fig. 5-5), it was a good candidate for protein functionalization of an SMR. Figure 6-3*B* and *C* shows the 2K1-specific adhesion of MBP to the cantilever. The cantilever was saturated with MBP-2K1 at an incubation concentration of 100 μg/mL, and resulted in a 6 Hz frequency shift. Conversely, MBP without 2K1 (MBP*) caused only about a 1 Hz shift at a ten-fold higher concentration of 1 mg/mL (Fig. 6-3*C*). These experiments demonstrate the potential of 2K1 as an affinity tag for reversible functionalization in an SMR. Further experiments would need to optimize buffer conditions and concentrations to ensure consistent functional layers. Even so, an advantage of these non-covalent schemes is that the functionalization process can be monitored in real time. This allows for faster optimization, better quality control, and more consistency between multiple functionalizations. Future work will focus on adding functionality to the 2K1-tag construct, such as a specific receptor for analyte sensing, or protein A domains for facile antibody capture.

6.4 Experimental

6.4.1 Protein patterning on oxide surfaces

μPlasma-Initiated Patterning of MBP-2K1polystyrene

A PDMS mask was cleaned by sonication in 70 % (v/v) ethanol in water for 20 minutes and then let dry in air. Polystyrene surfaces were cleaned with three rinses with warm soapy water followed by three rinses with ethanol and ultra-pure water before drying

in air. PDMS was placed on polystyrene and surfaces exposed to oxygen plasma for one minute. PDMS mask was then removed and a solution of 10 μg/mL MBP-2K1 in PBST was applied to polystyrene plasma treated surfaces for 20 minutes. Surface were washed three times with 1 mL PBST. Next, 1 mL of anti-MBP mouse IgG, diluted 1:2000 from a 1 mg/mL stock (New England Biolabs) in PBS-BSA was incubated for 30 minutes before washing three more times with 1 mL PBST. A second 30 minute antibody labeling step was performed with 1 mL of 10 μg/mL goat-anti-mouse IgG-AlexaFluor488 in PBS-BSA, followed by an additional three washes. Substrates were then imaged using FITC filter sets and standard fluorescent microscopy techniques.

μContact Printing of MBP-2K1 on TCT-ps

PDMS stamp was cleaned by sonication in 70 % (v/v) ethanol in water for 20 minutes and then let dry in air. PDMS was then exposed to oxygen plasma for one minute followed by one minute exposure to ambient air. A 10 μg/mL MBP-2K1 solution in PBST was applied onto the stamp and let sit for 15 minutes. Excess protein was washed off by submersing PDMS in ultra-pure water 3 times followed by drying under a nitrogen stream. The stamp was then pressed onto tissue culture treated-polystyrene (TCT-ps; BD-Falcon 6-well plates, 35-3046) and let sit for 20 minutes. The stamp was then removed and stained with primary and secondary antibodies as described above.

6.4.2 Electronic removal of tagged proteins

Glass slides with a thin film of Indium Tin Oxide (ITO) were obtained by Delta Technology (Resistivity ~13-30 Ωcm). To create patterned ITO slides, silicon tape was used as a mask. Unmasked ITO was etched away to glass by exposure to agua regia (100 mL H_2O, 80 mL Hydrochloric Acid, 35 mL Nitric Acid) for 15 minutes followed by several rinses in ultra-pure water. After removel of silicon tape to expose the remaining ITO, slides were cleaned in piranha solution (3:1 H_2SO_4: 30 wt% H_2O_2) for 10 minutes, followed by brief sonication in ultra-pure water, and 70 %

(v/v) ethanol in water. Clean ITO surfaces were connected to a power source with an aluminium adhesive electrode and wells were created on clean ITO/glass slides with 1 cm diameter silicon gaskets (holding volume: 0.2 mL). 180 μL of PBST was added to the well and Pt and Ag counter and reference electrodes, respectively, were lowered into the well approximately 1 mm below the top of the meniscus. Next, 20 μL of 10 μg/mL MBP-2K1 was mixed into the well by pipette, followed by immediate exposure to an applied bias for a predetermined length of time. After exposure, the well was washed three times with PBST followed by antibody staining as described above, with all volumes adjusted to 200 μL.

6.4.3 Functionalization of biosensor surfaces

A suspended mass resonator (SMR) was fabricated and operated as described in refs. [26, 25], respectively. Before application of protein to the SMR, stock solutions of MBP-2K1 and MBP* were buffer exchanged into 1 x PBS with Zeba Desalt Spin columns (Pierce), followed by filtration through Ultra Free-MC 0.22 μm filters (Millipore). After cantilever surface cleaning with piranha solution, a typical experimental run consisted of the following steps: (1) equilibration of the sensor in 1 x PBS running buffer, (2) injection of the protein from the bypass channel, (3) washout of unbound protein with buffer, and (4) stripping the surface with high-salt buffer (0.1 M phosphate buffer, 1 M NaCl). Raw data was collected as described in [25], and reported after a few algebraic manipulations. Briefly, raw data was adjusted by subtracting out spikes in vibrational frequency due to variations in solution density between running buffer and protein solutions, and then normalized to the pre-protein injected frequency.

6.5 Future Directions

The first examples of peptides specific for binding and nucleating inorganic materials led to great excitement over the potential to facilely interface the biological and inorganic worlds. Unfortunately, material-specific biomolecules have shown mod-

est applicability due to the lack of underlying physical principles guiding discovery. Therefore, the field is still dependent on discovery from random biomolecule pools. For the potential of material-specific biomolecules to be realized, a better understanding of peptide specificity and affinity, through careful characterization, is necessary. I envision this will lead to a paradigm shift away from random discovery towards more directed search and design methods. Also, with a clearer picture on the scope of potential applications, peptides will be better tailored for their final application.

This thesis has been an attempt to begin addressing the gap in understanding with facile techniques to study the biological-inorganic interface. Findings from this thesis could be used to help guide future peptide construction methods. To my knowledge, there have been no reports of material-peptide screens with an affinity maturation step during the selection process. This is most likely due to fact that the affinity maturation steps are time and labor intensive and the most common mutation generation techniques are not ideal for mutating small peptides. Meanwhile, it was shown in Chapter 3 that a limited number of amino acids could individually confer peptide adhesion to materials with transition metal ions, while Chapter 4 and 5 highlighted the importance of basic amino acids for adhesion in oxide surfaces. This information may be useful for creating peptide libraries that favorably bias the library towards relevant amino acids. This will allow a researcher to screen a library with greater sequence diversity within a smaller region of all sequence space each with a higher percentage of relevant amino acids.

Another interesting result of our work was that most material specificity was compositionally-based and not sequence-based. Since small peptides have limited structural integrity in an aqueous environment, they are unable to reliably match lock-and-key with material surfaces. Ideally, the ability to harness both the structural and chemical specificity of biomolecules would lead to more specific (and therefore more broadly applicable) material binders. One possible avenue is to screen libraries of small structural domains. Recently, there has been interest in the protein therapeutic field to find and screen small structural domains that facilitate library variants in order to find an alternative to therapeutic antibodies [17, 62, 113]. Of particular

interest are small scaffolds that present modifiable surfaces built into pre-existing into secondary structure. Examples of these type of scaffolds include affibodies, from the alpha-helical bacterial receptor Z domain [110], and ankyrin repeat domains [16, 103]. These scaffolds combine geometric rigidity with the chemical diversity on permissible surface residues, which may allow for lock-and-key interactions to inorganic materials.

Taking another cue from the biological receptor-ligand engineering, important design rules and novel interactions may be predicted and/or studied with computational modeling. Green et al. recently demonstrated the power of computational modeling to re-design the binding specificity of calmodulin [56]. To date, there have been few examples of computational modeling applied to peptide-inorganic interactions. Oren et al. used simple molecular dynamics simulations to model peptide interactions to metallic platinum in vacuum [115]. More recently, Tomasio et al. showed that atomistic modeling of peptides to carbon nanotubes compared favorably to experiment [147]. Mitternacht et al. used a Monte Carlo sampling method to study the solution structure of four GaAs and Si binding peptides and found then to be largely unstructured [101]. Finally, Schravendijk et al. present a general method combining first principles DFT and atomistic simulation for studying hydrated peptides on metal surfaces [132]. With the ability to resolve interactions to the atomic scale, computational modeling provides a level of insight not possible with experimental methods. Current challenges include the tradeoff of developing models that accurately reflect the physical reality and maximizing computational efficiency (S. Kottmann, personal communication). It is also important to validate models with continual interplay between simulation and experimentation. With the development of more realistic and faster models, it may be possible for *in silico* peptide screening or directed design of novel interactions. In this manner, the extensive use of computers with experiment should speed the discovery and characterization of inorganic binding biomolecules.

As mentioned earlier, a continuing problem with screens against inorganics is the low frequency of clones that are suitable for the desired end application. While much of this may be solved by meticulous characterization of clones to improve or even eliminate the necessity of screening altogether, there are additional issues to

consider. First is that inorganic material surfaces are often processed and maintained in various ways and therefore even the same surface may present many structural abnormalities (step edges, dislocations, dopants, contaminants etc.). In order to maximize success, it is best to screen on well characterized surfaces in a state directly related to the desired application. Second, in many cases the desired application for peptides is selective nucleation of material. Because the link between binding and nucleation is not necessarily linearly correlated [119], many current biopanning methods fail to provide clones for the desired nucleation process. An open challenge to the field is the development of growth-specific selection schemes for biomolecules. Currently, these methods are hampered by the inability to assay for nucleation and isolate respective clones in a high throughput manner. Also, nucleation depends on numerous parameters other than peptide properties, including temperature, time, and chemical precursors. Ideally, these would be optimized before the screening process. An approach may be to first study rationally designed peptides on a smaller scale, which would enable hypothesis testing and limit the scope of a larger peptide screen [119] . Recently, advances have been made in using microfluidic devices to rapidly screen protein crystallization conditions [57]. Eventually, these devices may be good medium-throughput candidates to screen for nucleating peptides.

The future application of material-specific biomolecules will largely depend on the progress of many of the above mentioned techniques. Even so, applications should be targeted that take advantage of the unique aspects of the biomolecules. In engineering any given interaction with an inorganic material, biology cannot match the chemical diversity of synthetic chemistry. Chemical diversity allows for a range of interactions, from weaker long-range interactions to covalent bonds, but the interactions are usually based on first principles or low-throughput empirical testing and require time consuming synthesis. Protein interactions, conversely, are limited to the chemical diversity of the naturally encoded amino acids, but can be discovered with convenient high-throughput biopanning methods. Assuming a suitable interaction is found, additional advantages of biomolecules include the ability to site-specifically fuse them in a modular fashion to a protein of interest or a biological scaffold, and

produce them with scalable biomanufacturing methods.

Taken together, the advantages suggest a few obvious applications of material-specific biomolecules. First, as described in introduction and body of this chapter, is the use as peptide affinity tags for facile surface functionalization with proteins and cells. They alleviate the need for prior chemical surface functionalization and the non-covalent attachment is ideal for multi-purpose surfaces which require reusability. Such surfaces include micro-fabricated sensors, such as the SMR, and bioseparation resins. Currently, only a few peptide affinity tags directly recognize the solid support for protein purifications, including the common polyhistidine tag. Finding other tags that specifically recognize common materials such as silica and alumina could greatly increase the versatility while decreasing the cost of bioseparations. Another ideal use of material-specific peptides is the supramolecular organization of inorganic material on biological scaffolds. While chemists and physicists are exploring methods to assemble materials with dimensions on the nanometer scale, biology has evolved proteinaceous scaffolds, such as viruses and structural filaments, on this scale with atomic level specificity. The ability to site-specifically place peptides at unique places on biological scaffolds adds versatility to the approach, as demonstrated by the ability to organize quantum dots [87] or create nanowires [95] on the same organism by utilizing different peptide attachment schemes. Peptide-based nucleation on biological scaffolds may also prove useful in low energy, large-scale production of inorganic materials. Used in only two ways, as affinity tags and nucleation tags, material-specific peptides have the potential to impact fields as diverse as medicine, biotechnology, and electronics. With continued efforts to understand the peptide-material interface, this potential hopefully will be realized in the near future.

Bibliography

[1] N. L. Abbott, C. B. Gorman, and G. M. Whitesides. Active control of wetting using applied electrical potentials and self-assembled monolayers. *Langmuir*, 11(1):16–18, 1995.

[2] J. Aizenberg, G. Lambert, S. Weiner, and L. Addadi. Factors involved in the formation of amorphous and crystalline calcium carbonate: a study of an ascidian skeleton. *J Am Chem Soc*, 124(1):32–9, 2002.

[3] J. Aizenberg, S. Weiner, and L. Addadi. Coexistence of amorphous and crystalline calcium carbonate in skeletal tissues. *Connect Tissue Res*, 44 Suppl 1:20–5, 2003.

[4] J. D. Andrade and V. Hlady. Protein adsorption and materials biocompatibility - a tutorial review and suggested hypotheses. *Advances in Polymer Science*, 79:1–63, 1986.

[5] A. R. Asthagiri, C. M. Nelson, A. F. Horwitz, and D. A. Lauffenburger. Quantitative relationship among integrin-ligand binding, adhesion, and signaling via focal adhesion kinase and extracellular signal-regulated kinase 2. *J Biol Chem*, 274(38):27119–27, 1999.

[6] V. R. S. Babu, M. A. Kumar, N. G. Karanth, and M. S. Thakur. Stabilization of immobilized glucose oxidase against thermal inactivation by silanization for biosensor applications. *Biosensors & Bioelectronics*, 19(10):1337–1341, 2004.

[7] Edmund Baeuerlein. *Biomineralization : from biology to biotechnology and medical application.* Wiley-VCH, Weinheim ; New York, 2000.

[8] I. A. Banerjee, L. Yu, and H. Matsui. Cu nanocrystal growth on peptide nanotubes by biomineralization: size control of cu nanocrystals by tuning peptide conformation. *Proc Natl Acad Sci U S A*, 100(25):14678–82, 2003.

[9] C. F. Barbas, J. S. Rosenblum, and R. A. Lerner. Direct selection of antibodies that coordinate metals from semisynthetic combinatorial libraries. *Proceedings of the National Academy of Sciences of the United States of America*, 90(14):6385–6389, 1993.

[10] J. P. Bearinger, J. Voros, J. A. Hubbell, and M. Textor. Electrochemical optical waveguide lightmode spectroscopy (ec-owls): A pilot study using evanescent-field optical sensing under voltage control to monitor polycationic polymer adsorption onto indium tin oxide (ito)-coated waveguide chips. *Biotechnology and Bioengineering*, 82(4):465–473, 2003.

[11] A. M. Belcher, P. K. Hansma, G. D. Stucky, and D. E. Morse. First steps in harnessing the potential of biomineralization as a route to new high-performance composite materials. *Acta Mater.*, 46(3):733–736, 1998.

[12] A. M. Belcher, X. H. Wu, R. J. Christensen, P. K. Hansma, G. D. Stucky, and D. E. Morse. Control of crystal phase switching and orientation by soluble mollusk-shell proteins. *Nature*, 381(6577):56–58, 1996.

[13] Angela M. Belcher and Erin E. Gooch. Protein components and inorganic structure in shell nacre. In *Biomineralization : from biology to biotechnology and medical application*, pages 221–249. Wiley-VCH, Weinheim ; New York, 2000.

[14] A. Bernard, E. Delamarche, H. Schmid, B. Michel, H. R. Bosshard, and H. Biebuyck. Printing patterns of proteins. *Langmuir*, 14(9):2225–2229, 1998.

[15] S. K. Bhatia, J. S. Swers, R. T. Camphausen, K. D. Wittrup, and D. A. Hammer. Rolling adhesion kinematics of yeast engineered to express selectins. *Biotechnol Prog*, 19(3):1033–7, 2003.

[16] H. K. Binz, P. Amstutz, A. Kohl, M. T. Stumpp, C. Briand, P. Forrer, M. G. Grutter, and A. Pluckthun. High-affinity binders selected from designed ankyrin repeat protein libraries. *Nature Biotechnology*, 22(5):575–582, 2004.

[17] H. K. Binz, P. Amstutz, and A. Pluckthun. Engineering novel binding proteins from nonimmunoglobulin domains. *Nature Biotechnology*, 23(10):1257–1268, 2005.

[18] E. T. Boder and K. D. Wittrup. Yeast surface display for screening combinatorial polypeptide libraries. *Nat Biotechnol*, 15(6):553–7, 1997.

[19] E. T. Boder and K. D. Wittrup. Optimal screening of surface-displayed polypeptide libraries. *Biotechnol Prog*, 14(1):55–62, 1998.

[20] E. T. Boder and K. D. Wittrup. Yeast surface display for directed evolution of protein expression, affinity, and stability. *Methods Enzymol*, 328:430–44, 2000.

[21] B. C. Braden, F. A. Goldbaum, B. X. Chen, A. N. Kirschner, S. R. Wilson, and B. F. Erlanger. X-ray crystal structure of an anti-buckminsterfullerene antibody fab fragment: biomolecular recognition of c(60). *Proc Natl Acad Sci U S A*, 97(22):12193–7, 2000.

[22] S. Brown. Engineered iron oxide-adhesion mutants of the escherichia coli phage lambda receptor. *Proc. Natl. Acad. Sci.*, 89(18):8651, 1992.

[23] S. Brown. Metal-recognition by repeating polypeptides. *Nature Biotechnol.*, 15(3):269–72, 1997.

[24] S. Brown, M. Sarikaya, and E. Johnson. A genetic analysis of crystal growth. *J Mol Biol*, 299(3):725–35, 2000.

[25] T. P. Burg, M. Godin, S. M. Knudsen, W. Shen, G. Carlson, J. S. Foster, K. Babcock, and S. R. Manalis. Weighing of biomolecules, single cells and single nanoparticles in fluid. *Nature*, 446(7139):1066–1069, 2007.

[26] T. P. Burg, A. R. Mirza, N. Milovic, C. H. Tsau, G. A. Popescu, J. S. Foster, and S. R. Manalis. Vacuum-packaged suspended microchannel resonant mass sensor for biomolecular detection. *Journal of Microelectromechanical Systems*, 15(6):1466–1476, 2006.

[27] F. Caruso, T. Serizawa, D. N. Furlong, and Y. Okahata. Quartz-crystal microbalance and surface-plasmon resonance study of surfactant adsorption onto gold and chromium-oxide surfaces. *Langmuir*, 11(5):1546–1552, 1995.

[28] J. G. Catalano, C. Park, Z. Zhang, and P. Fenter. Termination and water adsorption at the alpha-al2o3 (012) - aqueous solution interface. *Langmuir*, 22(10):4668–4673, 2006.

[29] G. P. Cereghino and J. M. Cregg. Applications of yeast in biotechnology: protein production and genetic analysis. *Curr Opin Biotechnol*, 10(5):422–7, 1999.

[30] J. N. Cha, G. D. Stucky, D. E. Morse, and T. J. Deming. Biomimetic synthesis of ordered silica structures mediated by block copolypeptides. *Nature*, 403(6767):289–92, 2000.

[31] M. Chiappalone, A. Vato, M. B. Tedesco, M. Marcoli, F. Davide, and S. Martinoia. Networks of neurons coupled to microelectrode arrays: a neuronal sensory system for pharmacological applications. *Biosens Bioelectron*, 18(5-6):627–34, 2003.

[32] E. Comini. Metal oxide nano-crystals for gas sensing. *Analytica Chimica Acta*, 568(1-2):28–40, 2006.

[33] H. X. Dai, C. K. Thai, M. Sarikaya, F. Baneyx, and D. T. Schwartz. Through-mask anodic patterning of copper surfaces and film stability in biological media. *Langmuir*, 20(8):3483–3486, 2004.

[34] P. S. Daugherty, B. L. Iverson, and G. Georgiou. Flow cytometric screening of cell-based libraries. *J Immunol Methods*, 243(1-2):211–27, 2000.

[35] A. L. de Lacey, V. M. Fernandez, and M. Rousset. Native and mutant nickel-iron hydrogenases: Unravelling structure and function. *Coordination Chemistry Reviews*, 249(15-16):1596–1608, 2005.

[36] E. Detrait, J. B. Lhoest, B. Knoops, P. Bertrand, and P. V. D. de Aguilar. Orientation of cell adhesion and growth on patterned heterogeneous polystyrene surface. *Journal of Neuroscience Methods*, 84(1-2):193–204, 1998.

[37] J. L. Dewez, J. B. Lhoest, E. Detrait, V. Berger, C. C. Dupont-Gillain, L. M. Vincent, Y. J. Schneider, P. Bertrand, and P. G. Rouxhet. Adhesion of mammalian cells to polymer surfaces: from physical chemistry of surfaces to selective adhesion on defined patterns. *Biomaterials*, 19(16):1441–1445, 1998.

[38] J. Doh and D. J. Irvine. Immunological synapse arrays: Patterned protein surfaces that modulate immunological synapse structure formation in t cells. *Proceedings of the National Academy of Sciences of the United States of America*, 103(15):5700–5705, 2006.

[39] C. C. Dupont-Gillain, B. Nysten, V. Hlady, and P. G. Rouxhet. Atomic force microscopy and wettability study of oxidized patterns at the surface of polystyrene. *Journal of Colloid and Interface Science*, 220(1):163–169, 1999.

[40] P. J. Eng, T. P. Trainor, G. E. Brown, G. A. Waychunas, M. Newville, S. R. Sutton, and M. L. Rivers. Structure of the hydrated alpha-al2o3 (0001) surface. *Science*, 288(5468):1029–1033, 2000.

[41] E. Eteshola, L. J. Brillson, and S. C. Lee. Selection and characteristics of peptides that bind thermally grown silicon dioxide films. *Biomolecular Engineering*, 22(5-6):201–204, 2005.

[42] Giuseppe Falini, Shira Albeck, Steve Weiner, and Lia Addadi. Control of aragonite or calcite polymorphism by mollusk shell macromolecules. *Science*, 271:67–69, 1996.

[43] J. Feder and I. Giaever. Adsorbtion of ferritin. *J Colloid Interface Sci*, 78(1):144–154, 1980.

[44] M. J. Feldhaus, R. W. Siegel, L. K. Opresko, J. R. Coleman, J. M. Feldhaus, Y. A. Yeung, J. R. Cochran, P. Heinzelman, D. Colby, J. Swers, C. Graff, H. S. Wiley, and K. D. Wittrup. Flow-cytometric isolation of human antibodies from a nonimmune saccharomyces cerevisiae surface display library. *Nat Biotechnol*, 21(2):163–70, 2003.

[45] J. P. Fitts, X. M. Shang, G. W. Flynn, T. F. Heinz, and K. B. Eisenthal. Electrostatic surface charge at aqueous/alpha-al2o3 single-crystal interfaces as probed by optical second-harmonic generation. *Journal of Physical Chemistry B*, 109(16):7981–7986, 2005.

[46] Christine E. Flynn, S.-W. Lee, B. R. Peelle, and A. M. Belcher. Viruses as vehicles for growth, organization and assembly of materials. *Acta Mater.*, 51(19):5867–5880, 2003.

[47] Christine E. Flynn, Chuanbin Mao, Andrew Hayhurst, Julie L. Williams, George Georgiou, Brent Iverson, and Angela M. Belcher. Synthesis and organization of nanoscale ii-vi semiconductor materials using evolved peptide specificity and viral capsid assembly. *J Mater Chem*, 13:2414–2421, 2003.

[48] G. V. Franks and L. Meagher. The isoelectric points of sapphire crystals and alpha-alumina powder. *Colloids and Surfaces a-Physicochemical and Engineering Aspects*, 214(1-3):99–110, 2003.

[49] D. J. H. Gaskin, K. Starck, and E. N. Vulfson. Identification of inorganic crystal-specific sequences using phage display combinatorial library of short peptides: A feasibility study. *Biotechnology Letters*, 22(15):1211–1216, 2000.

[50] G. Georgiou, C. Stathopoulos, P. S. Daugherty, A. R. Nayak, B. L. Iverson, and 3rd Curtiss, R. Display of heterologous proteins on the surface of microorganisms: from the screening of combinatorial libraries to live recombinant vaccines. *Nat Biotechnol*, 15(1):29–34, 1997.

[51] K. Goede, P. Busch, and M. Grundmann. Binding specificity of a peptide on semiconductor surfaces. *Nano Letters*, 4(11):2115–2120, 2004.

[52] J. J. Gooding and D. B. Hibbert. The application of alkanethiol self-assembled monolayers to enzyme electrodes. *Trac-Trends in Analytical Chemistry*, 18(8):525–533, 1999.

[53] K. Gorner, E. Holtorf, J. Waak, T. T. Pham, D. M. Vogt-Weisenhorn, W. Wurst, C. Haass, and P. J. Kahle. Structural determinants of the c-terminal helix-kink-helix motif essential for protein stability and survival promoting activity of dj-1. *Journal of Biological Chemistry*, 282(18):13680–13691, 2007.

[54] C. G. Granqvist and A. Hultaker. Transparent and conducting ito films: new developments and applications. *Thin Solid Films*, 411(1):1–5, 2002.

[55] J. J. Gray. The interaction of proteins with solid surfaces. *Curr Opin Struct Biol*, 14(1):110–5, 2004.

[56] D. F. Green, A. T. Dennis, P. S. Fam, B. Tidor, and A. Jasanoff. Rational design of new binding specificity by simultaneous mutagenesis of calmodulin and a target peptide. *Biochemistry*, 45(41):12547–12559, 2006.

[57] C. L. Hansen, S. Classen, J. M. Berger, and S. R. Quake. A microfluidic device for kinetic optimization of protein crystallization and in situ structure determination. *Journal of the American Chemical Society*, 128(10):3142–3143, 2006.

[58] T. Hayashi, K. Sano, K. Shiba, Y. Kumashiro, K. Iwahori, I. Yamashita, and M. Hara. Mechanism underlying specificity of proteins targeting inorganic materials. *Nano Letters*, 6(3):515–519, 2006.

[59] G. He, A. Ramachandran, T. Dahl, S. George, D. Schultz, D. Cookson, A. Veis, and A. George. Phosphorylation of phosphophoryn is crucial for its function as a mediator of biomineralization. *Journal of Biological Chemistry*, 280(39):33109–33114, 2005.

[60] A. Hecker, O. Testeniere, F. Marin, and G. Luquet. Phosphorylation of serine residues is fundamental for the calcium-binding ability of orchestin, a soluble matrix protein from crustacean calcium storage structures. *Febs Letters*, 535(1-3):49–54, 2003.

[61] D. Horakova, M. Rumlova, I. Pichova, and T. Ruml. Luminometric method for screening retroviral protease inhibitors. *Analytical Biochemistry*, 345(1):96–101, 2005.

[62] R. J. Hosse, A. Rothe, and B. E. Power. A new generation of protein display scaffolds for molecular recognition. *Protein Science*, 15(1):14–27, 2006.

[63] N. P. Huang, R. Michel, J. Voros, M. Textor, R. Hofer, A. Rossi, D. L. Elbert, J. A. Hubbell, and N. D. Spencer. Poly(l-lysine)-g-poly(ethylene glycol) layers on metal oxide surfaces: Surface-analytical characterization and resistance to serum and fibrinogen adsorption. *Langmuir*, 17(2):489–498, 2001.

[64] N. P. Huang, J. Voros, S. M. De Paul, M. Textor, and N. D. Spencer. Biotin-derivatized poly(l-lysine)-g-poly(ethylene glycol): A novel polymeric interface for bioaffinity sensing. *Langmuir*, 18(1):220–230, 2002.

[65] D. L. Huber, R. P. Manginell, M. A. Samara, B. I. Kim, and B. C. Bunker. Programmed adsorption and release of proteins in a microfluidic device. *Science*, 301(5631):352–354, 2003.

[66] K. Ichimura, S. K. Oh, and M. Nakagawa. Light-driven motion of liquids on a photoresponsive surface. *Science*, 288(5471):1624–1626, 2000.

[67] C. D. James, R. C. Davis, L. Kam, H. G. Craighead, M. Isaacson, J. N. Turner, and W. Shain. Patterned protein layers on solid substrates by thin stamp microcontact printing. *Langmuir*, 14(4):741–744, 1998.

[68] X. Y. Jiang, R. Ferrigno, M. Mrksich, and G. M. Whitesides. Electrochemical desorption of self-assembled monolayers noninvasively releases patterned cells from geometrical confinements. *Journal of the American Chemical Society*, 125(9):2366–2367, 2003.

[69] B. L. Johansson, A. Larsson, A. Ocklind, and A. Ohrlund. Characterization of air plasma-treated polymer surfaces by esca and contact angle measurements

for optimization of surface stability and cell growth. *Journal of Applied Polymer Science*, 86(10):2618–2625, 2002.

[70] W Kaim and B Schwederski. The bioinorganic chemistry of the quinessentially toxic metals. In G. N. A. Meyer, editor, *Bioinorgainc Chemistry: Inorganic Chemistry in the Cemistry of Life*, pages 330–350. John Wiley and Sons, 1991.

[71] R. S. Kane, S. Takayama, E. Ostuni, D. E. Ingber, and G. M. Whitesides. Patterning proteins and cells using soft lithography. *Biomaterials*, 20(23-24):2363–2376, 1999.

[72] D. Kase, J. L. Kulp, M. Yudasaka, J. S. Evans, S. Iijima, and K. Shiba. Affinity selection of peptide phage libraries against single-wall carbon nanohorns identifies a peptide aptamer with conformational variability. *Langmuir*, 20(20):8939–8941, 2004.

[73] E. Katz, O. Lioubashevsky, and I. Willner. Electromechanics of a redox-active rotaxane in a monolayer assembly on an electrode. *Journal of the American Chemical Society*, 126(47):15520–15532, 2004.

[74] G. L. Kenausis, J. Voros, D. L. Elbert, N. P. Huang, R. Hofer, L. Ruiz-Taylor, M. Textor, J. A. Hubbell, and N. D. Spencer. Poly(l-lysine)-g-poly(ethylene glycol) layers on metal oxide surfaces: Attachment mechanism and effects of polymer architecture on resistance to protein adsorption. *Journal of Physical Chemistry B*, 104(14):3298–3309, 2000.

[75] A. Khademhosseini, L. Ferreira, J. Blumling, J. Yeh, J. M. Karp, J. Fukuda, and R. Langer. Co-culture of human embryonic stem cells with murine embryonic fibroblasts on microwell-patterned substrates. *Biomaterials*, 27(36):5968–5977, 2006.

[76] H. Kim, R. E. Cohen, P. T. Hammond, and D. J. Irvine. Live lymphocyte arrays for biosensing. *Advanced Functional Materials*, 16(10):1313–1323, 2006.

[77] I. W. Kim, S. Collino, D. E. Morse, and J. S. Evans. A crystal modulating protein from molluscan nacre that limits the growth of calcite in vitro. *Crystal Growth & Design*, 6(5):1078–1082, 2006.

[78] K. Kjaergaard, J. K. Sorensen, M. A. Schembri, and P. Klemm. Sequestration of zinc oxide by fimbrial designer chelators. *Appl Environ Microbiol*, 66(1):10–4, 2000.

[79] D. M. Kuhn, J. Chandra, P. K. Mukherjee, and M. A. Ghannoum. Comparison of biofilms formed by candida albicans and candida parapsilosis on bioprosthetic surfaces. *Infect Immun*, 70(2):878–88, 2002.

[80] K. Kuroda, S. Shibasaki, M. Ueda, and A. Tanaka. Cell surface-engineered yeast displaying a histidine oligopeptide (hexa-his) has enhanced adsorption of

and tolerance to heavy metal ions. *Appl Microbiol Biotechnol*, 57(5-6):697–701, 2001.

[81] J. Lahann and R. Langer. Smart materials with dynamically controllable surfaces. *Mrs Bulletin*, 30(3):185–188, 2005.

[82] J. Lahann, S. Mitragotri, T. N. Tran, H. Kaido, J. Sundaram, I. S. Choi, S. Hoffer, G. A. Somorjai, and R. Langer. A reversibly switching surface. *Science*, 299(5605):371–374, 2003.

[83] B. A. Langowski and K. E. Uhrich. Microscale plasma-initiated patterning (mu pip). *Langmuir*, 21(23):10509–10514, 2005.

[84] C. Y. Lee, B. Illarionov, Y. E. Woo, K. Kemter, R. R. Kim, S. Eberhardt, M. Cushman, W. Eisenreich, M. Fischer, and A. Bacher. Ligand binding properties of the n-terminal domain of riboflavin synthase from escherichia coli. *Journal of Biochemistry and Molecular Biology*, 40(2):239–246, 2007.

[85] G. Lee, N. F. Scherer, and P. B. Messersmith. Single-molecule mechanics of mussel adhesion. *Proc Natl Acad Sci U S A*, 103(35):12999–13003, 2006.

[86] J. K. Lee, Y. G. Kim, Y. S. Chi, W. S. Yun, and I. S. Choi. Grafting nitrilotriacetic groups onto carboxylic acid-terminated self-assembled monolayers on gold surfaces for immobilization of histidine-tagged proteins. *Journal of Physical Chemistry B*, 108(23):7665–7673, 2004.

[87] S. W. Lee, C. Mao, C. E. Flynn, and A. M. Belcher. Ordering of quantum dots using genetically engineered viruses. *Science*, 296(5569):892–5, 2002.

[88] J. B. Lhoest, E. Detrait, J. L. Dewez, P. V. deAguilar, and P. Bertrand. A new plasma-based method to promote cell adhesion on micrometric tracks on polystyrene substrates. *Journal of Biomaterials Science-Polymer Edition*, 7(12):1039–1054, 1996.

[89] B. K. Li and B. E. Logan. Bacterial adhesion to glass and metal-oxide surfaces. *Colloids and Surfaces B-Biointerfaces*, 36(2):81–90, 2004.

[90] H. C. Lichtenegger, T. Schoberl, M. H. Bartl, H. Waite, and G. D. Stucky. High abrasion resistance with sparse mineralization: Copper biomineral in worm jaws. *Science*, 298(5592):389–392, 2002.

[91] Stephen J. Lippard and Jeremy Mark Berg. *Principles of bioinorganic chemistry*. University Science Books, Mill Valley, Calif., 1994.

[92] G. Ma, D. F. Liu, and H. C. Allen. Piperidine adsorption on hydrated alpha-alumina (0001) surface studied by vibrational sum frequency generation spectroscopy. *Langmuir*, 20(26):11620–11629, 2004.

[93] S. Mann, N. H. Sparks, and R. G. Board. Magnetotactic bacteria: microbiology, biomineralization, palaeomagnetism and biotechnology. *Adv Microb Physiol*, 31:125–81, 1990.

[94] Stephen Mann. *Biomineralization : principles and concepts in bioinorganic materials chemistry.* Oxford chemistry masters ; 5. Oxford University Press, Oxford ; New York, 2001.

[95] C. Mao, C. E. Flynn, A. Hayhurst, R. Sweeney, J. Qi, G. Georgiou, B. Iverson, and A. M. Belcher. Viral assembly of oriented quantum dot nanowires. *Proc Natl Acad Sci U S A*, 100(12):6946–51, 2003.

[96] C. Mao, D. J. Solis, B. D. Reiss, S. T. Kottmann, R. Y. Sweeney, A. Hayhurst, G. Georgiou, B. Iverson, and A. M. Belcher. Virus-based toolkit for the directed synthesis of magnetic and semiconducting nanowires. *Science*, 303(5655):213–7, 2004.

[97] J. R. Matthews, D. Tuncel, R. M. J. Jacobs, C. D. Bain, and H. L. Anderson. Surfaces designed for charge reversal. *Journal of the American Chemical Society*, 125(21):6428–6433, 2003.

[98] I. L. Medintz, J. H. Konnert, A. R. Clapp, I. Stanish, M. E. Twigg, H. Mattoussi, J. M. Mauro, and J. R. Deschamps. A fluorescence resonance energy transfer-derived structure of a quantum dot-protein bioconjugate nanoassembly. *Proceedings of the National Academy of Sciences of the United States of America*, 101(26):9612–9617, 2004.

[99] M. Mercier-Bonin, K. Ouazzani, P. Schmitz, and S. Lorthois. Study of bioadhesion on a flat plate with a yeast/glass model system. *Journal of Colloid and Interface Science*, 271(2):342–350, 2004.

[100] S. A. Mitchell, M. R. Davidson, and R. H. Bradley. Glow discharge modified tissue culture polystyrene: role of surface chemistry in cellular attachment and proliferation. *Surface Engineering*, 22(5):337–344, 2006.

[101] S. Mitternacht, S. Schnabel, M. Bachmann, W. Janke, and A. Irback. Differences in solution behavior among four semiconductor-binding peptides. *Journal of Physical Chemistry B*, 111(17):4355–4360, 2007.

[102] Y. Morita, T. Ohsugi, Y. Iwasa, and E. Tamiya. A screening of phage displayed peptides for the recognition of fullerene (c60). *Journal of Molecular Catalysis B-Enzymatic*, 28(4-6):185–190, 2004.

[103] L. K. Mosavi, D. L. Minor, and Z. Y. Peng. Consensus-derived structural determinants of the ankyrin repeat motif. *Proceedings of the National Academy of Sciences of the United States of America*, 99(25):16029–16034, 2002.

[104] M. Mrksich and G. M. Whitesides. Patterning self-assembled monolayers using microcontact printing - a new technology for biosensors. *Trends in Biotechnology*, 13(6):228–235, 1995.

[105] A. A. Mungikar and D. Forciniti. Conformational changes of peptides at solid/liquid interfaces: A monte carlo study. *Biomacromolecules*, 5(6):2147–2159, 2004.

[106] R. R. Naik, L. L. Brott, S. J. Clarson, and M. O. Stone. Silica-precipitating peptides isolated from a combinatorial phage display peptide library. *Journal of Nanoscience and Nanotechnology*, 2(1):95–100, 2002.

[107] R. R. Naik, S. E. Jones, C. J. Murray, J. C. McAuliffe, R. A. Vaia, and M. O. Stone. Peptide templates for nanoparticle synthesis derived from polymerase chain reaction-driven phage display. *Advanced Functional Materials*, 14(1):25–30, 2004.

[108] R. R. Naik, S. J. Stringer, G. Agarwal, S. E. Jones, and M. O. Stone. Biomimetic synthesis and patterning of silver nanoparticles. *Nat Mater*, 1(3):169–72, 2002.

[109] M. T. Neves-Petersen, T. Snabe, S. Klitgaard, M. Duroux, and S. B. Petersen. Photonic activation of disulfide bridges achieves oriented protein immobilization on biosensor surfaces. *Protein Science*, 15(2):343–351, 2006.

[110] K. Nord, E. Gunneriusson, J. Ringdahl, S. Stahl, M. Uhlen, and P. A. Nygren. Binding proteins selected from combinatorial libraries of an alpha-helical bacterial receptor domain. *Nature Biotechnology*, 15(8):772–777, 1997.

[111] W. Norde. Adsorption of proteins from solution at the solid-liquid interface. *Advances in Colloid and Interface Science*, 25(4):267–340, 1986.

[112] S Nygaard, R Wendelbo, and S Brown. Surface-specific zeolite-binding proteins. *Adv. Mat.*, 14(24):1853–1856, 2002.

[113] P. A. Nygren and A. Skerra. Binding proteins from alternative scaffolds. *Journal of Immunological Methods*, 290(1-2):3–28, 2004.

[114] E. Occhiello, M. Morra, F. Garbassi, D. Johnson, and P. Humphrey. Ssims studies of hydrophobic recovery - oxygen plasma treated ps. *Applied Surface Science*, 47(3):235–242, 1991.

[115] E. E. Oren, C. Tamerler, and M. Sarikaya. Metal recognition of septapeptides via polypod molecular architecture. *Nano Letters*, 5(3):415–419, 2005.

[116] P. Paoli, A. Modesti, F. Magherini, T. Gamberi, A. Caselli, G. Manao, G. Raugei, G. Camici, and G. Ramponi. Site-directed mutagenesis of two aromatic residues lining the active site pocket of the yeast ltp1. *Biochimica Et Biophysica Acta-General Subjects*, 1770(5):753–762, 2007.

[117] W. J. Parak, D. Gerion, T. Pellegrino, D. Zanchet, C. Micheel, S. C. Williams, R. Boudreau, M. A. Le Gros, C. A. Larabell, and A. P. Alivisatos. Biological applications of colloidal nanocrystals. *Nanotechnology*, 14(7):R15–R27, 2003.

[118] T. J. Park, S. Y. Lee, S. J. Lee, J. P. Park, K. S. Yang, K. B. Lee, S. Ko, J. B. Park, T. Kim, S. K. Kim, Y. B. Shin, B. H. Chung, S. J. Ku, D. H. Kim, and I. S. Choi. Protein nanopatterns and biosensors using gold binding polypeptide as a fusion partner. *Analytical Chemistry*, 78(20):7197–7205, 2006.

[119] B. Peelle. *Engineered Biomolecular Interactions with Inorganic Materials: Sequence, Binding, and Assembly.* Dissertation, Massachusetts Institute of Technology, 2005.

[120] B. Peelle, J. Lorens, W. Li, J. Bogenberger, D. G. Payan, and D. C. Anderson. Intracellular protein scaffold-mediated display of random peptide libraries for phenotypic screens in mammalian cells. *Chem Biol*, 8(5):521–34, 2001.

[121] B. R. Peelle, E. M. Krauland, K. D. Wittrup, and A. M. Belcher. Design criteria for engineering inorganic material-specific peptides. *Langmuir*, 21(15):6929–6933, 2005.

[122] B. R. Peelle, E. M. Krauland, K. D. Wittrup, and A. M. Belcher. Probing the interface between biomolecules and inorganic materials using yeast surface display and genetic engineering. *Acta Biomaterialia*, 1(2):145–154, 2005.

[123] R. Raiteri, M. Grattarola, H. J. Butt, and P. Skladal. Micromechanical cantilever-based biosensors. *Sensors and Actuators B-Chemical*, 79(2-3):115–126, 2001.

[124] B. D. Reiss, C. B. Mao, D. J. Solis, K. S. Ryan, T. Thomson, and A. M. Belcher. Biological routes to metal alloy ferromagnetic nanostructures. *Nano Letters*, 4(6):1127–1132, 2004.

[125] T. B. Reynolds and G. R. Fink. Bakers' yeast, a model for fungal biofilm formation. *Science*, 291(5505):878–81, 2001.

[126] M. A. Romanos, C. A. Scorer, and J. J. Clare. Foreign gene expression in yeast: a review. *Yeast*, 8(6):423–88, 1992.

[127] K. I. Sano and K. Shiba. A hexapeptide motif that electrostatically binds to the surface of titanium. *Journal of the American Chemical Society*, 125(47):14234–14235, 2003.

[128] M. Sarikaya, C. Tamerler, A. K. Jen, K. Schulten, and F. Baneyx. Molecular biomimetics: nanotechnology through biology. *Nat Mater*, 2(9):577–85, 2003.

[129] M. A. Schembri, K. Kjaergaard, and P. Klemm. Bioaccumulation of heavy metals by fimbrial designer adhesins. *FEMS Microbiol Lett*, 170(2):363–71, 1999.

[130] K. E. Schmalenberg, H. M. Buettner, and K. E. Uhrich. Microcontact printing of proteins on oxygen plasma-activated poly(methyl methacrylate). *Biomaterials*, 25(10):1851–1857, 2004.

[131] K. E. Schmalenberg and K. E. Uhrich. Micropatterned polymer substrates control alignment of proliferating schwann cells to direct neuronal regeneration. *Biomaterials*, 26(12):1423–1430, 2005.

[132] P. Schravendijk, L. M. Ghiringhelli, L. Delle Site, and N. F. A. van der Vegt. Interaction of hydrated amino acids with metal surfaces: A multiscale modeling description. *Journal of Physical Chemistry C*, 111(6):2631–2642, 2007.

[133] Nadrian C. Seeman and Angela M. Belcher. Emulating biology: Building nanostructures from the bottom up. *Proc. Natl. Acad. Sci.*, 99(2):6415, 2002.

[134] X. Shen, A. M. Belcher, P. K. Hansma, G. D. Stucky, and D. E. Morse. Molecular cloning and characterization of lustrin a, a matrix protein from shell and pearl nacre of haliotis rufescens. *J Biol Chem*, 272(51):32472–81, 1997.

[135] K. Shimizu, J. Cha, G. D. Stucky, and D. E. Morse. Silicatein alpha: cathepsin l-like protein in sponge biosilica. *Proc Natl Acad Sci U S A*, 95(11):6234–8, 1998.

[136] K. Shimizu, J. Cha, Y. Zhou, G. D. Stucky, and D. E. Morse. Molecular mechanism of biomineralization with silicon. *Abstracts of Papers of the American Chemical Society*, 217:U670–U670, 1999.

[137] S. S. Sidhu, W. J. Fairbrother, and K. Deshayes. Exploring protein-protein interactions with phage display. *Chembiochem*, 4(1):14–25, 2003.

[138] J. M. Slocik and D. W. Wright. Biomimetic mineralization of noble metal nanoclusters. *Biomacromolecules*, 4(5):1135–41, 2003.

[139] D. J. Solis and Y. Huang. Unpublished peptide sequences selected by phage display. *(personal communications)*.

[140] C. Sousa, A. Cebolla, and V. de Lorenzo. Enhanced metalloadsorption of bacterial cells displaying poly-his peptides. *Nat Biotechnol*, 14(8):1017–20, 1996.

[141] B. Straub, E. Meyer, and P. Fromherz. Recombinant maxi-k channels on transistor, a prototype of iono-electronic interfacing. *Nat Biotechnol*, 19(2):121–4, 2001.

[142] C. Tamerler, E. E. Oren, M. Duman, E. Venkatasubramanian, and M. Sarikaya. Adsorption kinetics of an engineered gold binding peptide by surface plasmon resonance spectroscopy and a quartz crystal microbalance. *Langmuir*, 22(18):7712–7718, 2006.

[143] C. S. Tang, M. Dusseiller, S. Makohliso, M. Heuschkel, S. Sharma, B. Keller, and J. Voros. Dynamic, electronically switchable surfaces for membrane protein microarrays. *Analytical Chemistry*, 78(3):711–717, 2006.

[144] H. Tang, W. Zhang, P. Geng, Q. J. Wang, L. T. Jin, Z. R. Wu, and M. Lou. A new amperometric method for rapid detection of escherichia coli density using a self-assembled monolayer-based bienzyme biosensor. *Analytica Chimica Acta*, 562(2):190–196, 2006.

[145] A. S. Templeton, T. P. Trainor, S. J. Traina, A. M. Spormann, and G. E. Brown. Pb(ii) distributions at biofilm-metal oxide interfaces. *Proceedings of the National Academy of Sciences of the United States of America*, 98(21):11897–11902, 2001.

[146] C. K. Thai, H. X. Dai, M. S. R. Sastry, M. Sarikaya, D. T. Schwartz, and F. Baneyx. Identification and characterization of cu2o- and zno-binding polypeptides by escherichia coli cell surface display: Toward an understanding of metal oxide binding. *Biotechnology and Bioengineering*, 87(2):129–137, 2004.

[147] S. D. Tomasio and T. R. Walsh. Atomistic modelling of the interaction between peptides and carbon nanotubes. *Molecular Physics*, 105(2-3):221–229, 2007.

[148] T. P. Trainor, P. J. Eng, G. E. Brown, I. K. Robinson, and M. De Santis. Crystal truncation rod diffraction study of the alpha-al2o3 (1(1)over-bar-0 2) surface. *Surface Science*, 496(3):238–250, 2002.

[149] T. G. van Kooten, H. T. Spijker, and H. J. Busscher. Plasma-treated polystyrene surfaces: model surfaces for studying cell-biomaterial interactions. *Biomaterials*, 25(10):1735–1747, 2004.

[150] C. Verdozzi, D. R. Jennison, P. A. Schultz, and M. P. Sears. Sapphire (0001) surface, clean and with d-metal overlayers. *Physical Review Letters*, 82(4):799–802, 1999.

[151] D. Y. Wang, Y. C. Huang, H. S. Chiang, A. M. Wo, and Y. Y. Huang. Microcontact printing of laminin on oxygen plasma activated substrates for the alignment and growth of schwann cells. *Journal of Biomedical Materials Research Part B-Applied Biomaterials*, 80B(2):447–453, 2007.

[152] S. Wang, E. S. Humphreys, S. Y. Chung, D. F. Delduco, S. R. Lustig, H. Wang, K. N. Parker, N. W. Rizzo, S. Subramoney, Y. M. Chiang, and A. Jagota. Peptides with selective affinity for carbon nanotubes. *Nat Mater*, 2(3):196–200, 2003.

[153] X. M. Wang, E. Katz, and I. Willner. Potential-induced switching of electrical contact by controlling droplet shapes at hydrophilic/hydrophobic interfaces. *Electrochemistry Communications*, 5(9):814–818, 2003.

[154] S. Weiner and H. D. Wagner. The material bone: structure-mechanical function relations. *Annual Review of Materials Science*, 28:271–298, 1998.

[155] Stephen Weiner and Lia Addadi. Design strategies in mineralized biological materials. *Journal of Materials Chemistry*, 7(5):689–702, 1997.

[156] S. R. Whaley, D. S. English, E. L. Hu, P. F. Barbara, and A. M. Belcher. Selection of peptides with semiconductor binding specificity for directed nanocrystal assembly. *Nature*, 405(6787):665–8, 2000.

[157] R. L. Willett, K. W. Baldwin, K. W. West, and L. N. Pfeiffer. Differential adhesion of amino acids to inorganic surfaces. *Proceedings of the National Academy of Sciences of the United States of America*, 102(22):7817–7822, 2005.

[158] K. D. Wittrup. Protein engineering by cell-surface display. *Curr Opin Biotechnol*, 12(4):395–9, 2001.

[159] R. G. Woodbury, C. Wendin, J. Clendenning, J. Melendez, J. Elkind, D. Bartholomew, S. Brown, and C. E. Furlong. Construction of biosensors using a gold-binding polypeptide and a miniature integrated surface plasmon resonance sensor. *Biosens Bioelectron*, 13(10):1117–26, 1998.

[160] X. Wu, H. Liu, J. Liu, K. N. Haley, J. A. Treadway, J. P. Larson, N. Ge, F. Peale, and M. P. Bruchez. Immunofluorescent labeling of cancer marker her2 and other cellular targets with semiconductor quantum dots. *Nat Biotechnol*, 21(1):41–6, 2003.

[161] B. A. Wustman, J. C. Weaver, D. E. Morse, and J. S. Evans. Structure-function studies of the lustrin a polyelectrolyte domains, rksy and d4. *Connect Tissue Res*, 44 Suppl 1:10–5, 2003.

[162] M. N. Yousaf, B. T. Houseman, and M. Mrksich. Using electroactive substrates to pattern the attachment of two different cell populations. *Proceedings of the National Academy of Sciences of the United States of America*, 98(11):5992–5996, 2001.

[163] B. Zhang, B. A. Wustman, D. Morse, and J. S. Evans. Model peptide studies of sequence regions in the elastomeric biomineralization protein, lustrin a. i. the c-domain consensus-pg-, -nvnct-motif. *Biopolymers*, 63(6):358–69, 2002.

[164] S. Zhang. Fabrication of novel biomaterials through molecular self-assembly. *Nat Biotechnol*, 21:1171–1178, 2003.

[165] X. M. Zhao, Y. N. Xia, and G. M. Whitesides. Soft lithographic methods for nano-fabrication. *Journal of Materials Chemistry*, 7(7):1069–1074, 1997.

[166] G. L. Zhen, D. Falconnet, E. Kuennemann, J. Voros, N. D. Spencer, M. Textor, and S. Zurcher. Nitrilotriacetic acid functionalized graft copolymers: A polymeric interface for selective and reversible binding of histidine-tagged proteins. *Advanced Functional Materials*, 16(2):243–251, 2006.

[167] H. Zlotnik, M. P. Fernandez, B. Bowers, and E. Cabib. Saccharomyces-cerevisiae mannoproteins form an external cell-wall layer that determines wall porosity. *Journal of Bacteriology*, 159(3):1018–1026, 1984.